



**UiT** The Arctic University of Norway

Faculty of Science and Technology  
Department of Geosciences

## **Upper Triassic to lower Cretaceous tectonostratigraphic development of the Barents Sea South East**

**Ådne Frostad Kristiansen**

*Master's thesis in Geology, GEO-3900  
May 2020*



## Abstract

The aim of this study is to investigate the tectonic- and evolutionary differences between major structural elements of the Barents Sea South East (BSSE) during the uppermost Triassic to lower Cretaceous. The study area comprises the following structural elements: the Bjarmeland- and Finnmark platforms, the Nordkapp- and Tiddlybanken basins, the Signalhorn-, Haapet- and Veslekari domes and the Fedynsky High.

Interpretation of seismic 2D- and well-data from the exploration well 7435/12-1 have provided the stratigraphic framework on the uppermost Triassic to lower Cretaceous, represented by the Realgrunnen Subgroup (late Norian to Bajocian), the Fuglen Formation (Callovian to Oxfordian) and the Hekkingen Formation (late Oxfordian to Tithonian). Thickness variations, and seismic stratigraphy as reflection geometries and terminations were applied to identify structural events such as uplift, subsidence and periods of erosion.

Insight in the tectono-stratigraphic evolution of the Barents Sea South East have been provided by variations in the thickness and termination patterns of the uppermost Triassic to lower Cretaceous units. This study suggests a late Norian to Bajocian (represented by the Realgrunnen Subgroup) elevation of the Fedynsky High, Finnmark Platform, Veslekari- and Signalhorn domes. During the same period, a relatively stable platform configuration was valid for the Bjarmeland Platform and northern section of the Finnmark Platform, and concurrent basin configuration of the Nordkapp Basin, what today is the Haapet Dome and the area northeast of the dome structure. The structural trends valid for the late Norian to Bajocian continued into the Callovian to Oxfordian (represented by the Fuglen Formation), excluding the Haapet Dome, Bjarmeland Platform and north part of the Finnmark Platform in which the former experienced uplift and the two latter experienced subsidence during this period. The tectono-stratigraphic evolution of the Callovian to Oxfordian persisted through the late Oxfordian to Tithonian, accompanied by a rise in relative sea-level (represented by the Hekkingen Formation), in addition to subsidence of the Tiddlybanken Basin.

Late Norian to Tithonian structuring of the BSSE are suggested to be linked to the possible reactivation of deep lineaments by the final upthrusting of the Novaya Zemlya (Late Triassic – Early Jurassic) and also the tectonic events that influenced the NE Atlantic rifting (Late Jurassic – Early Cretaceous) and later opening.





## Acknowledgements

Fem år går fort, og før man vet ordet av det så har man en mastergrad innenfor geologi. Det siste året har vært lærerikt, utfordrende og spennende, med både gledens øyeblikk samt noen søvnløse netter.

Jeg vil først og fremst tildele en utrolig stor takk til min hovedveileder Stig-Morten Knutsen og mine bi-veiledere; Tom Arne Rydningen og Vegard Heiberg. Dere har kommet med utrolig gode innspill og diskusjoner, samt litteratur, forklaringer, motivasjon og sannsynligvis mer korrekturlesing enn dere hadde håpet på. Jeg kan trygt si at oppgaven ikke hadde blitt til det den er uten deres hjelp!

Videre vil jeg takke mine utrolig flotte klassekamerater gjennom disse fem årene på geologi. Studietiden har vært en fantastisk opplevelse fra dagen vi startet på studiet til hvor vi er nå, og denne turen hadde ikke vært den samme uten hver og en av dere! Jeg vil også gi en spesiell takk til familien min, som alltid har vært der for meg, spesielt på de søvnløse nettene. Til slutt vil jeg takke Cris Tandy og Dag Julian Eilertsen for å ha tatt seg tiden til å lese korrektur.



# Table of Contents

1	Introduction .....	1
1.1	Objective.....	1
1.2	Study area .....	2
2	Geological background .....	3
2.1	Structural development.....	3
2.1.1	Precambrian.....	4
2.1.2	Paleozoic .....	4
2.1.3	Mesozoic .....	5
2.1.4	Cenozoic.....	6
2.2	Stratigraphic and depositional environment .....	7
2.2.1	Mesozoic .....	8
2.3	Stratigraphic units.....	17
2.3.1	Realgrunnen Subgroup.....	17
2.3.2	Snadd Formation .....	17
2.3.3	Stø Formation.....	17
2.3.4	Fuglen Formation .....	17
2.3.5	Hekkingen Formation.....	18
2.4	Structural elements .....	18
2.4.1	Bjarmeland Platform .....	19
2.4.2	Finnmark Platform .....	19
2.4.3	Nordkapp Basin.....	19
2.4.4	Tiddlybanken Basin.....	21
2.4.5	Haapet Dome.....	21
2.4.6	Veslekari Dome.....	21
2.4.7	Signalhorn Dome.....	21

2.4.8	Fedynsky High .....	22
3	Theory .....	23
3.1	Seismic reflection theory .....	23
3.1.1	Seismic resolution .....	24
3.1.2	Vertical resolution .....	26
3.1.3	Horizontal resolution.....	27
4	Data and Methods.....	30
4.1	Data.....	30
4.1.1	Phase and polarity .....	32
4.1.2	Vertical and horizontal resolution of 2D data .....	33
4.2	Method.....	38
4.2.1	Seismic stratigraphy .....	38
4.2.2	Seismic attributes .....	40
5	Results .....	41
5.1	Snadd horizon (Base Realgrunnen) .....	51
5.2	The Realgrunnen Subgroup (Top Snadd – Top Stø) .....	58
5.3	Top Stø (Top Realgrunnen).....	61
5.4	Fuglen Formation .....	64
5.5	Top Fuglen horizon .....	67
5.6	Hekkingen Formation .....	70
5.7	Top Hekkingen horizon .....	73
6	Discussion .....	81
6.1	Depositional and structural development .....	81
7	Conclusion.....	98
8	Future work .....	100
	References .....	102



# 1 Introduction

The Barents Sea South East (BSSE) was opened to petroleum exploration in 2013, following the signing of a delimitation agreement between Norway and Russia in 2010 (Jensen, 2011; Nagell & Berthelsen, 2016). Subsequent to the agreement and the following 22-24th licensing rounds, the geological knowledge of the area has increased considerably. With the acquisition of seismic 2D and 3D data, drilling of exploration wells (NPD, 2019), and a number of scientific studies conducted on the area (Mattingsdal et al., 2015; Gernigon et al., 2018; Müller et al., 2019; Hassaan et al., 2020).

## 1.1 Objective

The objective of the study is to map, interpret and describe the uppermost Triassic to lower Cretaceous units in the Barents Sea South East (BSSE) in order to evaluate any tectonic- and evolutionary differences between major structural elements of the area. The stratigraphic focus is represented by the Hekkingen Formation, Fuglen Formation and Realgrunnen Subgroup, with some of the key tasks listed below:

- Interpret the top and base of the above listed stratigraphic units (Hekkingen Formation, Fuglen Formation and Realgrunnen Subgroup).
- Generate time-thickness maps of the units and identify possible unconformities/ terminations.
- Investigate thickness variations and relations to unconformities/ terminations of the units.
- Identify the internal and external reflection geometry and amplitude of the units and correlate it to their possible lithological composition and environmental setting.
- Establish a possible uppermost Triassic to lower Cretaceous structural evolution for each element, basing it on the documented findings, and previously published literature.

## 1.2 Study area

The study area – the Barents Sea South East (BSSE) - is situated along the Norwegian – Russian border, covering an area of 44 000 square kilometers (NPD, 2013). It comprises the Bjarmeland and Finnmark platforms, Nordkapp and Tiddlybanken basins, Veslekari, Signalhorn and Haapet domes and the Fedynsky High (Figure 1.1).

The following chapter will give background information on the structural and sedimentary aspects of this study.

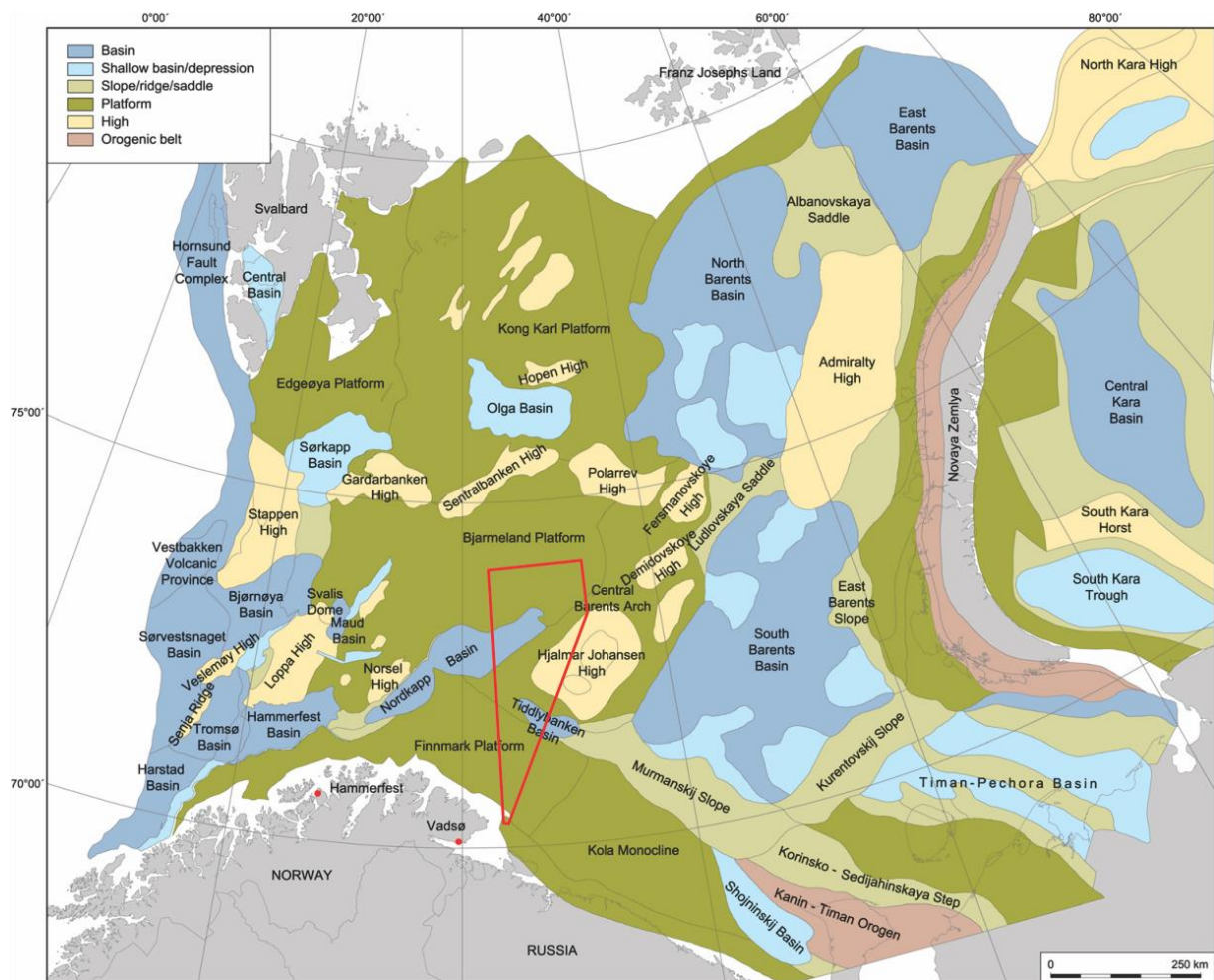


Figure 1.1 Regional Barents Sea map indicating some of the major structural elements and the location of the study area (red polygon). The Haapet, Signalhorn and Veslekari domes were defined after the creation of the structural map, and are as of this not indicated in this figure. The Norwegian-Russian border is indicated in Figure 2.11. Modified from (Henriksen et al., 2011)

## **2 Geological background**

The Barents Sea shelf (Figure 1.1) is situated north of the Norwegian and Russian mainland, covering an area of 1.3 million square km. It stretches from the Norwegian-Greenland Sea in the west, to the Novaya Zemlya archipelago in the east while bounded by the Svalbard and Franz Josef Land archipelagos in the northwest and north (Doré, 1995; Worsley, 2008; Smelror et al., 2009). The Barents Sea has an average water depth of 300 m and no area surpasses 500 m (Rønnevik et al., 1982; Doré, 1995).

The southern Barents Sea can be divided into an eastern and western province based on stratigraphic and tectonic differences in both time, trend and magnitude (Smelror et al., 2009). Separated by the N-S to NNE-SSE trending Ringvassøy-Loppa and Bjørnøyrenna Fault Complexes (Halland et al., 2014). Tectonically the western province was most active throughout the late Mesozoic and Cenozoic, which was a period of extensive rifting and sedimentation. This resulted in a NNE-SSW, NE-SW and N-S regional fault orientation as well as extensive sedimentation within the Harstad, Tromsø and Bjørnøya Basins (Faleide et al., 1993; Halland et al., 2014). Structurally the western province consists of several smaller, shallower basins and highs, when compared to the south eastern Barents Sea region. In the eastern region there are two significant offshore sedimentary basins, which are the North and South Barents Sea basins, as well as the semi-offshore Timian-Pechora Basin (Figure 1.1) (Smelror et al., 2009). The North and South Barents Sea Basins are known as sag basins, which has formed in the foredeep zone, west of Novaya Zemlya peninsula (Doré, 1995; Smelror et al., 2009). These basins have the most significant areal extent and sedimentary thickness within the Barents Sea, possibly exceeding 12 km of post-Carboniferous sediments (Doré, 1995), with primarily Upper Paleozoic and Mesozoic deposits dominating this sedimentary package (Halland et al., 2014).

### **2.1 Structural development**

The Barents Sea shelf has since the Precambrian experienced several compressional and extensional episodes, in its evolution to become the mosaic of structural highs and lows of today (Figure 1.1). The western Barents Sea shelf has mainly been shaped by the compressional regime of the Caledonian orogeny and the following onset of extensional regimes. The post Caledonian rifting occurred in pulses, with three main phases of rifting occurring during the Late Devonian – Carboniferous, Middle Jurassic – Early Cretaceous and early Cenozoic (Faleide et al., 1993). The east Barents Sea shelf has mainly experienced



compressional regimes in the shape of the Timanian and Uralian orogenies (Smelror et al., 2009).

### **2.1.1 Precambrian**

The first known large scale tectonic event of the Barents Sea shelf took place in the late Neoproterozoic (Ediacaran) time, known as the Timanian Orogeny (Klitzke et al., 2015; Gernigon et al., 2018). It developed along the north-eastern passive margin of Baltica, as a fold-and-thrust belt, stretching from the Varanger Peninsula of northern Norway to the southern Ural Mountains of Kazakhstan (Gee & Pease, 2004; Gernigon et al., 2018; Hassaan et al., 2020). The opening of the Iapetus Ocean occurred in the transition from the Precambrian to the Paleozoic, following passive margin extension and subsequent rifting along the northwest of the Baltic Plate (Gernigon et al., 2018).

### **2.1.2 Paleozoic**

The Caledonian Orogeny (approx. 400 ma) represents the consolidation of the Laurentian (Greenland, North America) and the Baltic plates (Scandinavian, western Russia) into the Laurasian continent, as well as the closure of the Iapetus (Doré, 1995; Smelror et al., 2009; Henriksen et al., 2011; Gernigon et al., 2018). According to Henriksen et al. (2011) deformation initiated during the Middle Ordovician, with a deformation maximum in the Silurian. It represents large parts of the regional basement in the western Barents Sea, and influenced the structural foundation for the subsequent structural evolution (E. Glørstad-Clark et al., 2011). Present day evidence of this orogeny can be traced for almost 2000 km, stretching from the south-western part of Norway all the way to the western part of Svalbard (Smelror et al., 2009; Gernigon et al., 2018).

The compressional regime of the Caledonian Orogeny was followed by crustal extensions in the Late Paleozoic, affecting much of the western Barents Sea shelf (Faleide et al., 1993; Henriksen et al., 2011). These crustal extensions occurred episodically just as in the following Mesozoic and Cenozoic, with the main episodes taking place in the mid-Carboniferous, Carboniferous - Permian and Permian - Early Triassic times (Faleide et al., 2008; E. Glørstad-Clark et al., 2011).

The Uralian Orogeny (Mid to Late Paleozoic), represents the consolidation of Baltica and Kazakhstania and the creation of the Ural Mountains (Berzin et al., 1996; Puchkov, 2009; Smelror et al., 2009). In the present-day Barents and Kara Sea, evidence of the Uralian Ocean

closure can be observed on seismic profiles as folds dated to a Carboniferous to Permian age (Smelror et al., 2009).

### **2.1.3 Mesozoic**

The Mesozoic in comparison to the Precambrian and Paleozoic, was modest when it comes to tectonic activity, with only minor occurrences of movement documented on the Bjarmeland and Finnmark platforms (Doré, 1995; Smelror et al., 2009; Henriksen et al., 2011). The Barents Sea shelf experienced passive regional subsidence during this period, with especially high rates in the eastern Barents Sea Basins during the Triassic (O'leary et al., 2004; Smelror et al., 2009). Folding in the east Barents Sea occurred along the Novaya Zemlya at the Triassic/ Jurassic boundary as a late response to the Uralian Orogeny (Ritzmann & Faleide, 2009; Gernigon et al., 2018). Foreland uplift west of the Novaya Zemlya is believed to have occurred as a response to the compressional event (Müller et al., 2019).

Tectonic activity increased into the Middle Jurassic, with episodic rifting being a normal occurrence in the west Barents Sea during the Middle, Late-Jurassic and Early Cretaceous, as a result of the long-lived Paleozoic-Mesozoic pre-opening rifting of the North Atlantic (Faleide et al., 1993; Smelror et al., 2009; Faleide et al., 2010; Gernigon et al., 2018). The gradual westward migration of the focus area of these rifting episodes, resulted in younger as well as deeper pull-apart basins in the west (Figure 2.1) (Faleide et al., 1993; Faleide et al., 2008; Faleide et al., 2010; E. Glørstad-Clark et al., 2011; Klitzke et al., 2015).

In the Early Cretaceous the north Barents Sea shelf experienced extensive magnetism (Faleide et al., 2010; Klitzke et al., 2015). The magnetism was part of a High Arctic Large Igneous Province (HALIP) located in the Arctic, most active in the Barremian-Aptian times (Faleide et al., 2010). The magnetism caused a regional uplift of the north Barents Sea shelf, altering the regional depositional pattern (Faleide et al., 2008; Faleide et al., 2010; E. Glørstad-Clark et al., 2011; Klitzke et al., 2015).

## 2.1.4 Cenozoic

The Cenozoic opening of the Norwegian-Greenland Sea had a noticeable effect on the structural evolution of the Barents Sea, with the western margin experiencing lithospheric breakup of Norway and Greenland at the Paleocene-Eocene boundary (Faleide et al., 1993; Faleide et al., 2008; E. Glørstad-Clark et al., 2011; Henriksen et al., 2011; Hassaan et al., 2020). This was followed by a transition from an active to a passive margin, believed to have happened in the Oligocene (Faleide et al., 1993; Faleide et al., 2008; Henriksen et al., 2011). In the north of the Barents Sea, the early Eocene marked the creation of the Eurasian Basin, with the Atlantic and Eurasian being connected by the regional De Geer megashear system (Doré, 1995; Faleide et al., 2008; Gernigon et al., 2018).

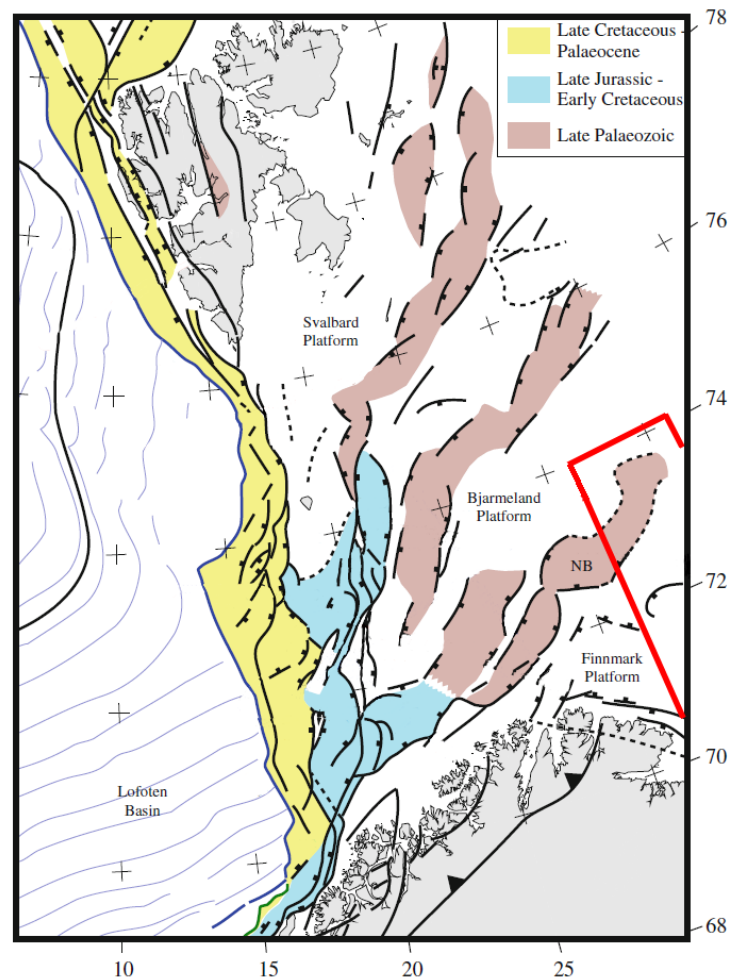


Figure 2.1 A map of the orientation and positioning of the rift system from the western Barents Sea shelf to the BSSE, with colours indicating the area influenced by Paleozoic (Brown), Late Jurassic – Early Cretaceous (Blue) and Late Cretaceous – Paleocene rifting. Illustrating how the rifting gradually migrated westward. The Paleozoic evolution is indicated with brown, while the following Mesozoic (Late Jurassic – Early Cretaceous) and Mesozoic - Cenozoic (Late Cretaceous – Paleocene) is indicated in blue and yellow. The study area is indicated with the red polygon, with NB = Nordkapp basin. Modified from (Faleide et al., 2010)

## 2.2 Stratigraphic and depositional environment

Stratigraphically, this study has its focus on the Realgrunnen Subgroup and the Teistengrunnen Group of the Late Triassic to Early Cretaceous. The Realgrunnen Subgroup is comprised of four formations, being the Fruholmen, Tubåen, Nordmela and Stø (Halland et al., 2014; Klausen et al., 2019). While the Teistengrunnen Group consists of the Late Jurassic, Fuglen Formation (Callovian –Oxfordian) and Hekkingen Formation (upper Oxfordian – Tithonian). This subchapter will give a short brief on the depositional environments of the Mesozoic and its correlating formations illustrated in (Figure 2.2).

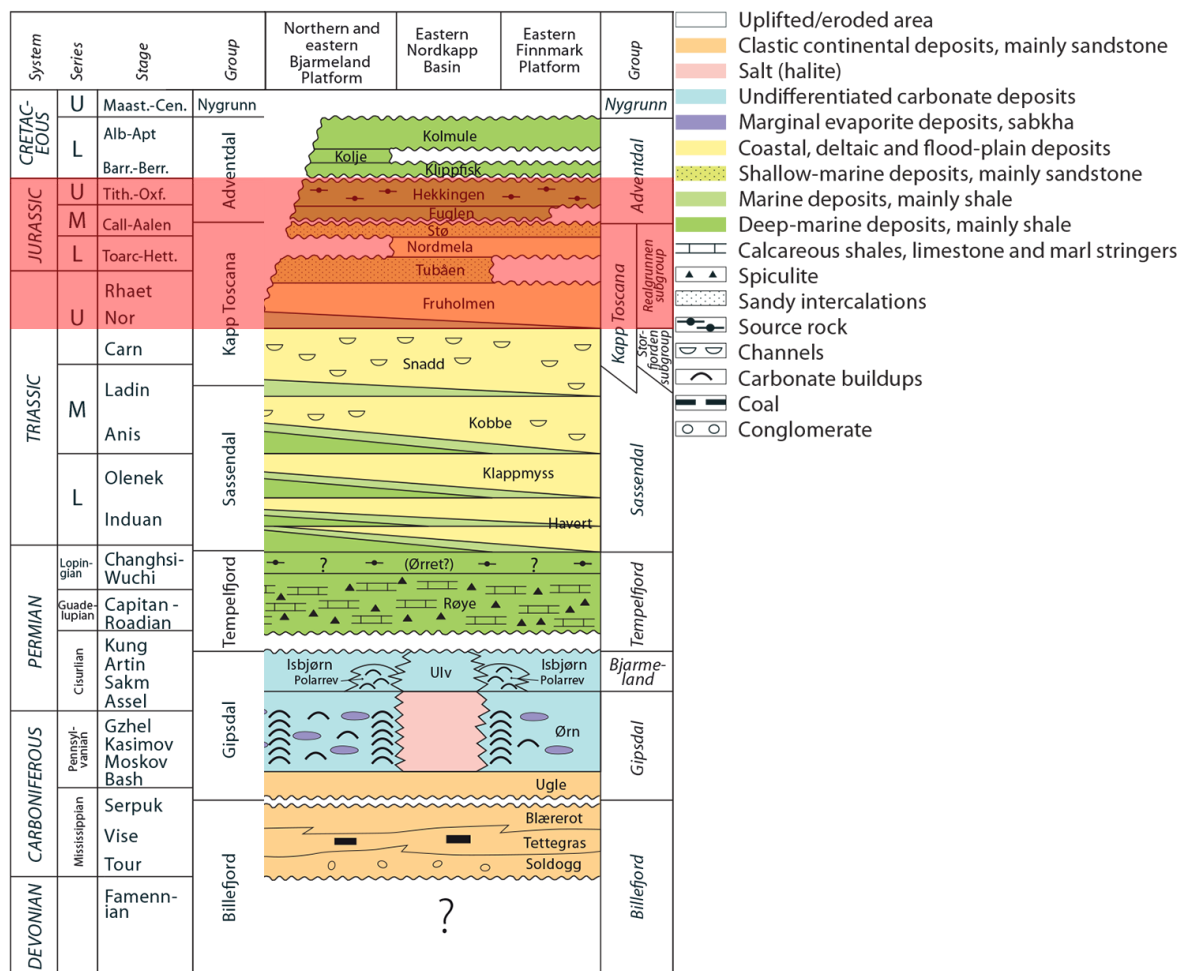


Figure 2.2 Chronostratigraphic chart of the East Barents Sea, with the red square indicating the focus stratigraphy for this study (Top Snadd – Top Hekkingen). Modified from (NPD, 2017)

## **2.2.1 Mesozoic**

### **2.2.1.1 Triassic**

During the Triassic the Svalbard Archipelago drifted northward, from approximately 40° to 60°N, causing a climatic transition from an arid to a humid environment (E. Glørstad-Clark et al., 2011; Ryseth, 2014). At the time a marine environmental setting characterized the western Barents Sea shelf, while a terrestrial environmental setting characterized the eastern parts (Figure 2.3) (Bugge et al., 2002; Smelror et al., 2009; Faleide et al., 2010). The greatest water depths were possibly located in the Hammerfest Basin to the northern part of the Finnmark Platform, Nordkapp Basin and Tiddlybanken Basin (Smelror et al., 2009).

The Barents Sea shelf experienced a high rate of sedimentation during the Lower Triassic, with the newly developed Uralian Highlands supplying the rapidly subsiding North and South Barents basins in the east. In the west, the Fennoscandian Shield, and locally uplifted/exposed areas supplied the Finnmark Platform, Hammerfest Basin and Nordkapp Basin (Bugge et al., 2002; Smelror et al., 2009; Faleide et al., 2010; E. Glørstad-Clark et al., 2011; Lundschien et al., 2014; Mørk et al., 2014; Hassaan et al., 2020).

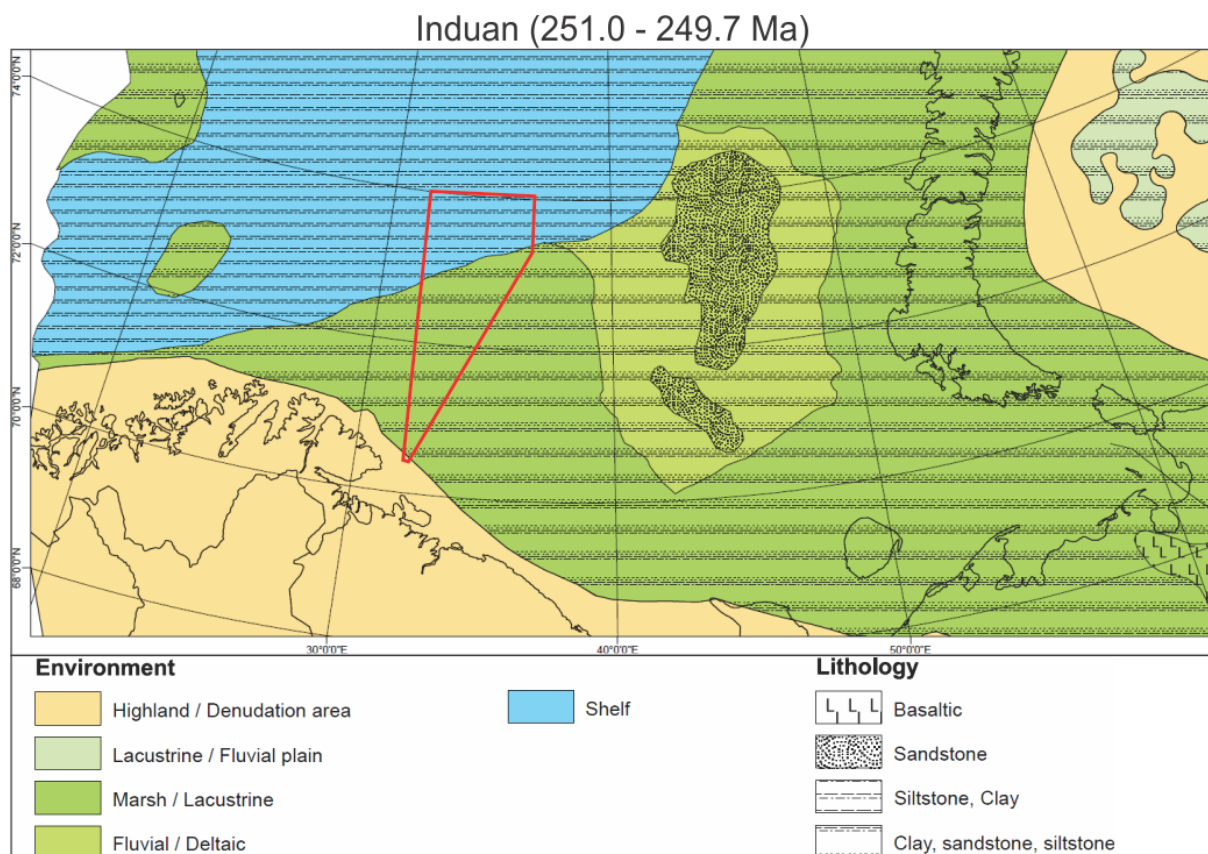
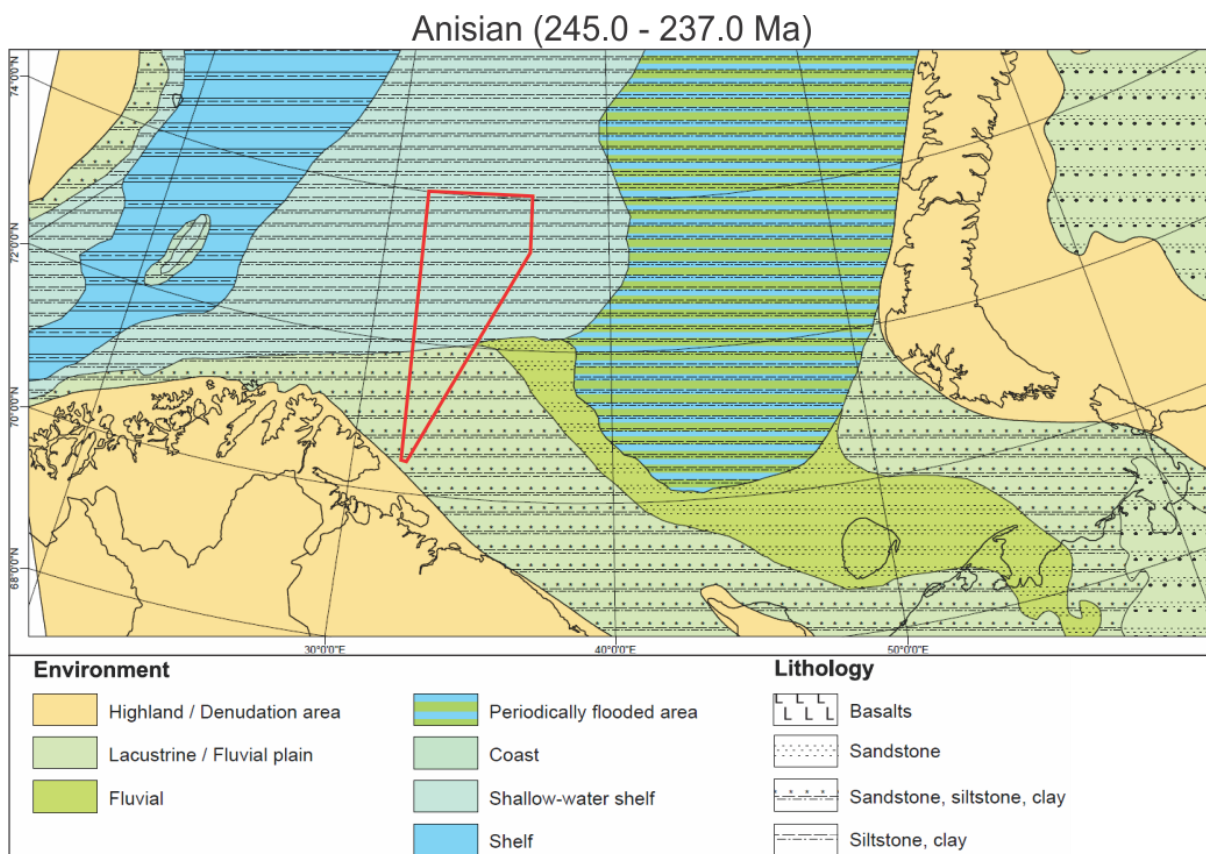


Figure 2.3 Paleogeographic map illustrating the environmental and lithological distribution at the Induan. The study area is located within the red polygon, illustrating that there possibly was a marsh / lacustrine setting in the south of the study area while a shelf setting in the north. Modified from (Smelror et al., 2009)

The transition from Lower to Middle Triassic is characterized by regression, and much of the Lower Triassic shelf in the western Barents Sea became terrestrial landmasses (Smelror et al., 2009; Faleide et al., 2010). The marine shelf was reduced to a central marine basin, bracted by the western margin (Greenland), Fennoscandian Shield in the south and a coastal setting in the east, possibly having a marine connection in the southwest (Figure 2.4) (Smelror et al., 2009). The eastern shore of the central marine basin, had much of the same sedimentary supply as in the Lower Triassic, with the Fennoscandian Shield and Ural in the south and east (Smelror et al., 2009; Evy Glørstad-Clark et al., 2010; Lundschieen et al., 2014). In the east Barents Sea shelf a combination of lacustrine and floodplain settings dominated during the Middle Triassic, represented in the stratigraphy by non-marine clayey siltstones of the Anguranskaya Formation (Smelror et al., 2009).



*Figure 2.4 Paleogeographic map illustrating the environmental and lithological distribution at the Anisian. The study area is located within the red polygon, illustrating that there possibly was a lacustrine / fluvial plain setting in the south of the study area while a shallow-water shelf setting in the north. Modified from (Smelror et al., 2009)*

Sedimentation rates decreased gradually into the Late Triassic, reducing to only 5% of that in the Lower Triassic (Worsley, 2008). The regressive trend of the early Middle Triassic continued into the Late Triassic, transforming the central marine basin in the west into a shallow-water shelf and a coastal plain in the east (Figure 2.5) (Smelror et al., 2009; Lundschieen et al., 2014; Klausen et al., 2015). During the early Norian to late Rhaethian/early Hettangian a succession of fine-grained distal marine shales to coastal sands and terrestrial coals were deposited in the Troms I area and the Hammerfest basin (Dalland et al., 1988; Dallmann, 1999, p. 182; Henriksen et al., 2011). These deposits are the oldest formation of the Realgrunnen Subgroup and are known as the Fruholmen Formation, reflecting a northward fluviodeltaic progradation (Dalland et al., 1988; Dallmann, 1999; Henriksen et al., 2011; Ryseth, 2014).



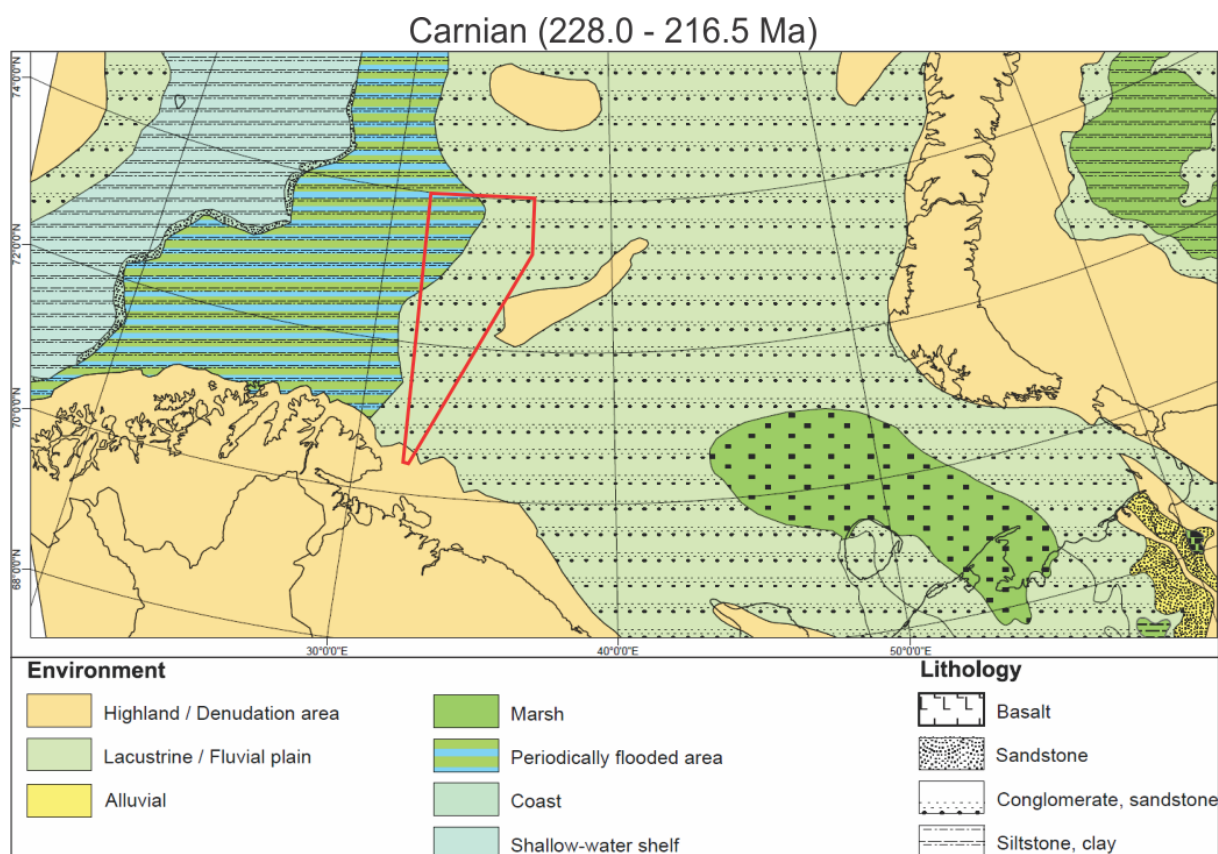


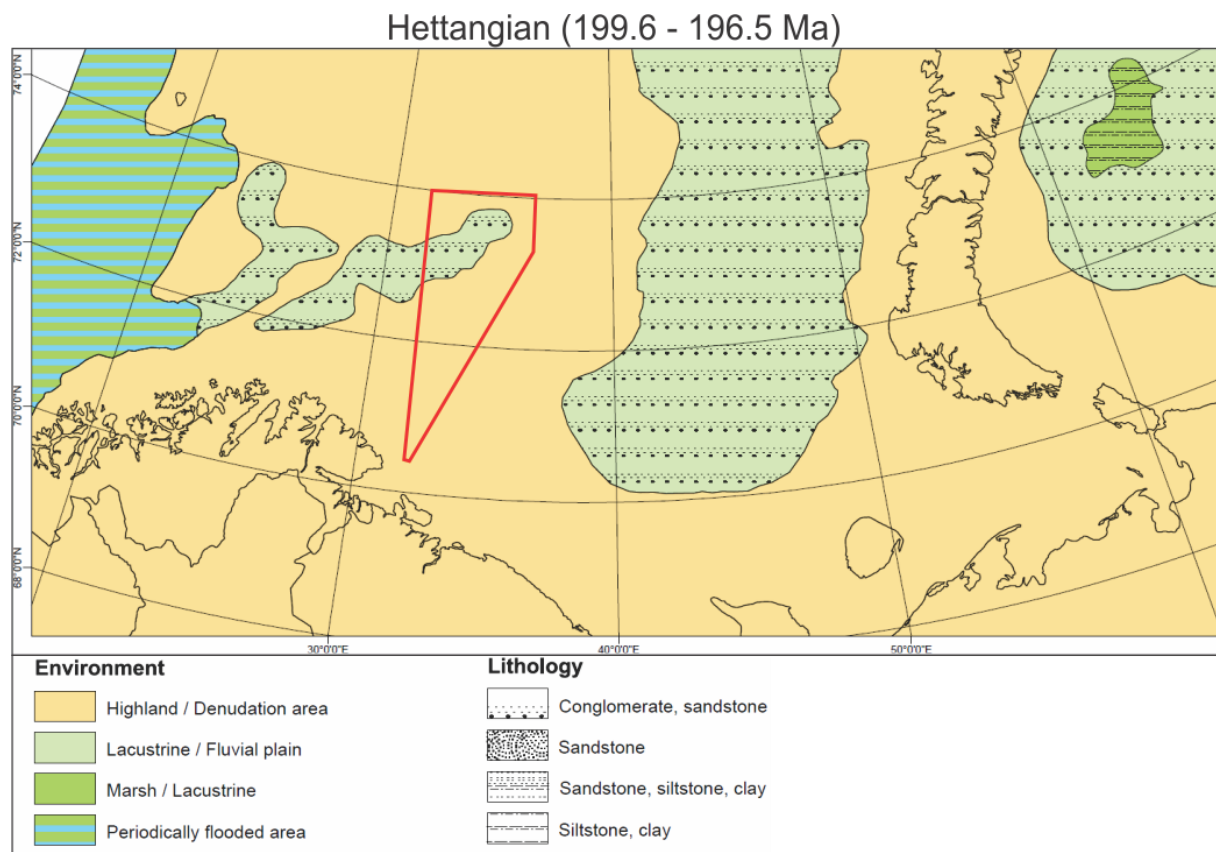
Figure 2.5 Paleogeographic map illustrating the environmental and lithological distribution at the Carnian. The study area is located within the red polygon, illustrating that there possibly was a lacustrine / fluvial plain setting in the east of the study area while a periodically flooded area in the west. Modified from (Smelror et al., 2009).

### 2.2.1.2 Jurassic

In the transition from the Late Triassic to the Early Jurassic an episode of regional uplift and regression occurred, resulting in wide continental lowlands comprised of the Loppa High, Franz Josef Land, Svalbard and Timan-Pechora area (Smelror et al., 2009; Henriksen et al., 2011). The regression maximum is assumed to have been reached during the Hettangian to Sinemurian (Figure 2.6) (Henriksen et al., 2011; Ryseth, 2014). A change from arid to humid climatic condition accompanied this uplift, increasing clastic transportation and deposition onto the Barents Sea shelf (E. Glørstad-Clark et al., 2011; Ryseth, 2014). Present day deposits are most frequently found in the Hammerfest, Nordkapp and Tromsø Basins, represented in the stratigraphy as a sandy sequence known as the Tubåen Formation. Which at the time (Rhaetian to Sinemurian) was primarily deposited in lagoons, tidal inlets and estuaries (Smelror et al., 2009; Henriksen et al., 2011; Ryseth, 2014).



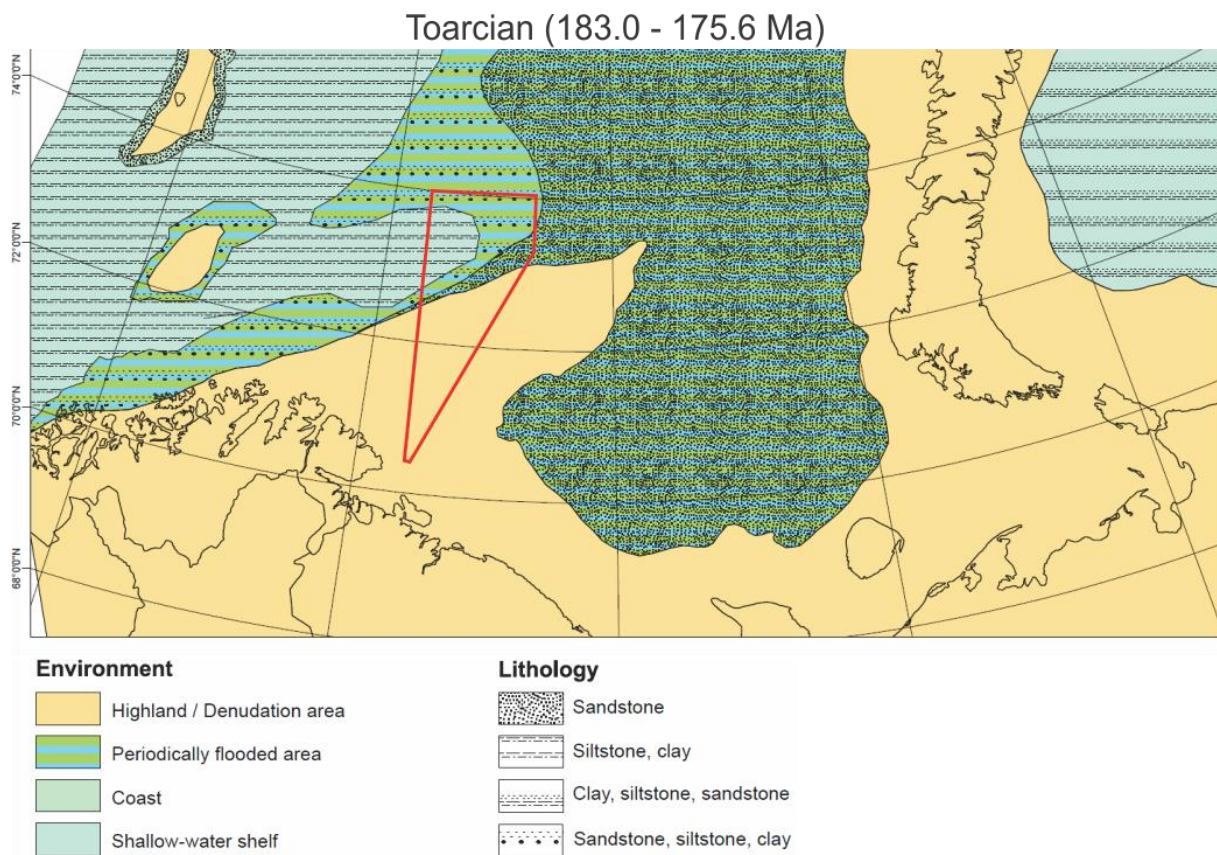
Overlying the Tubåen Formation lies the Sinemurian to late Pliensbachian Nordmela Formation. The Nordmela Formation is documented to primarily consist of sandstone with a tidal origin (on the Bjarmeland Platform) (Henriksen et al., 2011). Its lower boundary (Sinemurian to late Pliensbachian) is indicated by a rapid transition into floodplain and tidal flat deposits lower component (siltstones), followed by an upper fine-grained sandy component (Dalland et al., 1988; Dallmann, 1999, p. 184; Ryseth, 2014).



*Figure 2.6 Paleogeographic map illustrating the environmental and lithological distribution at the Hettangian. The study area is located within the red polygon, illustrating that a highland / denudation environmental setting probably covered most of the study area. A small lacustrine / fluvial plain setting most likely existed within the Nordkapp basin. Modified from (Smelror et al., 2009).*

In the Early Jurassic – Middle Jurassic (Toarcian), a regional transgression of the Barents Sea transpired (Figure 2.7 and 2.8) (Smelror et al., 2009; Henriksen et al., 2011). Giving rise to a shallow-marine environment covering most of the western Barents Sea, while the eastern Barents Sea became a periodically flooded area (Smelror et al., 2009). A Middle Jurassic uplift and regression phase occurred, reaching its maximum in the Bajocian age (Figure 2.8) (Dallmann, 1999, p. 184; Smelror et al., 2009; Henriksen et al., 2011). This restricted marine environments to only the deepest basins within the Barents Sea, with a possible seaway connecting the east and west Barents Sea through the Hammerfest and Nordkapp basins

(Figure 2.8) (Smelror et al., 2009). The deposits of both the transgression and the following regression are poorly preserved in much of the Barents Sea region. The transgressive deposits can be found in the Hammerfest, Nordkapp and Bjørnøya basins and on the Bjarmeland Platform (Dallmann, 1999, p. 184; Smelror et al., 2009). While deposits of the regressive stage are only preserved in basins that did not experience erosion, such as the Hammerfest and Nordkapp basins (Smelror et al., 2009). Deposits from this Middle Jurassic epoch are today known as the Stø Formation, represented as stacked shoreface deposits, with a sandy to silty composition (Dallmann, 1999, p. 184; Smelror et al., 2009).



*Figure 2.7 Paleogeographic map illustrating the environmental and lithological distribution at the Toarcian. The study area is located within the red polygon, illustrating that there possibly were a highland / denudation environmental setting in the south of the study area. The northeast were possibly characterized by a periodically flooded area, while the northwest were a shallow-water shelf. Modified from (Smelror et al., 2009).*

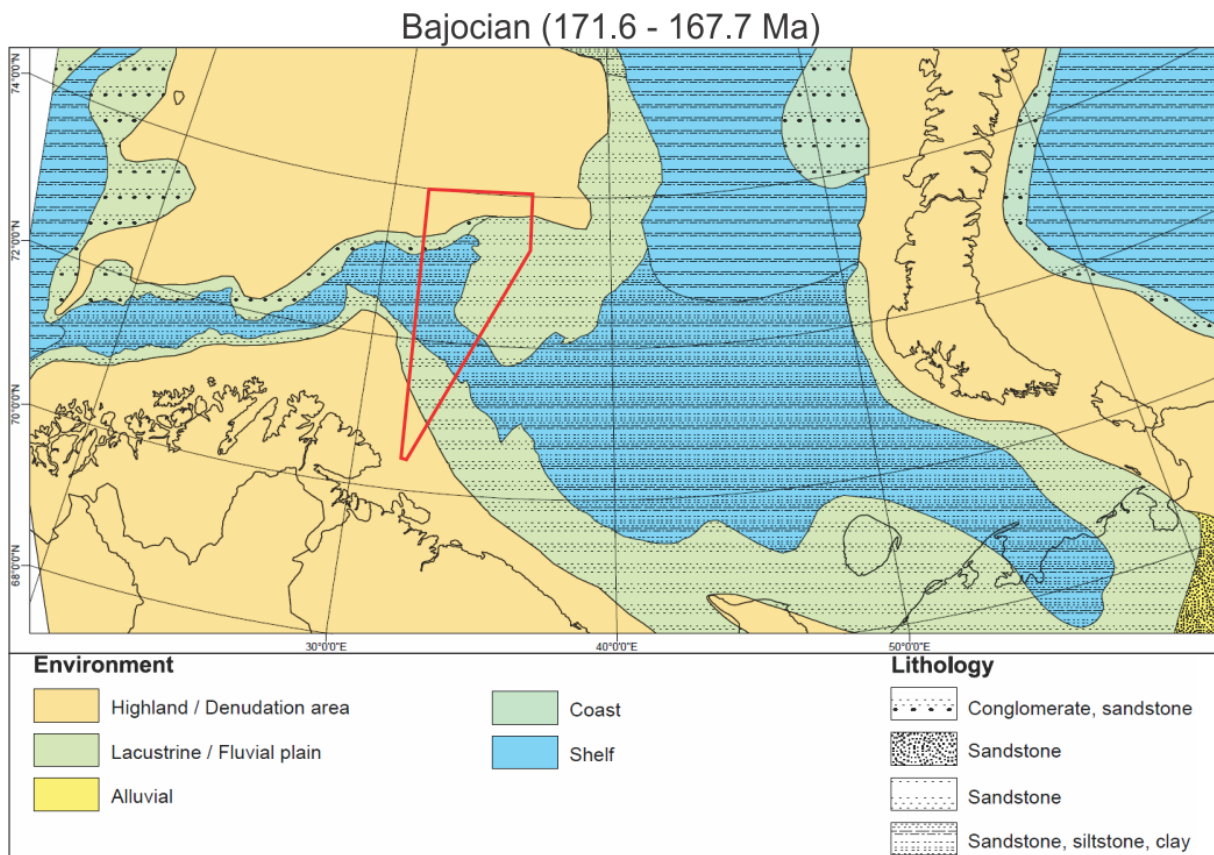


Figure 2.8 Paleogeographic map illustrating the environmental and lithological distribution at the Bajocian. The study area is located within the red polygon, illustrating that the north and south of the study area were possibly a highland / denudation area. The middle part illustrates the basin restricted marine connection of the east and west, being a lacustrine / fluvial plain to a shelf in the middle. Modified from (Smelror et al., 2009).

In the Late Jurassic, a transgression occurred reaching its maximum in the Tithonian (Figure 2.9) (Smelror et al., 2009; Klausen et al., 2019), at which point most of the Barents Sea shelf was submerged, with water depth of up to 200-300 m (Smelror et al., 2009). During this time predominantly shale and mudstone were deposited in the distal coastal areas, at a suspected low sedimentation rate (Worsley, 2008; Smelror et al., 2009; Henriksen et al., 2011). During the first part of the transgression (late Callovian to Oxfordian) pyritic mudstone, shale and limestone were primarily deposited, known as the Fuglen Formation (Dalland et al., 1988; Klausen et al., 2019). In the second half of the transgression anoxic water-bottom conditions and high organic productivity, lead to the deposition and preservation of shale with a high organic content (Smelror et al., 2009; Henriksen et al., 2011). In the western Barents Sea these high organic shales are represented by the Hekkingen Formation, being one of the most important source rock in the Barents as well as in the Norwegian Sea and the North Sea (Smelror et al., 2009; Henriksen et al., 2011).



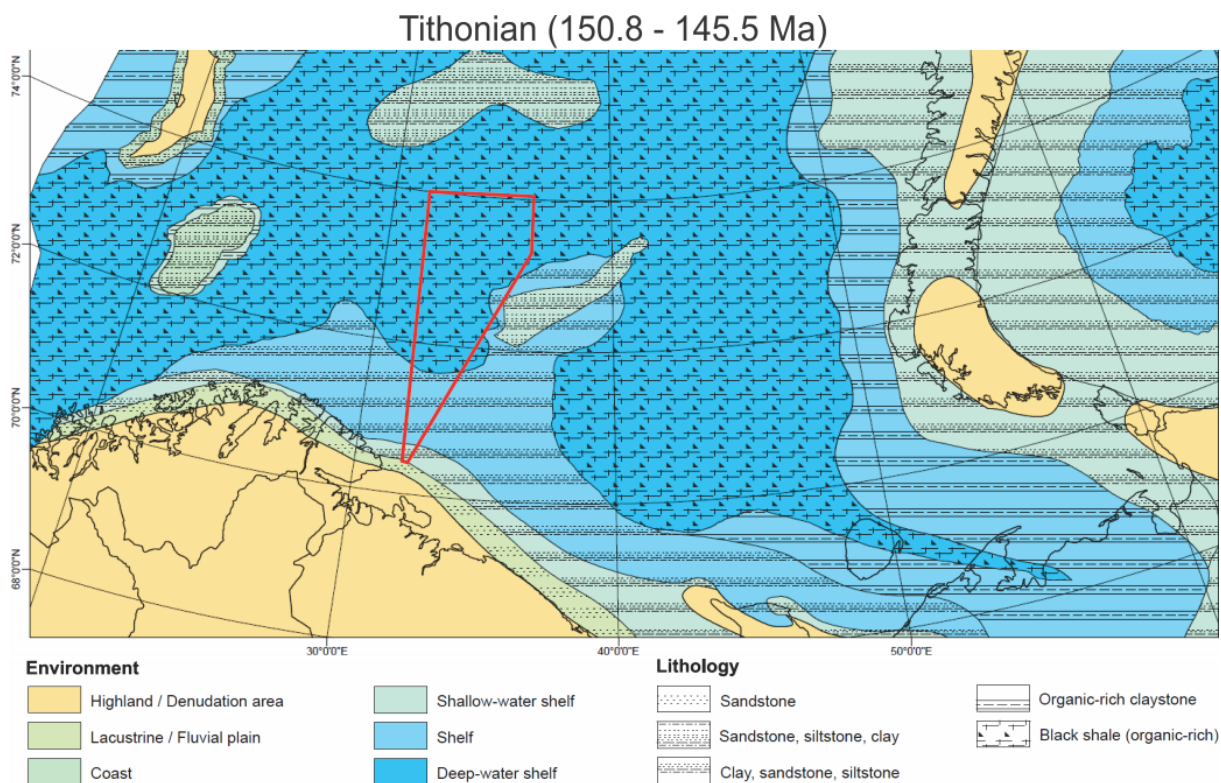


Figure 2.9 Paleogeographic map illustrating the environmental and lithological distribution at the Tithonian, with this illustrating the transgressional maximum. The study area is located within the red polygon, illustrating the possible transition from a lacustrine / fluvial plain setting, followed by a shallow-water shelf, shelf and deep-water shelf form south to north within the study area. Modified from (Smelror et al., 2009).

### 2.2.1.3 Cretaceous

The Late Jurassic to the Early Cretaceous is characterized by a major change in depositional environment (Worsley, 2008). A regional uplift of the north Barents shelf was caused by the HALIP (Section 2.1.3), shifting the coastline south and altering the deep-marine circulation pattern of the western Barents Sea (Worsley, 2008; Smelror et al., 2009; Faleide et al., 2010). This changed the anoxic environment of the Late Jurassic into a circulated oxygenated deep-sea environment in the Early Cretaceous (Worsley, 2008; Faleide et al., 2010). Reducing the preservation of organic material, while establishing a southward progradation of terrestrial sediments (Faleide et al., 2008; Smelror et al., 2009; Faleide et al., 2010). This alteration is the reason the basinal deposits of the Early Cretaceous mainly consist of shale, while some carbonates were deposited on platform areas (Worsley, 2008). During the Cretaceous some intrabasinal highs were exposed due to uplift, with the Fedynsky High being the most relevant example for this study (Figure 2.10) (Klausen et al., 2017a). The Jurassic and Triassic succession is absent on parts of the Fedynsky high, following the uplift and subsequent erosion (Klausen et al., 2017a).

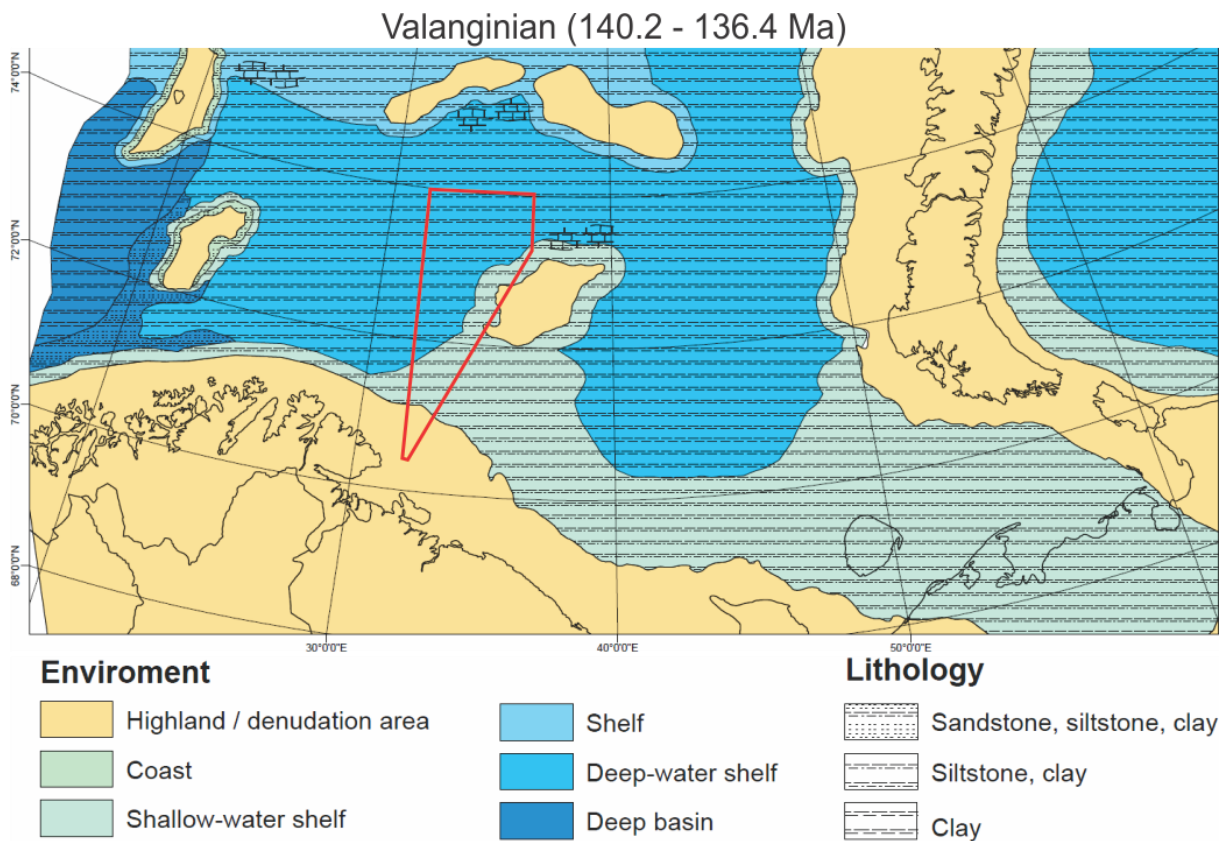


Figure 2.10 Paleogeographic map illustrating the environmental and lithological distribution at the Valanginian, with this illustrating the uplift of the Fedynsky High. The study area is located within the red polygon, illustrating the possible transition from a highland / denudation area in the south and on the Fedynsky High in the east. In the west and northwest a possible deep-water shelf existed, with a shallow-water shelf stretching between the Fedynsky High and the highland / denudation area in the south. Modified from (Smelror et al., 2009).

## **2.3 Stratigraphic units**

### **2.3.1 Realgrunnen Subgroup**

The Realgrunnen Subgroup was deposited during the late Norian to Bajocian. The subgroup is comprised of the offshore to deltaic deposits of the Fruholmen (Norian-Rhaetian), Tubåen (Rhaetian-Sinemurian), Nordmela (Sinemurian-Pliensbachian) and Stø (Pliensbachian-Bajocian) formations (Müller et al., 2019). The Fruholmen and Tubåen formations were deposited in a regressive regime, while the Nordmela and Stø formations were deposited in a transgressive regime. The primary component of the subgroup are mature sandstones, with the Fruholmen Formation having a higher proportion of fine-grained immature deposits (Dallmann, 1999, p. 133; Henriksen et al., 2011; Mulrooney et al., 2018; Müller et al., 2019).

### **2.3.2 Snadd Formation**

The Snadd Formation was deposited during the late Ladinian to early Norian (Dalland et al., 1988; Dallmann, 1999, p. 168; Ryseth, 2014; Klausen et al., 2015). It is geographically widespread, with a substantial unit thickness of non-marine deltaic deposits (Ryseth, 2014; Klausen et al., 2015). The formation consists primarily of mature sands, deposited in a river setting, in combination with some terrestrial organic content (coal) and mud (Ryseth, 2014; Klausen et al., 2015). The transition from the Snadd Formation into the overlying Fruholmen Formation (Base Realgrunnen Subgroup) is marked by a regional flooding surface of organic mudrock (Ryseth, 2014; Klausen et al., 2015; Klausen et al., 2019; Müller et al., 2019).

### **2.3.3 Stø Formation**

The Stø Formation is comprised of highly reworked, shallow marine sandstone deposits of the Pliensbachian to Bajocian, being the youngest formation within the Realgrunnen Subgroup (Henriksen et al., 2011; Klausen et al., 2017b; Nygaard et al., 2017). The formation is relatively condensed and eroded, covering an area of more than 180 000 square km (Klausen et al., 2017b). The top of the Stø Formation is represented by a middle Bathonian flooding surface (Klausen et al., 2019; Müller et al., 2019).

### **2.3.4 Fuglen Formation**

The Fuglen Formation was deposited during the Callovian to Oxfordian, as an offshore marine, pyritic mud-, shale- and lime-stone (Dalland et al., 1988; Dallmann, 1999, p. 136; Klausen et al., 2019). It is documented at the Haapet Dome at well 7435/12-1 as a 38m thick unit (NPD, 2019).

### 2.3.5 Hekkingen Formation

The Hekkingen Formation is a deep marine, highly organic shale, deposited during the upper Oxfordian –Tithonian (Henriksen et al., 2011; Halland et al., 2014). Its primary composition is shale and mudstone, deposited on a regional extent in anoxic conditions (Dallmann, 1999, p. 136; Henriksen et al., 2011). Gamma ray readings from well 7435/12-1 at the Haapet Dome reflect the elevated organic content of the formation (NPD, 2019).

### 2.4 Structural elements

This section will give a short introduction to each of the elements located within the study area illustrated in Figure 2.11, starting at the platforms in the area, followed by the basins, domes and highs.

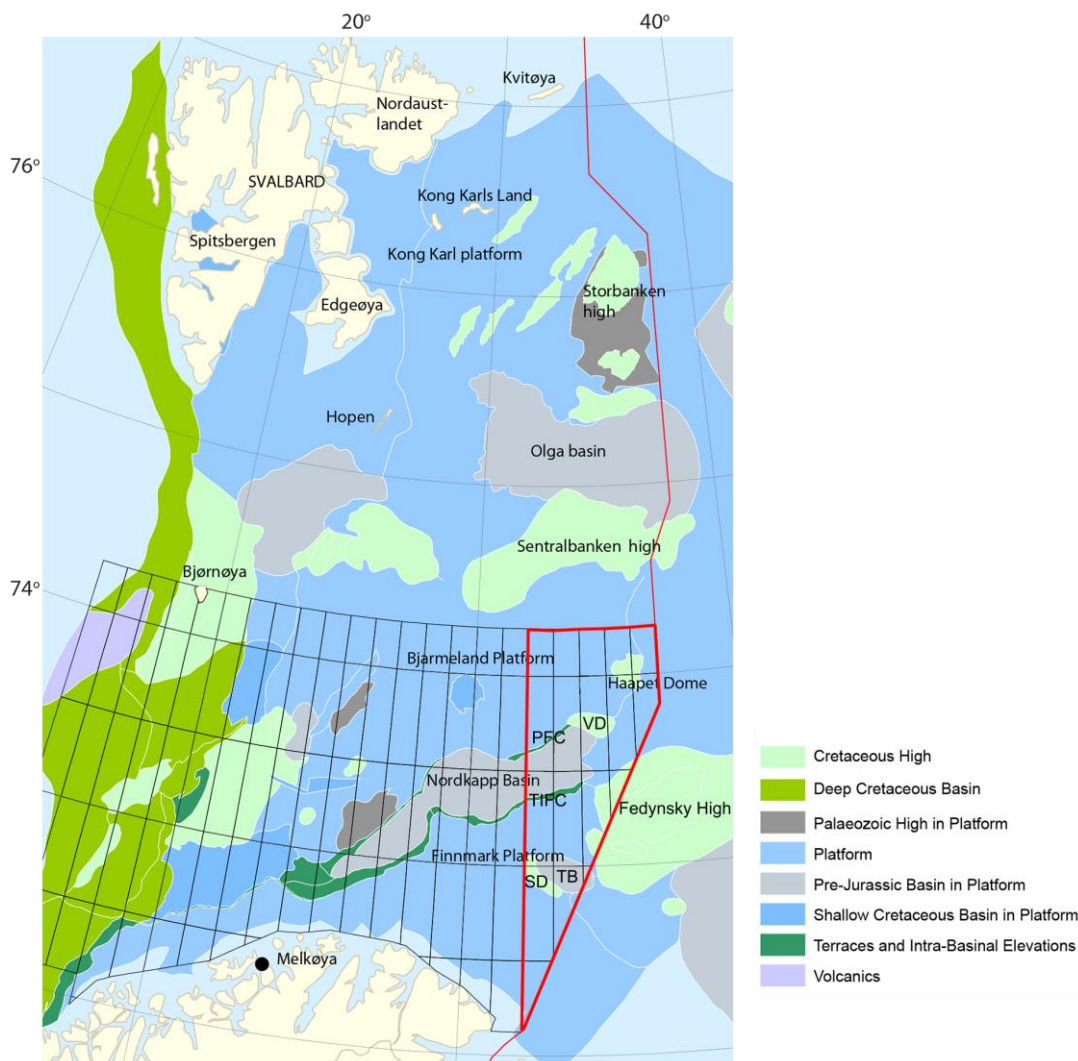


Figure 2.11 Map of the structural elements within the BSSE (red polygon) and the north Barents Sea. SD=Signalhorn Dome, VD=Veslekari Dome, TB=Tiddlybanken Basin, TIFC=Tor-Iversen Fault Complex, PFC=Polarstjerna Fault Complex. Modified from (NPD, 2017)

### **2.4.1 Bjarmeland Platform**

The Bjarmeland Platform is one of the main structural elements within the study area and the Norwegian Barents Sea (Figure 2.11). It stretches from the Sentralbanken and Gardarbanken highs in the north, to the Hammerfest and Nordkapp basins in the south and southeast respectively, terminating at the Fingerdjupet Subbasin and the Loppa High in the west (Gabrielsen et al., 1990; Larssen et al., 2002). The transition of the structural element into a platform is believed to have occurred in the Late Carboniferous to Permian period, based on the transition from Carboniferous clastics to Permian carbonates (Gabrielsen et al., 1990; Larssen et al., 2002). A following stable configuration of the structural elements is believed to have prevailed since the Late Paleozoic (Gabrielsen et al., 1990).

### **2.4.2 Finnmark Platform**

The Finnmark Platform is located in the southern part of the study area (Figure 2.11). It is bounded by the Norwegian mainland in the south and the Hammerfest and Nordkapp basins to the north. Its western border is a south-western extension of the Ringvassøy-Loppa Fault Complex, while in the east it is delineated by the Tiddlybanken Basin (Gabrielsen et al., 1990; Larssen et al., 2002; Halland et al., 2014). It shows much of the same features as the Bjarmeland platform as to pre-platform to platform development, with Early Carboniferous clastics transitioning into Late Carboniferous to Permian carbonates (Gabrielsen et al., 1990; Larssen et al., 2002). Structurally the platform shows a gentle northward tilt, with younger to older strata sub cropping the Quaternary base in chronological order from north to south (Gabrielsen et al., 1990). Tectonically the platform has been mostly stable since the Late Paleozoic, with the northward tilt being the primary result of Ceneozoic tectonism and uplift (Gabrielsen et al., 1990; Larssen et al., 2002; Halland et al., 2014).

### **2.4.3 Nordkapp Basin**

The last major structural element of the study area is the more than 300 km long and 30-80 km wide Nordkapp Basin (Figure 2.11). Located north of the Finnmark Platform and southwest of the Bjarmeland Platform (Gabrielsen et al., 1990; Bugge et al., 2002; Halland et al., 2014). It has a WSW-ENE orientation, and its margins are defined by the Måsøy, Nysleppen, Polarstjernen and Thor Iversen Fault complexes (Gabrielsen et al., 1990; Bugge et al., 2002; Halland et al., 2014; Gernigon et al., 2018). The basin is of Paleozoic age, presumably Late Devonian to Early Carboniferous, as the result of crustal extension between Greenland and Norway (Gabrielsen et al., 1990; Koyi et al., 1995; Bugge et al., 2002; Larssen



et al., 2002). Following the rifting, a large sequence of Late Carboniferous evaporites were deposited, subsequently being overlain by clastic sediments (Gabrielsen et al., 1990; Koyi et al., 1995; Larssen et al., 2002; Hassaan et al., 2020). Sedimentary loading in combination with faulting in the Lower Triassic possibly resulted in the first formation of salt pillows as well as rollover structures within the basin (Bugge et al., 2002; Larssen et al., 2002; Faleide et al., 2010; Gernigon et al., 2018). This is assumed due to the geometry of the wedge and rim synclines, as well as salt piercing its overburden in late Lower Triassic (Gabrielsen et al., 1990; Gernigon et al., 2018). Rapid diapirism and subsidence of the Lower to Middle Triassic were followed by a reduction in subsidence from Late Triassic to the Late Jurassic (Gabrielsen et al., 1990; Gernigon et al., 2018). Tectonic events in Late Jurassic, Early Cretaceous and Tertiary times have resulted in episodes of diapiric reactivation, a theory supported by the thinning of Cretaceous sediments draping the diapirs (Gernigon et al., 2018)

#### **2.4.3.1 Polarstjernen Fault Complex**

The Polarstjernen Fault Complex represents the south-eastern termination margin of the Bjarmeland Platform into the Nordkapp Basin (Figure 2.11) (Mattingsdal et al., 2015; Gernigon et al., 2018). It has an overall ENE-WSW orientation, terminating at the Veslekari Dome in the east (Mattingsdal et al., 2015). The fault complex has indications of dip-slip movements, suggesting extensional movements (Mattingsdal et al., 2015). Fault displacement suggest the faults were most active up until the Middle-Triassic (Mattingsdal et al., 2015; Gernigon et al., 2018). In resemblance to that of the Tor-Iversen Fault Complex, fault activity is the result of a combination of extensional forces and salt migration within and along the margins of the Nordkapp Basin (Mattingsdal et al., 2015; Gernigon et al., 2018).

#### **2.4.3.2 Tor-Iversen Fault Complex**

The Tor-Iversen Fault Complex is located at the southeast margin of the Nordkapp Basin, separating the basin from the Finnmark Platform in the southeast (Figure 2.11). It has a WNW-ESE orientation in the westernmost parts, transitioning into an E-W in the centre of the fault complex, followed by a NE-SW orientation in the east (Gabrielsen et al., 1990; Gernigon et al., 2018). The first signs of fault activity are documented at the Early Carboniferous, with reactivation in the Mesozoic and Tertiary (Gabrielsen et al., 1990). This is indicated by the thickness increase of the units deposited at the time, transitioning into the Nordkapp Basin from the Finnmark Platform (Gabrielsen et al., 1990). The initial faulting is the believed effect of Late Paleozoic to Mesozoic extension, with salt migration later reactivating the faults (Gabrielsen et al., 1990).

#### **2.4.4 Tiddlybanken Basin**

The Tiddlybanken Basin is situated south of the Fedynsky High, north on the Finnmark Platform and east of the Signalhorn Dome (Figure 2.11). The basin shares several similarities with the Nordkapp Basin, with both experiencing a suggested Triassic salt mobilization, most likely caused by prograding delta deposits. The diapiric growth has caused a positive relief on the seabed above the Tiddlybanken Basin, in similarity to several diapiric structures within the Nordkapp Basin (NPD, 2013).

#### **2.4.5 Haapet Dome**

The Haapet Dome is located in the east on the Bjarmeland Platform (Figure 2.11) (Mattingsdal et al., 2015; Gernigon et al., 2018). It is a circular shaped dome with an approximate diameter of 40 km at base Cretaceous (Mattingsdal et al., 2015; Gernigon et al., 2018). The dome is the result of an accumulation of salt within a four-way closure. The salt is interpreted to be of Carboniferous to Early Permian age (Mattingsdal et al., 2015). Mattingsdal et al. (2015) suggest the doming possibly occurred as early as the Lower-Cretaceous, with a most likely activation in the Paleogene.

#### **2.4.6 Veslekari Dome**

The Veslekari Dome is 50 km long and 25 km wide (base Cretaceous) dome, located in the easternmost margin of the Nordkapp Basin (Figure 2.11) (Mattingsdal et al., 2015). The salt responsible for the dome structure is in similarity to the Haapet Dome and Nordkapp Basin salt of Carboniferous to Early Permian age (Mattingsdal et al., 2015). Mattingsdal et al. (2015) suggest a post-Cretaceous doming, as no thinning of the pre-Cenozoic strata is documented.

#### **2.4.7 Signalhorn Dome**

The Signalhorn Dome is an approximately 60 km long and 15 km wide elliptical shaped dome on the north-eastern part of the Finnmark Platform, at the western edge of the Tiddlybanken Basin (Figure 2.11) (Mattingsdal et al., 2015; Gernigon et al., 2018). The structure's core is made up of a salt dome of a pre-Cretaceous age, indicated by the thinning of the Upper Triassic, Jurassic and lowermost Cretaceous (Mattingsdal et al., 2015).

#### **2.4.8 Fedynsky High**

The Fedynsky High is located east of the Nordkapp Basin, east to northeast of the Finnmark Platform, southeast of the Haapet Dome and north of the Tiddlybanken Basin (Figure 2.11). It originally acted as a basin with a later inversion, indicated by the graben structures cutting into the Carboniferous/ Permian strata (NPD, 2013). Extensive erosion has affected the high at several occasions, with the erosional effect reaching the Triassic strata (NPD, 2013; Klausen et al., 2017a).

## 3 Theory

### 3.1 Seismic reflection theory

The basic concept of seismic reflection theory is built upon the generation, propagation and reflection of elastic strain energy, also known as seismic waves. These seismic waves are a combination of compressional waves (P-waves) and shear waves (S-waves), propagating through a medium in a compressional (P-waves) and shearing (S-waves) manner (Sheriff, 2002; Kearey et al., 2013). A key difference to be noted is that P-waves are able to transmit through gas and liquids as well as solids, while S-waves can only transmit through solids. The seismic waves propagate outwards from a source and are generated by natural and artificial sources such as naturally occurring earthquakes and artificial man-made explosions. The main purpose for applying these concepts in a seismic survey is to generate and record reflected seismic waves, in order to establish a better understanding of the depositional and structural configuration in the subsurface. The reflection of wave energy within the sub surface is determined by the properties of the medium through which it travels (Kearey et al., 2013, pp. 22-24).

In order for seismic wave energy to be reflected there has to be a difference in density ( $\rho$ ) and/ or velocity ( $v$ ) at the interface of two mediums through which the wavelet is propagating (Sheriff, 2002; Kearey et al., 2013). The amount of energy that is reflected and transmitted at a given interface is determined by the difference in the acoustic impedance  $Z$ , of the two mediums, with the acoustic impedance  $Z$  being a product of density ( $\rho$ ) and velocity ( $v$ ), shown as:

*Equation 1:*

$$Z = \rho v$$

By comparing the  $Z$  value of medium one ( $M_1$ ) and medium two ( $M_2$ ), it can be determined if there is a difference between the two, and if the interface acts as a reflector. In order to get a better understanding of the relationship between the reflected and transmitted energy at an interface, the reflection coefficient  $R$  has to be calculated. The reflection coefficient  $R$  is a numerical measure between -1 and 1 portraying the effect that an interface has on a propagating wave (Kearey et al., 2013, pp. 28-29). A large difference in acoustic impedance  $Z$  from one layer to the next will result in an  $R$  value close to -1 or 1, while negligible

differences in  $Z_1$  and  $Z_2$  will come close to 0 (Sheriff, 2002; Kearey et al., 2013, pp. 28-29). A transition from a dense (hard) unit to a less dense (soft) unit, will be reflected by a negative reflection coefficient, and vica versa. The reflection coefficient R is calculated with the use of the following equation:

*Equation 2:*

$$R = \frac{\rho_2 v_2 - \rho_1 v_1}{\rho_2 v_2 + \rho_1 v_1} = \frac{Z_2 - Z_1}{Z_2 + Z_1}$$

### 3.1.1 Seismic resolution

Seismic resolution refers to what degree it is possible to differentiate between objects recorded by a seismic survey (Kearey et al., 2013, p. 34). For an object to be recorded it has to have a sufficient acoustic impedance compared with its surroundings, as well as being within the seismic resolution of the survey. In other words, it is the seismic acquisition and later the seismic processing of the acquired data which determines the final resolution (Kearey et al., 2013, p. 27). It is also important to note that seismic resolution has both a vertical and a horizontal aspect to it (Brown, 2004).

The resolution of a seismic survey is always measured in terms of wavelength ( $\lambda$ ) (Brown, 2004). With the wavelength ( $\lambda$ ), being a product of the relationship between velocity ( $v$ ) and frequency ( $f$ ). This can be calculated with the use of the following equation:

*Equation 3:*

$$\lambda = \frac{v}{f}$$

When seismic waves travels through the subsurface, their energy is gradually attenuated by internal frictional losses caused by the oscillation of rock particles (Kearey et al., 2013, pp. 27-28). This means that higher rates of oscillation, results in an faster attenuation rate (Kearey et al., 2013). The rate at which particles oscillate is determined by the frequency of the propagating soundwaves, hence higher frequencies attenuate faster than low frequencies (Kearey et al., 2013, p. 28). This means that lower frequencies have a limited range of

penetration into the subsurface, causing a gradual removal of the lower frequency spectrum with depth (Kearey et al., 2013).

Another aspect of seismic wave propagation is the increase in velocity with depth, which has an effect on the wavelength ( $\lambda$ ) (Brown, 2004; Kearey et al., 2013, pp. 26-28). As sediments and rocks are buried with time they become gradually more compacted, resulting in a higher rock density and velocity (Brown, 2004; Kearey et al., 2013, p. 52). When combining both the attenuation of seismic energy and the increase in velocity with depth it becomes clear that the seismic resolution decreases as a function of depth, as shown by (Figure 3.1) (Brown, 2004).

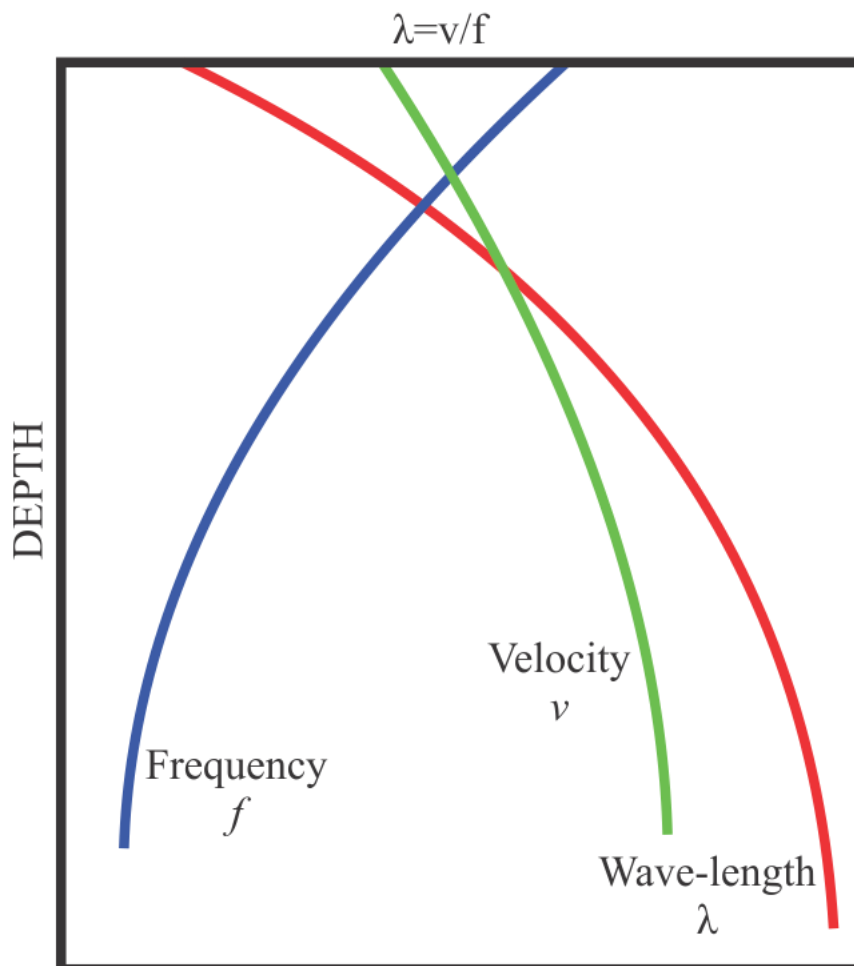


Figure 3.1 Illustration of the relationship between frequency ( $f$ ), velocity ( $v$ ) and wave-length ( $\lambda$ ) with depth. Frequency ( $f$ ) will decrease and wave-length ( $\lambda$ ) and velocity ( $v$ ) will increase with depth, causing a reduction in resolution. Modified from (Brown, 2004)

### 3.1.2 Vertical resolution

The vertical resolution of a seismic dataset is defined as the ability to differentiate between closely spaced individual reflectors (layers and objects) in a seismic section (Kearey et al., 2013, p. 52). The lower limit of vertical resolution is defined as  $\frac{1}{4}$  of the dominate wavelength ( $\frac{1}{2}$  of a period) used in the survey, also known as the limit of separability (*equation 4*) (Brown, 2004; Kearey et al., 2013).

*Equation 4:*

$$\text{limit of separability} = \frac{1}{4} \lambda$$

According to Brown (2004) there are specified two limits when it comes to vertical resolution, being the “limit of separability” and the “limit of visibility” (Figure 3.2). The limit of separability ( $\frac{1}{4}$  of the dominate wavelength) indicates the point at which it becomes impossible to differentiate the upper and lower reflector of a layer. When surpassing the limit of separability, the amplitude will gradually be attenuated by the upper and lower reflected wavelet until reaching the point of visibility (Figure 3.2). Defined as the point at which a layer becomes obscured by the seismic background noise. This usually occurs within the range of  $\frac{1}{8}$  to  $\frac{1}{30}$  of the dominant wavelength, dependent on the data quality and the medium through which the seismic wave travels (Brown, 2004). It is also important to note that the vertical resolution decreases with depth caused by seismic attenuation, and that the vertical resolution may be increased at the data processing stage with the use of deconvolution dependent on the quality of the gathered data (Kearey et al., 2013).

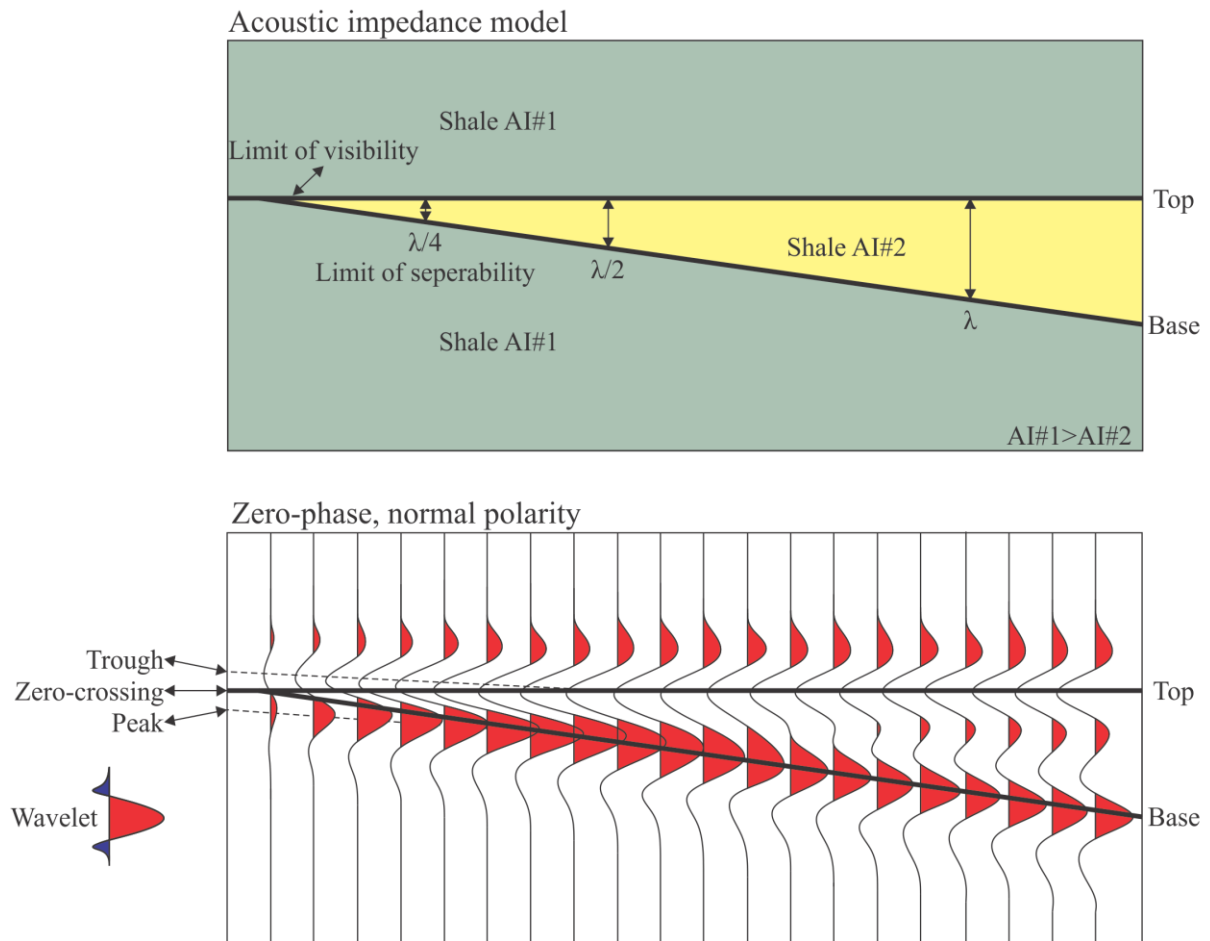


Figure 3.2 Wedge model showing the gradual increase in acoustic interference with decreased separability of the upper and lower reflector. Modified from (Aminzadeh & Dasgupta, 2013)

### 3.1.3 Horizontal resolution

Horizontal resolution is determined by two main factors, being the receiver spacing and the Fresnel zone. The receiver spacing is a rather simple concept, where the horizontal sample rate is  $\frac{1}{2}$  of the receiver spacing. This makes it important to have receivers closely packed in order to get a sufficient sampling rate, especially in areas of diverse/ complex geology (Kearey et al., 2013). The Fresnel zone is more of a complex concept, in need of a more detailed explanation.

When conducting a seismic survey, waves of energy are generated at the surface. These waves prograde in a three-dimensional, spherical manner through the subsurface being reflected at boundaries of sufficient acoustic impedance contrast. When recording these reflections, only those arriving at the receivers within  $\frac{1}{2}$  of the wavelength are desired, as they will have a constructive interference in building the reflection (Sheriff, 2002; Kearey et al., 2013). This interval is commonly known as the Fresnel zone, representing the absolute limit



of horizontal resolution of a seismic survey (Figure 3.3) (Kearey et al., 2013). In other words, gaps along a reflector will not be individually distinguished if they are less than the width of the Fresnel zone (Kearey et al., 2013). In an unmigrated stacked dataset, the radius of the Fresnel zone can be calculated with the use of:

Equation 5:

$$rf = \frac{v}{2} \sqrt{\frac{t}{f}}$$

With,

- $rf$  = Radius of the Fresnel Zone (m)
- $v$  = Seismic velocity of the propagating wave (m/s)
- $t$  = Two-way-travel-time of the recorded wave (s)
- $f$  = Frequency of the seismic wave (Hz)

By looking at this equation we can see that the radius of the Fresnel zone will increase as a function of depth. This is caused by the attenuation of lower frequencies ( $f$ ) with distance travelled, increase in two-way-travel-time (TWT) ( $t$ ) and increase in velocity ( $v$ ) with compaction.

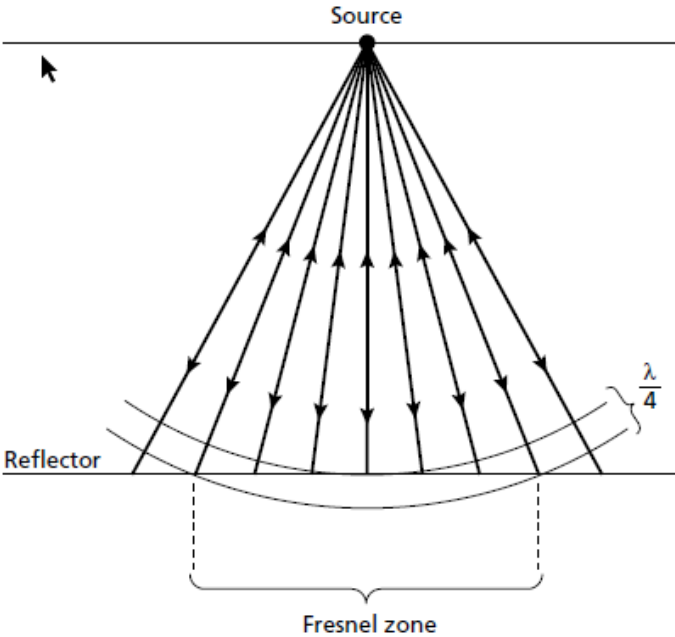


Figure 3.3 The zone at which energy is reflected and returned within half a wavelength is known as the Fresnel zone. Modified from (Kearey et al., 2013)

In order to improve the horizontal resolution of a dataset one main technique is often utilized, known as migration (Brown, 2004; Kearey et al., 2013). This technique is performed in three main steps: the repositioning of out-of-place reflections, focusing of energy within the Fresnel zone and collapsing diffracted energy (Brown, 2004; Kearey et al., 2013). Repositioning of out-of-place reflections is necessary in areas of a dipping reflector, as the reflector will appear gentler than it really is. While focusing of energy and collapsing of diffracted energy will increase the accuracy of amplitudes, by refocusing energy to its actual point of origin (Brown, 2004; Kearey et al., 2013), the degree of migration that is possible to perform on the data is dependent upon if it is 2D or 3D data (Brown, 2004; Kearey et al., 2013). With 3D data energy can be migrated back to its point of origin as it is possible to work in the x, y and z dimension, effectively reducing the Fresnel zone to a single point. In a 2D dataset the energy can only be migrated in the x and y dimension, resulting in scattered energy from the z dimension still present in the migrated data. This results in the Fresnel zone having the shape of an ellipse (Figure 3.4) (Brown, 2004).

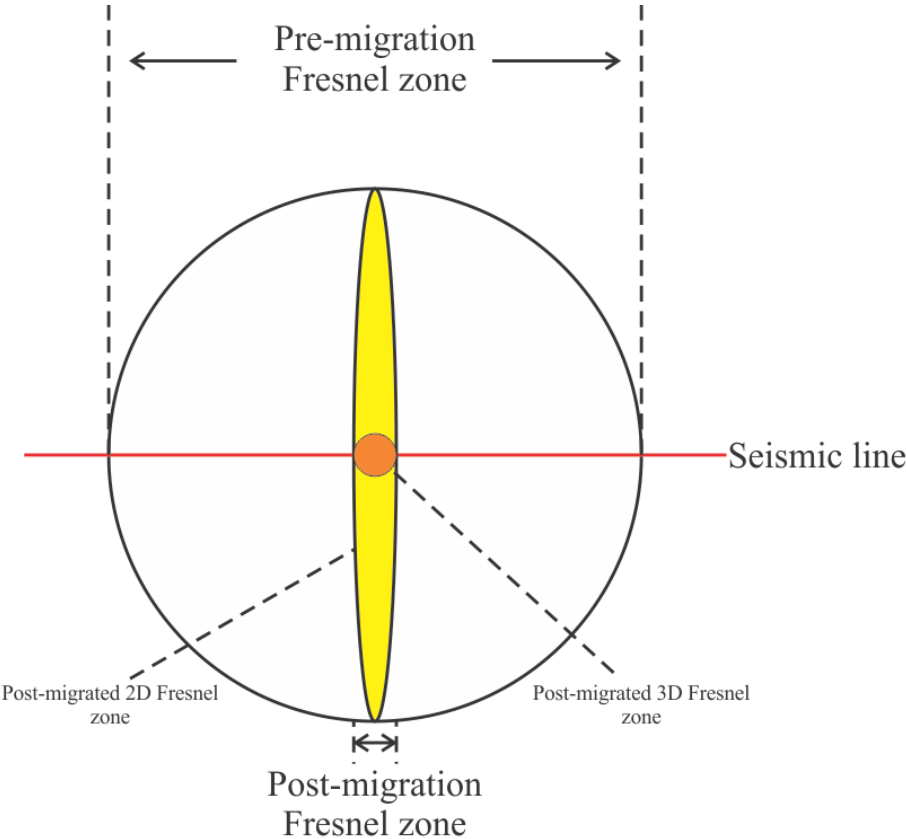


Figure 3.4 Illustration of the effect migration has on the size of the Fresnel zone in 2D and 3D data. Notice that the post-migrated Fresnel zone is focused into a single point while the 2D migrated data is an ellipse. Modified from (Brown, 2004)

## 4 Data and Methods

### 4.1 Data

The seismic 2D datasets applied in this study are NPD-BA-11 and NPD1201, acquired in 2011 and 2012, respectively (Table 1). Exploration well 7435/12-1 (Korpfjell) was drilled by Statoil (now Equinor Energy) AS in 2017, and has been used for stratigraphic correlation of the seismic units. Schlumberger's Petrel 2018 software package has been used for interpreting the seismic data.

The NPD-BA-11 dataset covers the majority of the study area with majority of lines in a primary N-S orientation, and tie-lines running E-W and NE-SW (Figure 4.1). The spacing between lines (grid size) ranges from 3-4 km in the west of the Veslekari Dome and 8-10 km in the east. The overall quality of the N-S and E-W seismic lines are very good in the south of the Nordkapp Basin, with a mediocre quality in the north. The quality of the NE-SW seismic lines are significantly reduced in comparison to the rest of the seismic.

The NPD1201 dataset is primarily located on the Signalhorn Dome, Veslekari Dome, Fedynsky High and Haapet Dome, with some additional lines throughout the study area (Figure 4.1). The primary orientation of the seismic lines is NE-SW on the Veslekari Dome and Tiddlybanken Basin, N-S and NE-SW on the Fedynsky High, N-S and NW-SE on the Haapet Dome (Figure 4.1). The additional lines throughout the study area have an overall E-W orientation, consolidating the N-S orientated seismic lines of the above mentioned NPD-BA-11 (Figure 4.1). The spacing of seismic lines ranges from 4-8 km, except for the E-W orientated lines in the north of the study area, which average 7-16 km. The quality of the data is overall very good, but with the NW-SE oriented seismic lines on the Haapet Dome grading to poor quality. The combination of the two seismic datasets (NPD-BA-11 and NPD1201) significantly reduce the listed line-spacing down to an average of 4-6 km, resulting in a very good data coverage and an overall good to very good quality of the two datasets (Figure 4.1). However, on the Bjarmeland Platform and the south basin of the Tiddlybanken Basin good tie of interpreted units are more complex due to fewer E-W oriented seismic lines. Large distances (400 km) from well 7435/12-1 (Korpfjell) to the southernmost parts of the study area, might cause some uncertainty for the detailed tie of the stratigraphy to these areas.

Table 1 General information on the NPD-BA-11 and NPD-1201 datasets, compiled from NPD factpages.

NPD-BA-11								
Format	Phase	Polarity	Shot by (Contractor)	Shot for (Operator)	Acquisition year	Number of lines	Length (km)	Data quality
SEG-Y	Zero	Normal	PGS	NPD	2011	41	11543	Good
NPD-1201								
SEG-Y	Zero	Normal	Dolphin AS	NPD	2012	57	6766	Very Good

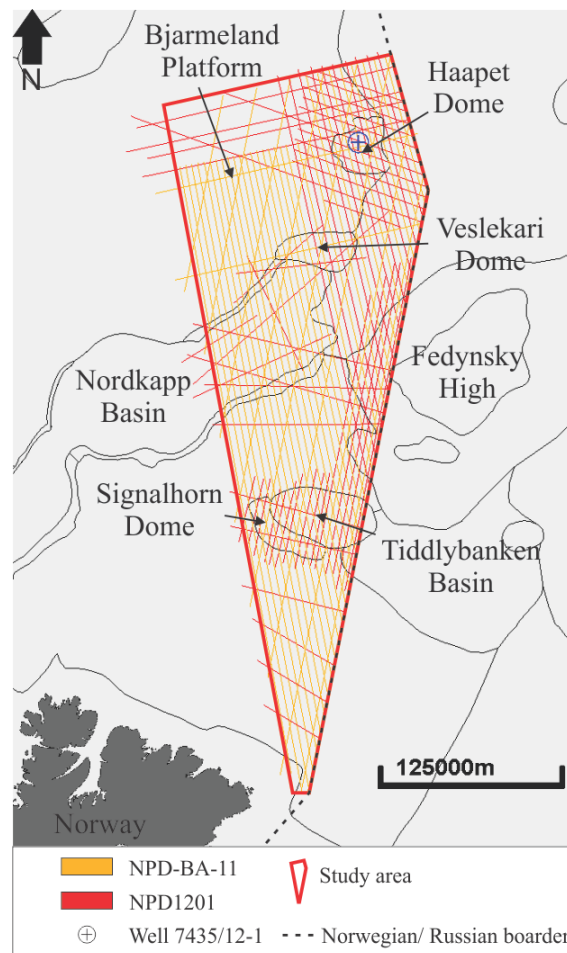
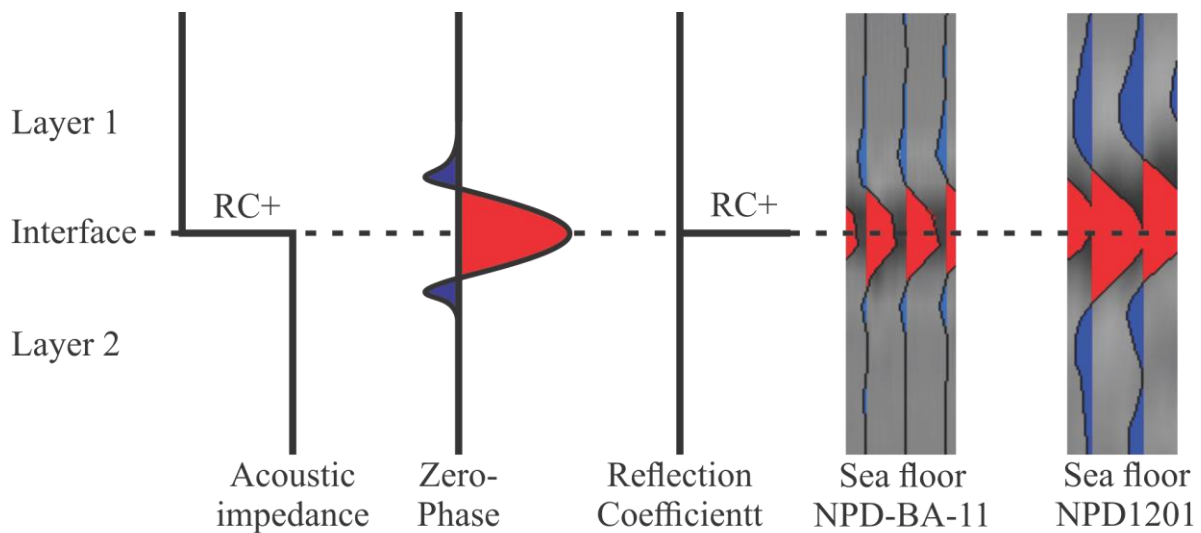


Figure 4.1 Seismic database. NPD-BA-11 (orange lines) and NPD1201 (red lines) datasets, with study area limit (red polygon), reference well 7435/12-1 ("Korpfjell" - blue cross and circle) and Norwegian/ Russian boarder (dotted line) indicated. Structural elements compiled from (NPD, 2019), Norwegian/ Russian boarder compiled from (NPD, 2017).

### 4.1.1 Phase and polarity

According to the Society of Exploration Geophysicists (SEG) the datasets used in this study are regarded as normal polarity, indicated by a peak following a downwards increase in impedance contrast (Figure 4.2) (Bacon et al., 2003). The seismic phase of the data is also determined according to the SEG standard, defining both datasets as zero-phase. This is illustrated in Figure 4.2, where the seafloor for both datasets show a central red peak, with blue troughs on each side.



*Figure 4.2 An illustration of a zero-phase signal at a reflection interface, with corresponding acoustic impedance and reflection coefficient. An example of the seismic response at the sea floor in both the NPD-BA-11 and NPD1201 are illustrated on the right side of the figure.*

### 4.1.2 Vertical and horizontal resolution of 2D data

Well 7435/12-1 (Korpfjell) was used to acquire formation depths in two-way-travel-time and meters, enabling the calculations of the interval velocity of each unit (Table 2). The calculation was performed with the use of the following equation, with the initial values used and results listed in (Table 2) below:

*Equation 6:*

$$v_{unit} = \frac{d_{unit}}{t_{unit}}$$

With,

$v_{unit}$  = Internal velocity of unit x (Velocity (m/s))

$d_{unit}$  = Thickness of unit x (Distance (m))

$t_{unit}$  = One way travel time within unit (Time (s))

The seismic lines of both the NPD-BA-11 and NPD1201 datasets were cropped to a depth of 1800ms (TWT), limiting the frequency spectra to the depth interval for the units. The seismic lines were added to the “frequency spectra” function in Petrel with (Figure 4.3 and 4.4) being the resulting graphs from the NPD-BA-11 and NPD1201 respectively.

Peak-values (frequency value at which the Power (dB) is 0) of each graph were collected and a median value for each dataset were calculated (Table 3). Wavelengths and vertical resolution within each specific unit, of the two datasets were calculated with the use of *equation 3* and *equation 4*, respectively. The horizontal resolutions of the datasets were calculated with the use of *equation 5*, using well 7425/12-1 at the Haapet Dome as a reference for formation depths. Values used/calculated for the vertical and horizontal resolution are listed in (Table 3 and 4).

The vertical resolution of NPD-BA-11 and NPD1201 ranges from 25m to 31m, while unmigrated horizontal resolution ranges from 184m to 292m. It is important to note that calculations were conducted with the use of values extracted from well 7435/12-1 (Figure 4.1, Table 2). The horizon/unit depth and thickness will fluctuate with location, while the velocity is dependent on consolidation of the sediments at said location. The frequency spectrums in Figures 4.3 and 4.4 shows a range, and it should be mentioned that the median frequency applied in Tables 3 and 4 are at the low end of the spectrum. Higher frequencies will give

better resolution. The actual horizontal resolution of the datasets can thus be expected to be better than calculated and presented in Table 4. Both the vertical and horizontal resolution reflect a trend of decreased resolution with an increase in depth (Table 3 and 4).

*Table 2 The table below list the values used for the calculation of the internal velocity of each unit. The depth of the formation tops (in both meters and milliseconds) was taken from the well-tops. Unit thicknesses in (s) and (m) were calculated by subtracting the formation base depth from formation top depth. Unit thickness (m) was then divided by the one-way travel time (s) to acquire the velocity (v).*

Formation/Unit	Depth TWT (ms)	Unit thickness TWT (ms)	Unit thickness (s)	Depth (m)	Unit thickness (m)	Velocity (m/s)
Top Hekkingen Formation	524.06ms			465.49m		
Hekkingen Formation		32.52ms	0.01626s		41m	2521m/s
Top Fuglen Formation	556.58ms			506.49m		
Fuglen Formation		29.44ms	0.01472s		38m	2581m/s
Top Stø Formation	586.02ms			544.49m		
Realgrunnen Subgroup		139.85ms	0.069925s		203m	2903m/s
Top Snadd Formation	725.87ms			747.49m		
Top Snadd - Top Kobbe		233.82ms	0.11691s		388.44m	3322m/s
Top Kobbe (Formation)	959.69ms			1135.93m		

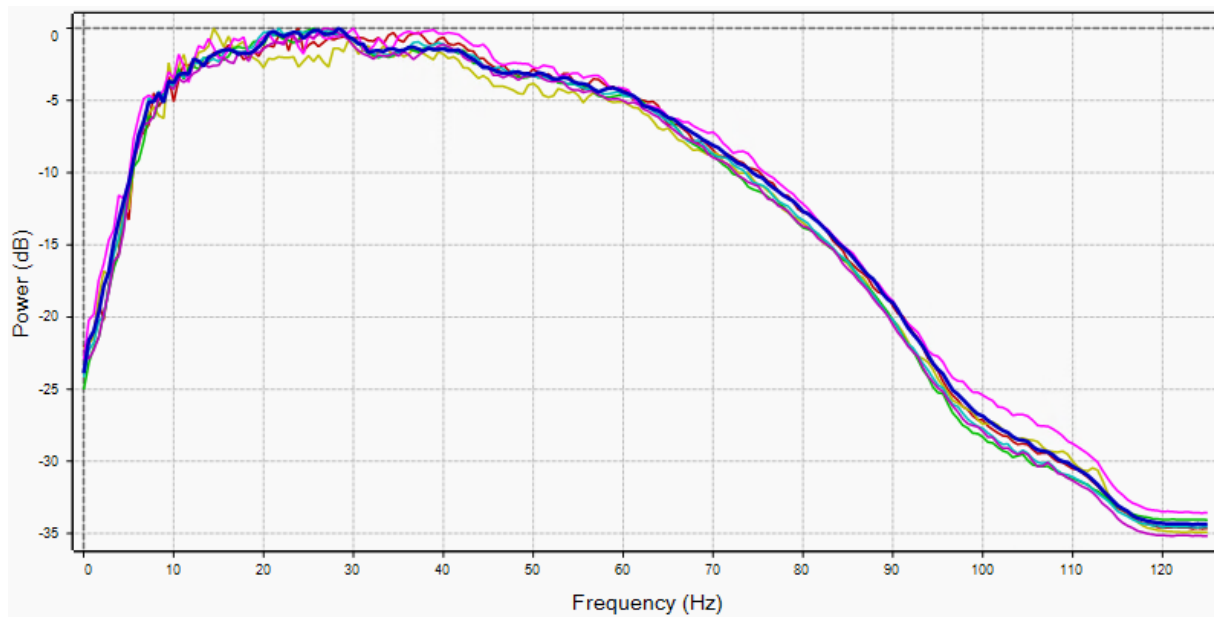


Figure 4.3 “Frequency spectra” of seismic lines from the NPD-BA-11 dataset, within a depth interval from 0ms to 1800ms (TWT). Illustrating the relationship between Frequency (Hz) and Power (dB). The figure does not consist of the entire dataset, but rather a sample range of those used to create figures in the result for this study (Section 5). Each of the colored lines represent one of these seismic lines, with each colored line illustrating the main frequencies of said line. The frequencies were sampled at the point where the line is closes to or touches the dotted horizontal line at 0 dB. The median frequency of the sample group were calculated to be 24.36Hz, giving an adequate representation of the frequency spectra of the NPD-BA-11 dataset. The location of the seismic lines are illustrated in (Figure 5.3 and 5.11).

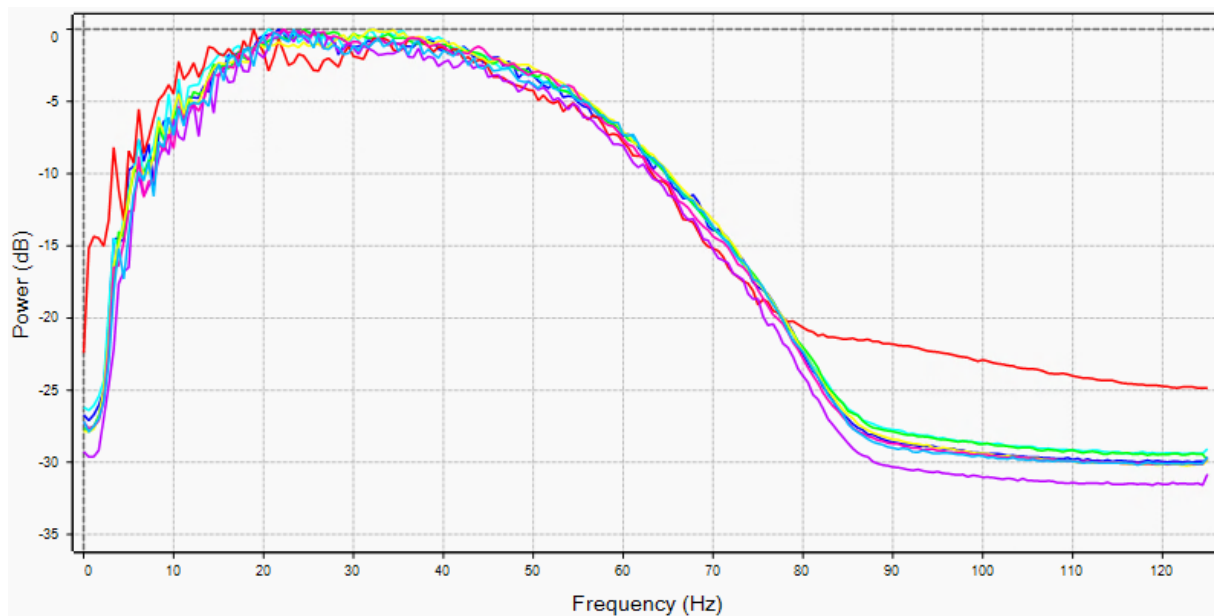


Figure 4.4 “Frequency spectra” of seismic lines from the NPD1201 dataset, within a depth interval from 0ms to 1800ms (TWT). Illustrating the relationship between Frequency (Hz) and Power (dB). The figure does not consist of the entire dataset, but rather a sample range of those used to create figures in the result for this study (Section 5). Each of the colored lines represent one of these seismic lines, with each colored line illustrating the main frequencies of said line. The median frequency of the sample group were calculated to be 23.4Hz, giving an adequate representation of the frequency spectra of the NPD1201 dataset. The location of the seismic lines are illustrated in (Figure 5.3 and 5.11).



Table 3 Median frequency (Hz) and velocity (m/s) were used to calculate the wavelength (m), these were then used to calculate the vertical resolution (m) of each unit in their respective dataset. The top section of the table is the values used/calculated for dataset NPD-BA-11 and the base section is for dataset NPD1201.

<b>NPD-BA-11</b>				
Unit	Median frequency (Hz)	Velocity (m/s)	Wavelength (m)	Vertical resolution (m)
Hekkingen Formation	24.36Hz	2521m/s	103m	26m
Fuglen Formation	24.36Hz	2581m/s	105.95m	26.5m
Realgrunnen Subgroup	24.36Hz	2903m/s	119.17m	30m
<b>NPD-1201</b>				
Hekkingen Formation	23.4Hz	2521m/s	107.73m	27m
Fuglen Formation	23.4Hz	2581m/s	110.30m	27.5m
Realgrunnen Subgroup	23.4Hz	2903m/s	124.05m	31m

Table 4 Median frequency (Hz), velocity (m/s) and depth TWT (s), were used to calculate the horizontal resolution (m) of the NPD-BA-11 and NPD1201 datasets. The horizontal resolution calculated is representative for that of an unmigrated datasets, hence the horizontal resolution of data used in this study is presumably higher than calculated.

<b>NPD-BA-11</b>				
Horizon	Median frequency (Hz)	Velocity (m/s)	Depth TWT (s)	Horizontal resolution unmigrated (m)
Top Hekkingen	24.36Hz	2521m/s	0.52406s	185m
Top Fuglen	24.36Hz	2581m/s	0.55658s	195m
Top Stø	24.36Hz	2903m/s	0.58602s	225m
Top Snadd	24.36Hz	3322m/s	0.72587s	287m
<b>NPD1201</b>				
Top Hekkingen	23.4Hz	2521m/s	0.52406s	189m
Top Fuglen	23.4Hz	2581m/s	0.55658s	199m
Top Realgrunnen	23.4Hz	2903m/s	0.58602s	230m
Top Snadd	23.4Hz	3322m/s	0.72587s	293m

## 4.2 Method

### 4.2.1 Seismic stratigraphy

Seismic stratigraphy according to Vail and Mitchum (1977) is “a geologic approach to the stratigraphic interpretation of seismic data” (Vail & Mitchum, 1977, p. 51). It is used to associate the seismic reflection configuration of seismic units to a specific chronostratigraphic depositional interval (Vail & Mitchum, 1977; Catuneanu et al., 2011). By carrying out a seismic sequence analysis, seismic facies analysis and analysis of relative sea-level changes, paleo-environmental reconstructions can be conducted. The mapping of chronostratigraphic correlation makes it possible to reconstruct the syn- and post-depositional environments (Vail & Mitchum, 1977; Van Wagoner et al., 1987; Catuneanu et al., 2011).

#### 4.2.1.1 Seismic sequence analysis

Seismic sequence analysis involves the identification of genetically related and relatively conformable successions of strata. Such a succession is bounded by its top and base by unconformities and/or their correlative conformities (Mitchum et al., 1977b; Vail & Mitchum, 1977; Van Wagoner et al., 1987; Catuneanu et al., 2011). The seismic sequence boundaries can be identified by the geometrical relationship of the seismic section to its upper and lower unconformities and/or conformities. These geometrical relationships are known as onlap, toplap, downlap and truncations (Figure 4.5) (Mitchum et al., 1977b; Vail & Mitchum, 1977; Veeken, 2007).

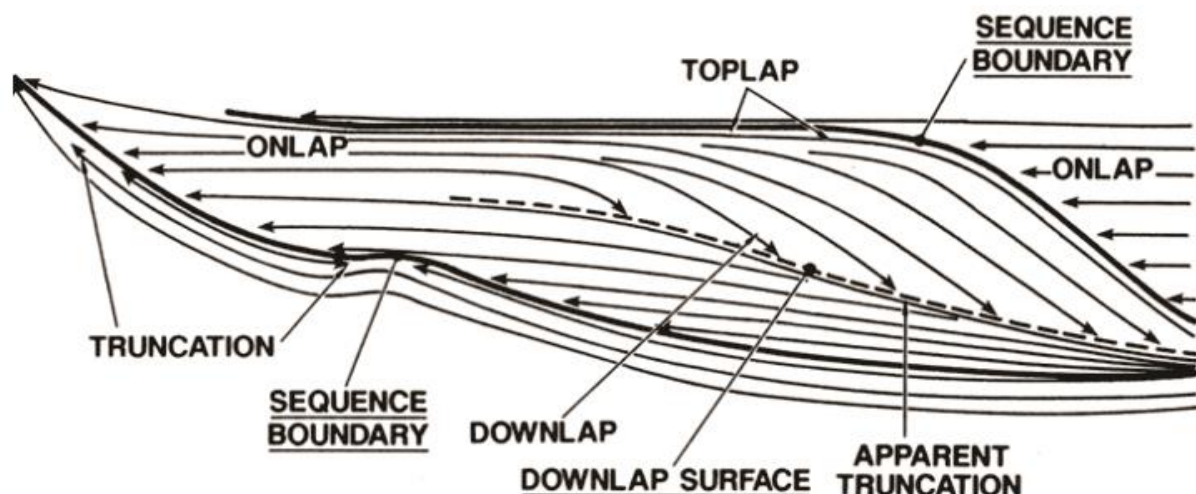


Figure 4.5 Illustration of the internal relationship of units/ sequences in the case of onlap, toplap, downlap and truncations. Modified from (Van Wagoner et al., 1987).

**Onlap, toplap, downlap and truncations**

Onlap occurs where younger sedimentary deposits progressively overlap each other, terminating along an higher incline stratigraphic surface (Mitchum et al., 1977b; Veeken, 2007). Toplap develops where inclined strata terminates towards an upper boundary in a depositional manner (Mitchum et al., 1977b; Veeken, 2007). Downlap occurs when inclined strata terminates into a under laying, inclined or horizontal surface (Mitchum et al., 1977b; Veeken, 2007). The truncation is an erosional feature, at which older sediment terminate toward an erosional surface (Mitchum et al., 1977b; Veeken, 2007).

**4.2.1.2 Seismic facies**

Seismic facies analysis is the process of mapping the reflection amplitude, geometry and continuity, among other parameters (Figure 4.6) (Mitchum et al., 1977a; Mitchum et al., 1977b). This is done in order for the interpreter to make a prediction on the depositional environment, and a potential lithological correlation of the unit (Mitchum et al., 1977a; Mitchum et al., 1977b; Veeken, 2007, p. 113).


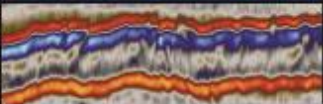



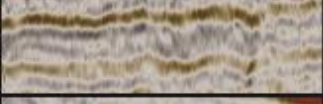




Reflection geometry	Reflection amplitude	Seismic facies (Veeken, 2007)	Seismic facies in this study
Parallel continuous	High amplitude		
Parallel continuous	Medium amplitude		
Parallel continuous	Low amplitude		
Sub-parallel discontinuous	Medium-low amplitude		
Chaotic	Low amplitude		

Figure 4.6 An illustration of reflection geometries and reflection amplitudes from the seismic data utilized in this study, with a comparison from data used in (Veeken, 2007).

## **4.2.2 Seismic attributes**

Seismic attributes are properties extracted from seismic data, which can be used in order to enhance the understanding of the subsurface. In this study used to better visualize the depositional and erosional differences of formations.

### **4.2.2.1 Time-thickness map (Isochore map)**

A time-thickness map is a lateral surface, illustrating the vertical distance between an upper and lower horizon in ms (TWT). The time difference is calculated in Petrel and was in this study utilized to project regional and local thickness variations of the Hekkingen and Fuglen formations and the Realgrunnen Subgroup.

### **4.2.2.2 RMS Amplitude (Root-mean-square)**

An attribute which calculates the root-mean-square of squared amplitudes, divided by a user specified sample size (Chopra & Marfurt, 2008). It is useful in visualizing variations in amplitude, within seismic volumes and along seismic horizons. As for this study it is used in the visualization of amplitude variations on the Fedynsky High.

## 5 Results

This section portrays documentation of interpretations and observations conducted in this study. It gives an overview in chronological order of the horizons and their subsequent units, from the Top Snadd horizon to the Top Hekkingen horizon, illustrated in (Figure 5.1) below.

Horizon	Seismic/ Stratigraphic unit
Top Hekkingen	Hekkingen
Top Fuglen	
Top Stø	Fuglen
Top Snadd	Realgrunnen

Figure 5.1 An overview of the units and their corresponding top and base horizons, with horizons on the left and seismic/ stratigraphic unit on the right.

Seismic interpretation of Top Snadd – Top Hekkingen horizons were conducted, using well 7435/12-1 (Korpfjell) as a reference (Figure 5.2). (Figure 5.3) shows the location and orientation of the regional profiles (Figure 5.4 – 5.10) used to illustrate the regional trend of the horizons and units interpreted in this study. The depth of the seismic profiles and thickness of units used in this study are all given in milliseconds (ms) two-way-travel-time (TWT).



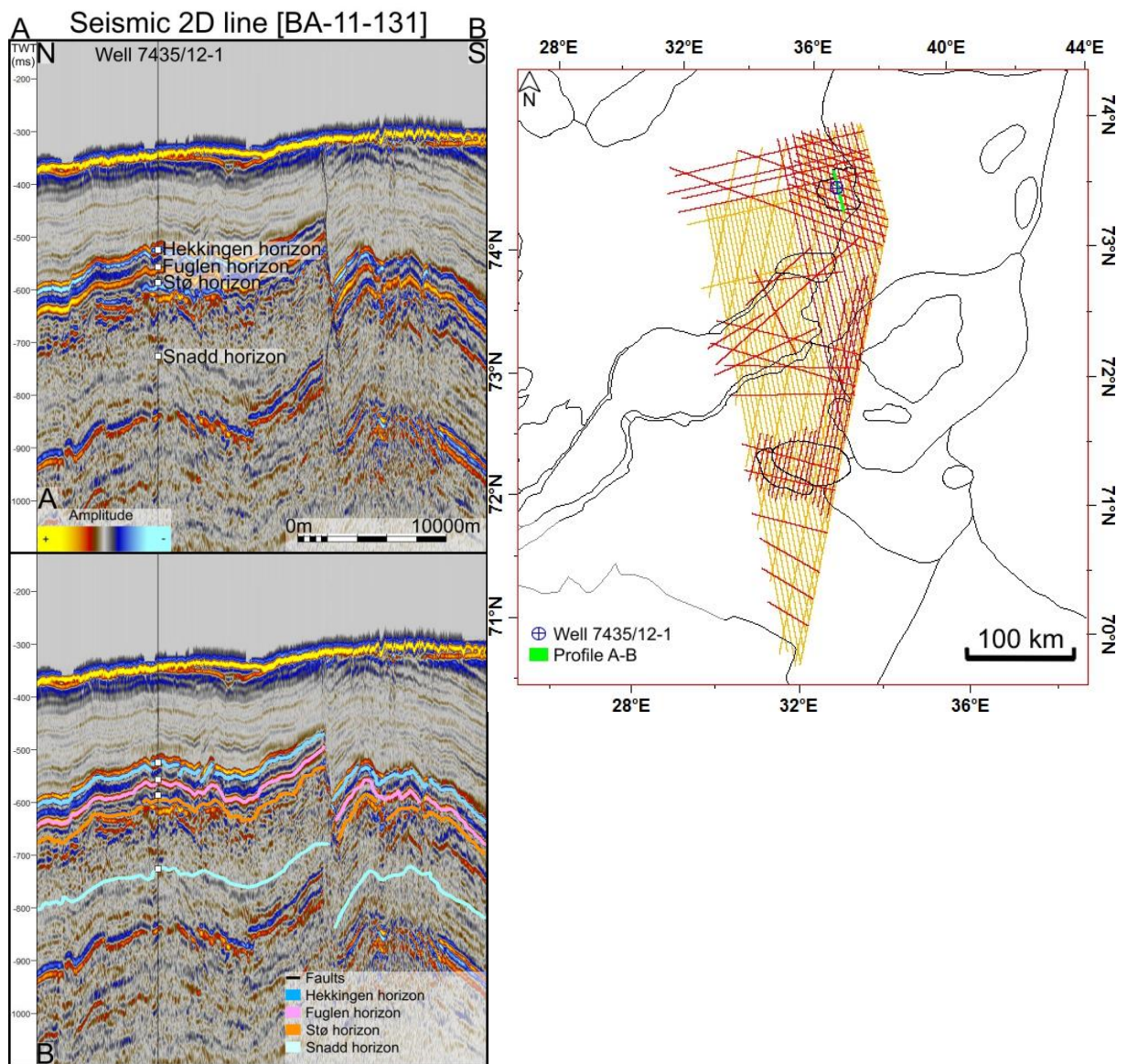


Figure 5.2 Map overview of well location and seismic profile BA-11-131 (right). Seismic profile BA-11-131 (left), illustrating the location of the formation well tops Hekkingen-Snadd.

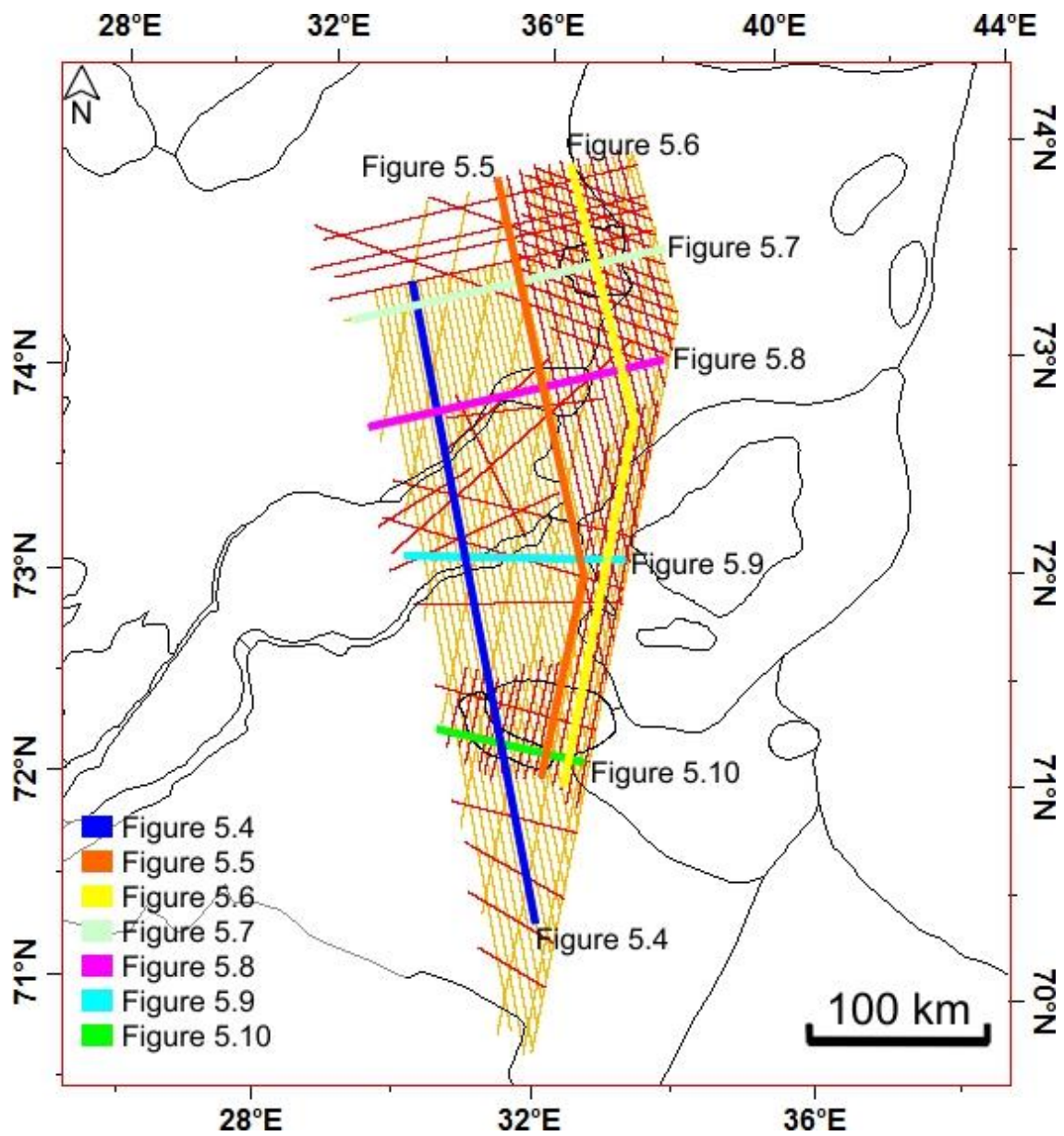


Figure 5.3 Seismic database with regional profiles illustrated in (Figure 5.4 – 5.10) highlighted. Basemap is outline of structural elements from NPD.



### Seismic 2D line [BA-11-104]

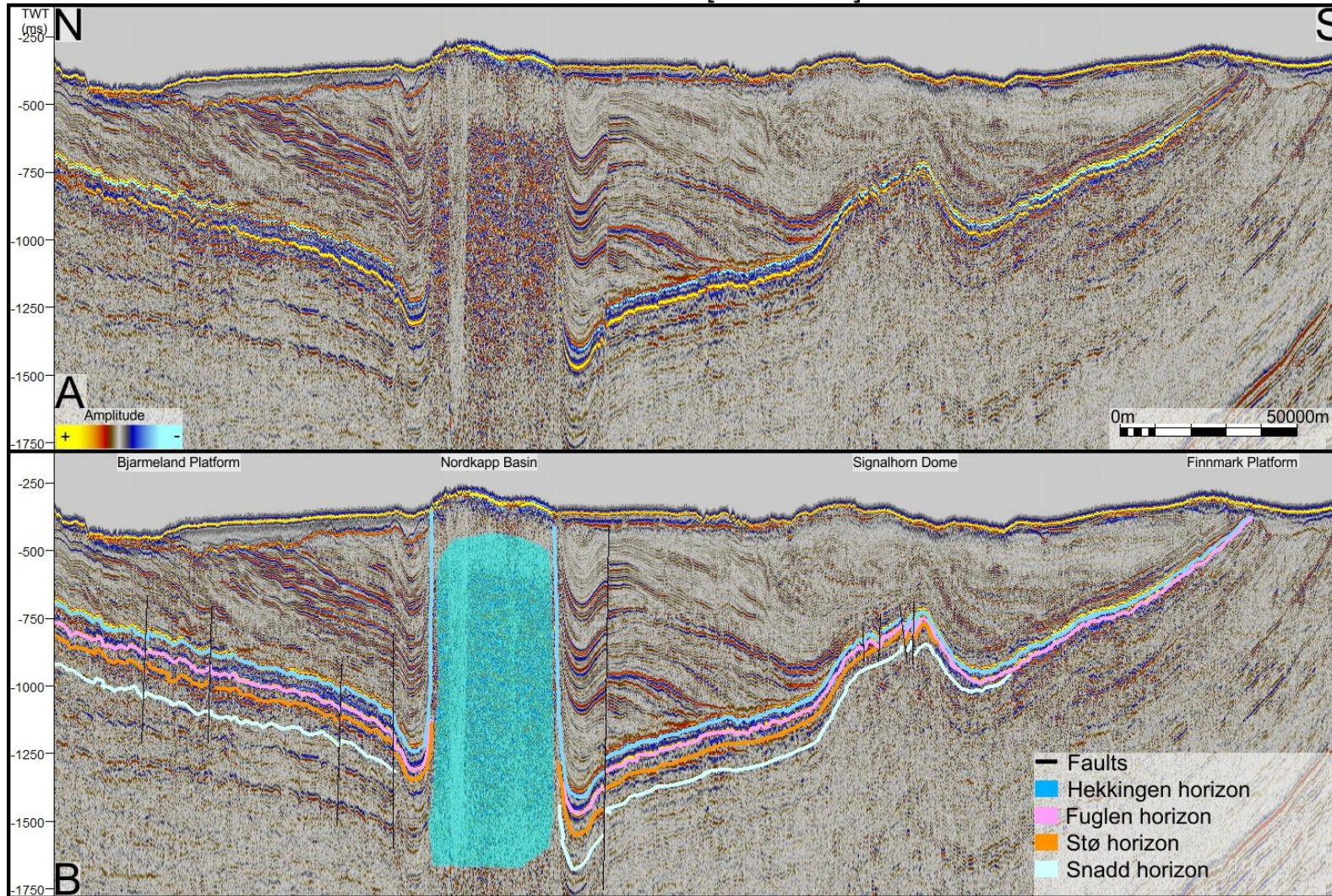


Figure 5.4 Seismic 2D line [BA-11-104] from the Bjarmeland Platform in the north to the Finnmark Platform in the south, illustrating the Nordkapp Basin followed by the Tiddlybanken Basin and Signalhorn Dome. The location of the profile is indicated with blue in (Figure 5.3). A) Without interpretations. B) With interpretations



Seismic 2D line [NPD1201-016]

Seismic 2D line [NPD1201-032]

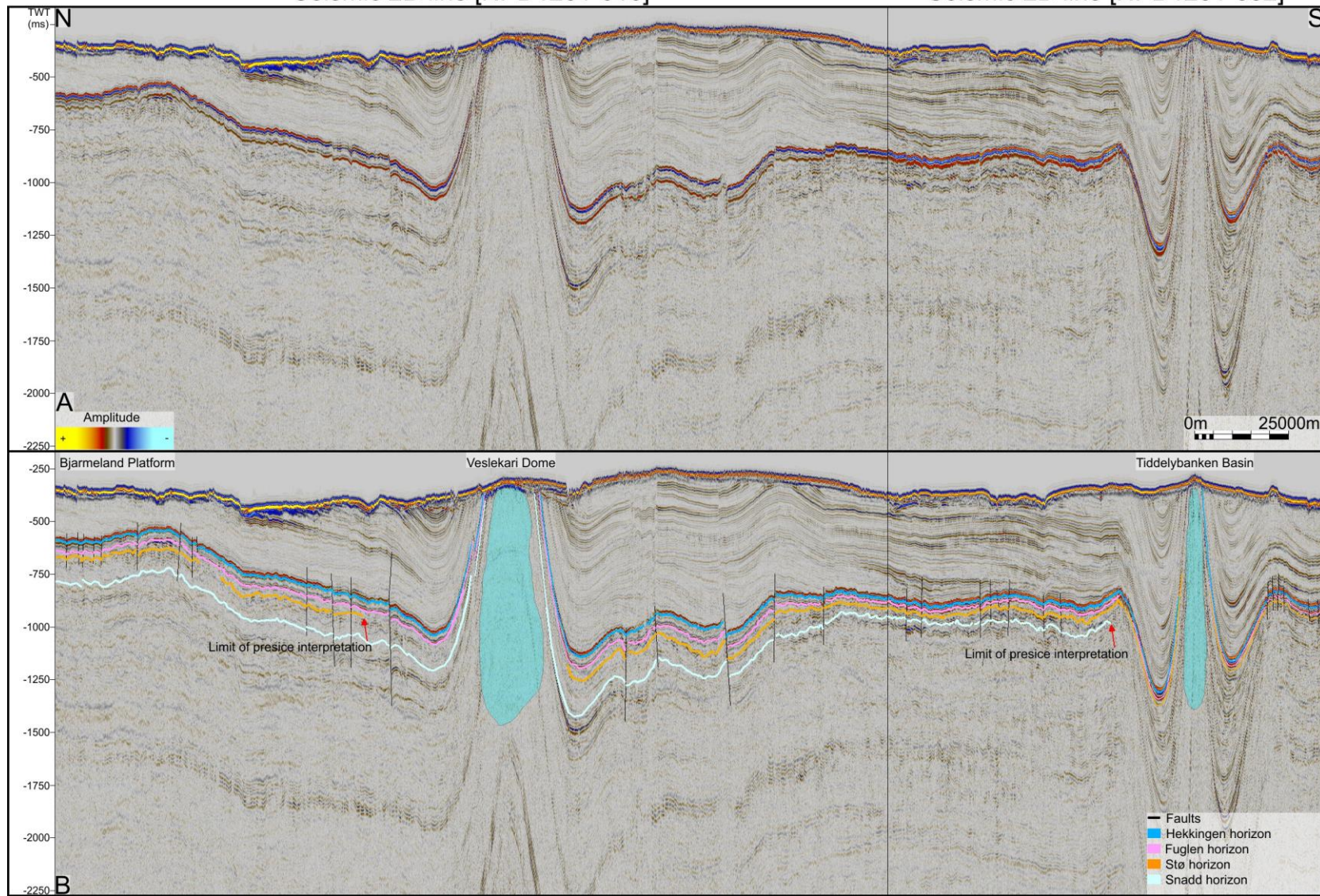


Figure 5.5 Seismic composited 2D line [NPD1201-016] and [NPD1201-032] from the Bjarmeland Platform in the north to the Tiddlybanken Basin and Signalhorn Dome in the South, illustrating the Bjarmeland Platform, Veslekari Dome, Tiddlybanken Basin and Signalhorn Dome. The location of the profile is indicated with orange in (Figure 5.3). A) Without interpretations. B) With interpretations



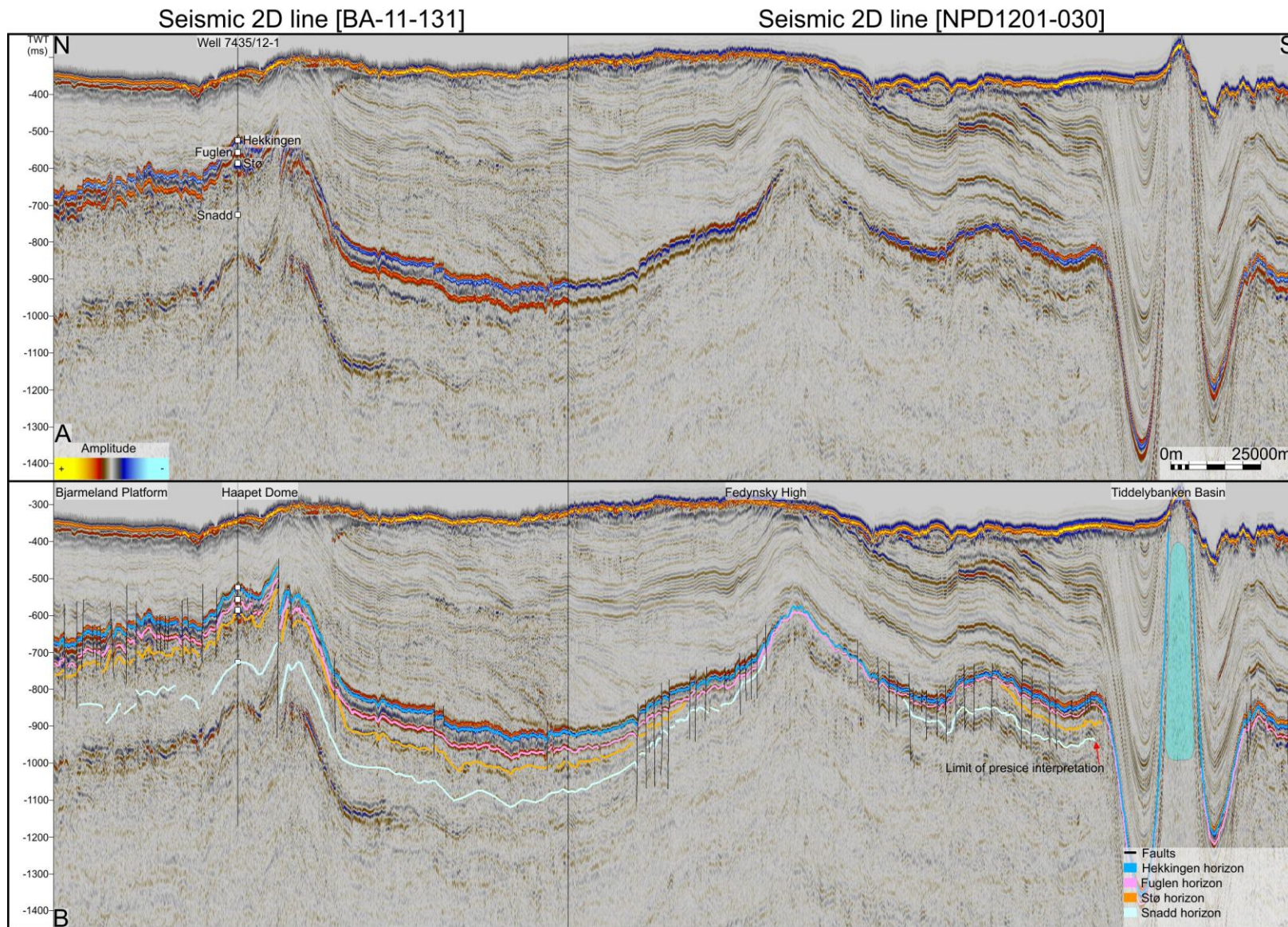
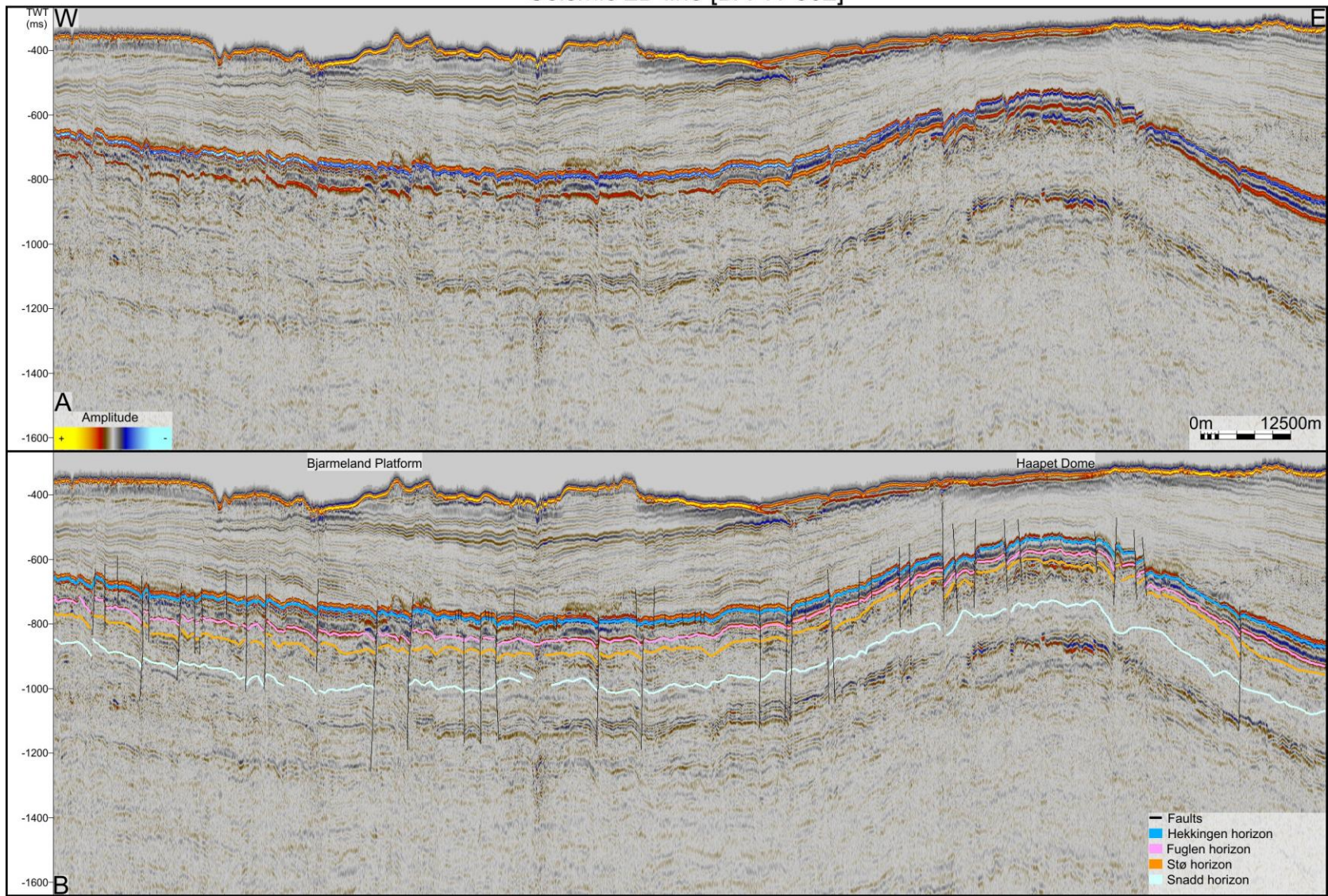


Figure 5.6 Seismic composite 2D line [BA-11-131] and [NPD1201-030] from the Haapet Dome to the north to the Tiddlybanken Basin in the south, illustrating the Haapet Dome, Fedynsky High and Tiddlybanken Basin. The location of the profile is indicated with yellow in (Figure 5.3). A) Without interpretations. B) With interpretations



### Seismic 2D line [BA-11-302]





### Seismic 2D line [BA-11-301]

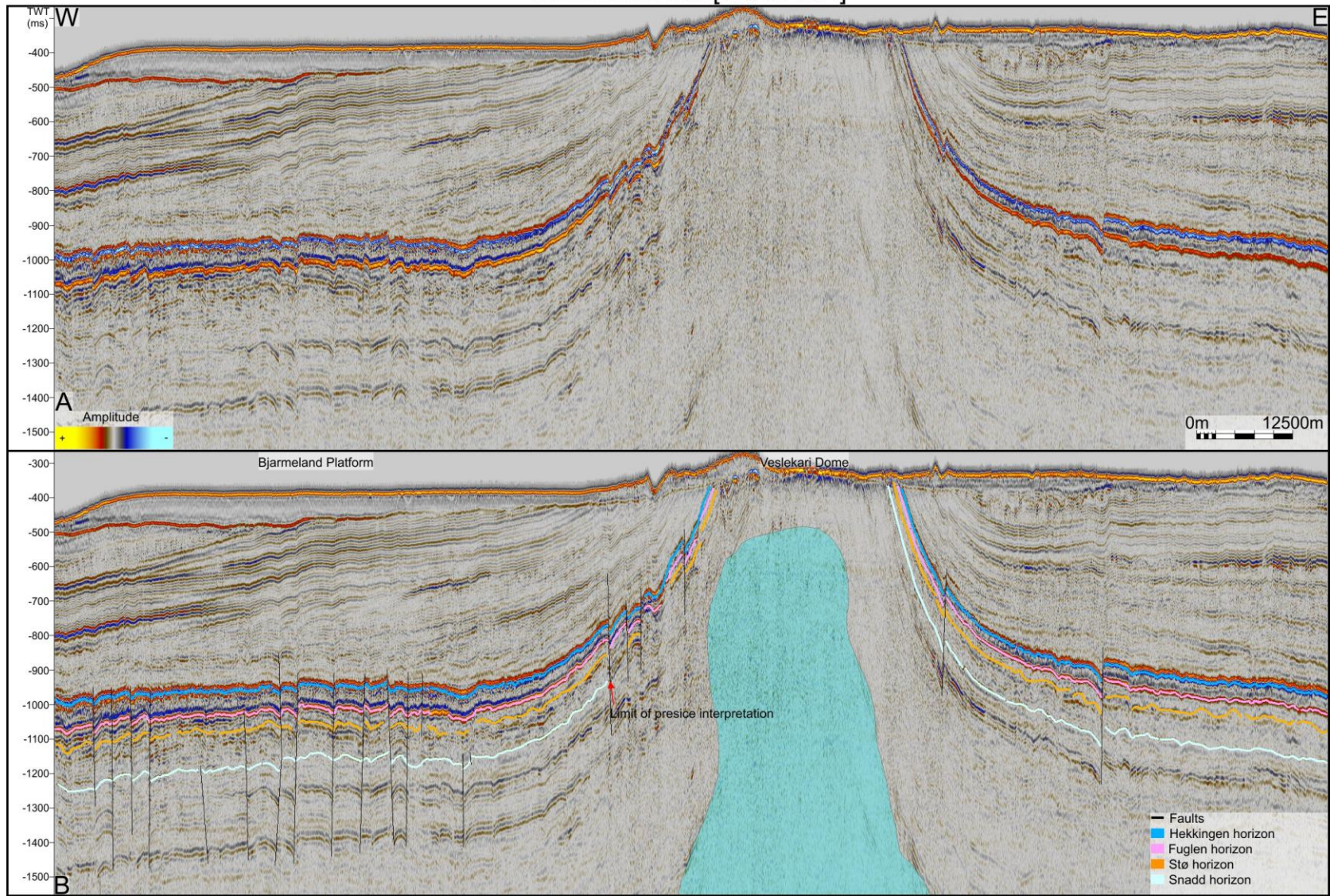


Figure 5.8 Seismic 2D line [BA-11-301] from the Bjarmeland Platform in the west through the Veslekari Dome in the east illustrating the Bjarmeland Platform and Veslekari Dome. The location of the profile is indicated with purple in (Figure 5.3). A) Without interpretations. B) With interpretations



Seismic 2D line [NPD1201-053]

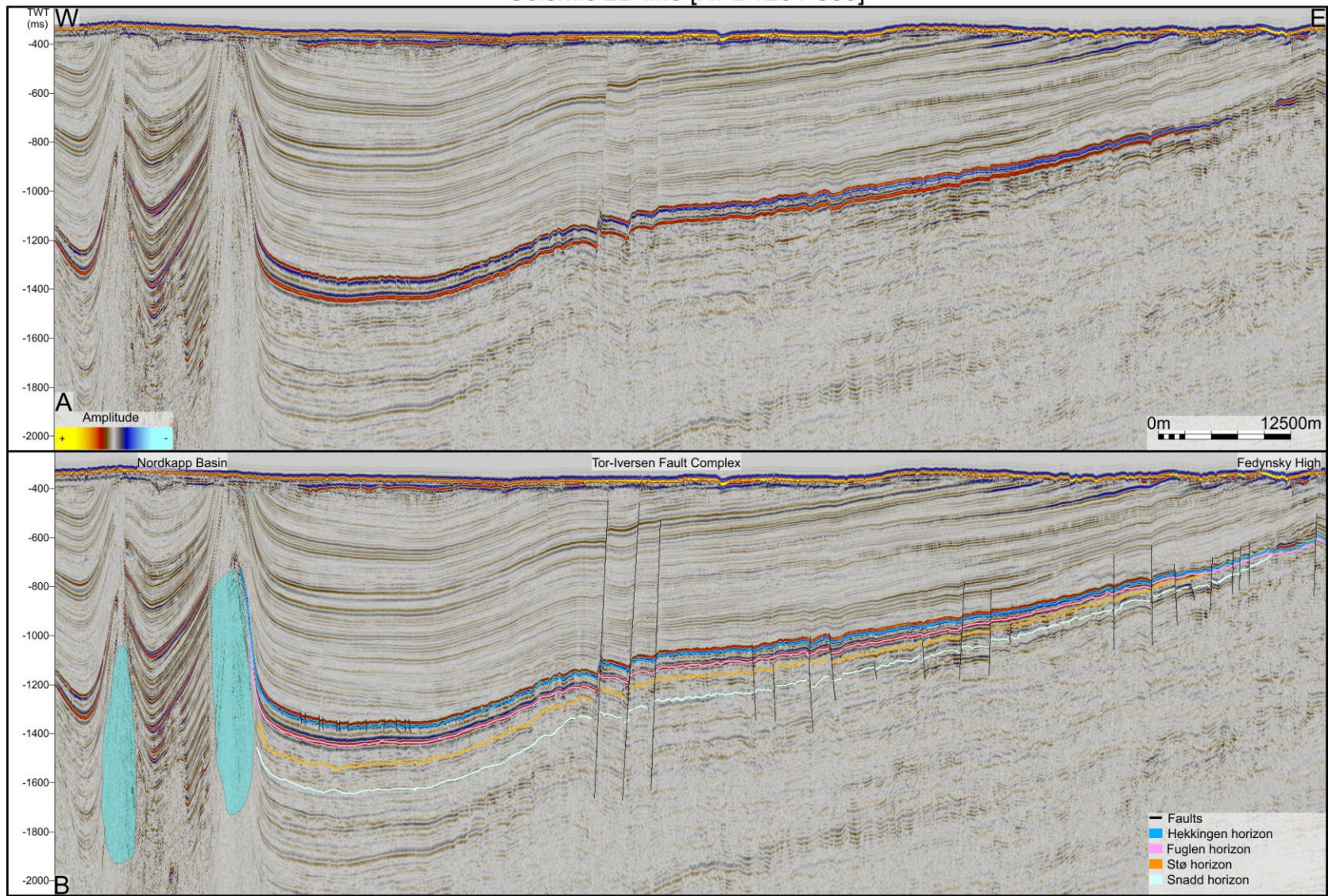


Figure 5.9  
 Seismic 2D line [NPD1201-053] from the Nordkapp Basin in the west to the Fedynsky High in the east, illustrating the south.eastern margin of the Nordkapp Basin and the west of the Fedynsky High. The location of the profile is indicated with light blue in (Figure 5.3). A) Without interpretations. B) With interpretations



### Seismic 2D line [NPD1201-047]

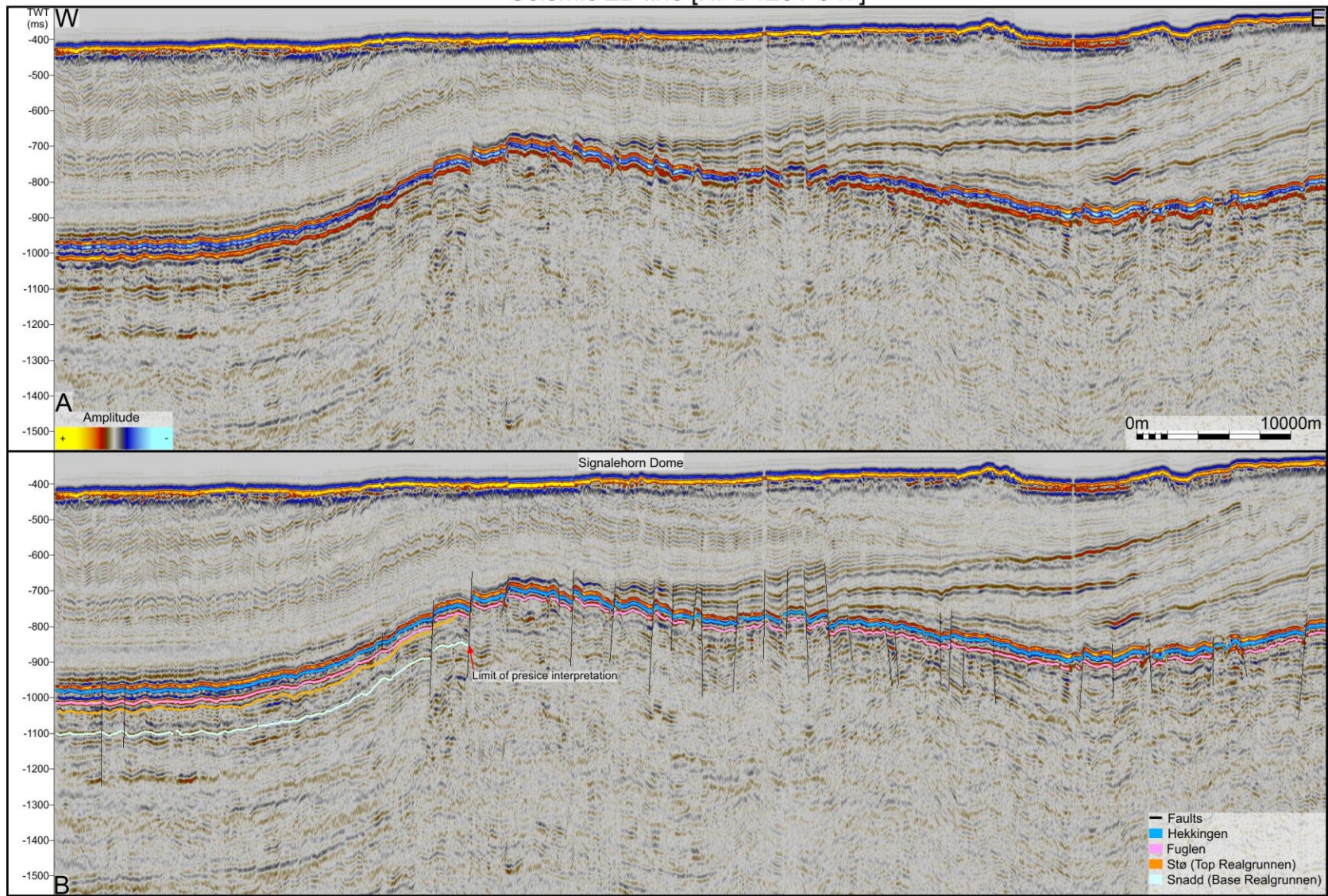


Figure 5.10  
 Seismic 2D line  
 [NPD1201-047]  
 from the west to  
 east on the  
 Signalhorn Dome,  
 illustrating the  
 Signalhorn Dome.  
 The location of the  
 profile is indicated  
 with green in  
 (Figure 5.3). A)  
 Without  
 interpretations. B)  
 With  
 interpretations

## 5.1 Snadd horizon (Base Realgrunnen)

The Top Snadd horizon represents the lower boundary of the Realgrunnen Subgroup (Figure 5.1, Section 2.3). The boundary is represented by a positive reflection coefficient, with a low to very low amplitude throughout the study area.

The strongest and most continuous reflections (continuous, low amplitude) are found on the southwest section of the Bjarmeland Platform (Figure 5.4 and 5.7), the north and west section of the Fedynsky High (Figure 5.6 and 5.9) and the north section of the Finnmark Platform (the area between the Tor-Iversen Fault Complex and the Tiddlybanken Basin) (Figure 5.4).

The horizon has the lowest amplitudes and is discontinuous on the Haapet Dome and the areas northeast of the dome (Figure 5.6 and 5.7). On the dome and the adjacent Bjarmeland Platform the continuity of the horizon is influenced by faulting, averaging a reflection separation of 25-50ms (TWT) and 155ms (TWT) at the most, observable in (Figure 5.4 – 5.8 and 5.12).

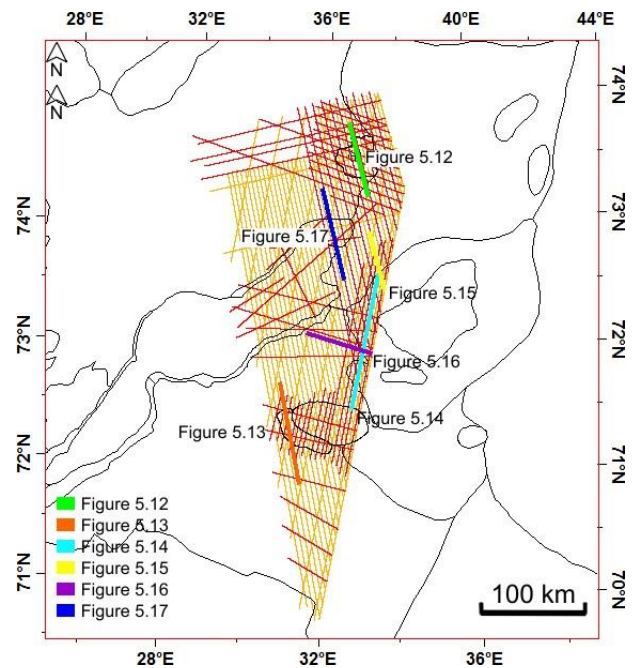


Figure 5.11 Seismic database with local profiles, illustrated in (Figure 5.12 to 5.17) highlighted. Basemap is outline of structural elements from NPD.



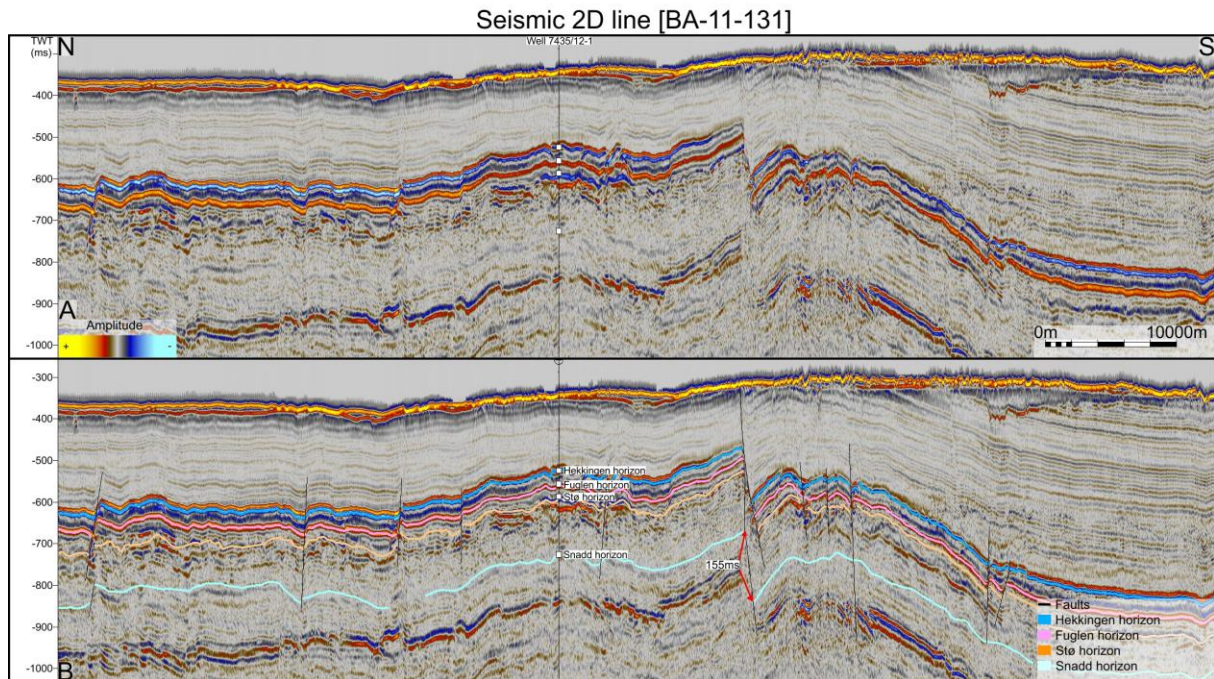


Figure 5.12 Seismic 2D line [BA-11-131] from north to south on the Haapet Dome. The location of the profile is indicated with green in (Figure 5.11).

In the Nordkapp Basin, the Top Snadd horizon is continuous to semi-continuous with low amplitudes (Figure 5.4). The Tor-Iversen Fault Complex and Polarstjernen Fault Complex (PFC) are areas where the reflection is discontinuous, with a low amplitude. Extensive faulting separates the horizon as much as 70ms (TWT) along the margins of the Nordkapp Basin (Figure 5.4), limiting seismic correlation into the basin.

The seismic signature at the Tiddleybanken Basin is similar to that of the Nordkapp Basin, showing a decrease to a low amplitude and a discontinuous configuration at the margins (Figure 5.4 – 5.6). On the Signalhorn Dome, the reflection is discontinuous, with a low to medium amplitude. Fault influence separate the horizon by throws of 20-60ms (TWT) on the dome (Figure 5.4 – 5.6, 5.10 and 5.13). South of the Signalhorn Dome and on the Fedynsky High to the northeast, the Top Snadd horizon is truncated at the base of the Hekkingen Formation (Figure 5.4 and 5.13 to 5.16).

Onto the Veslekari Dome the reflection is discontinuous, with a low amplitude in all directions. The west and south of the dome is extensively faulted, limiting seismic correlation onto the dome (Figure 5.5, 5.8 and 5.17).



Seismic 2D line [BA-11-104]

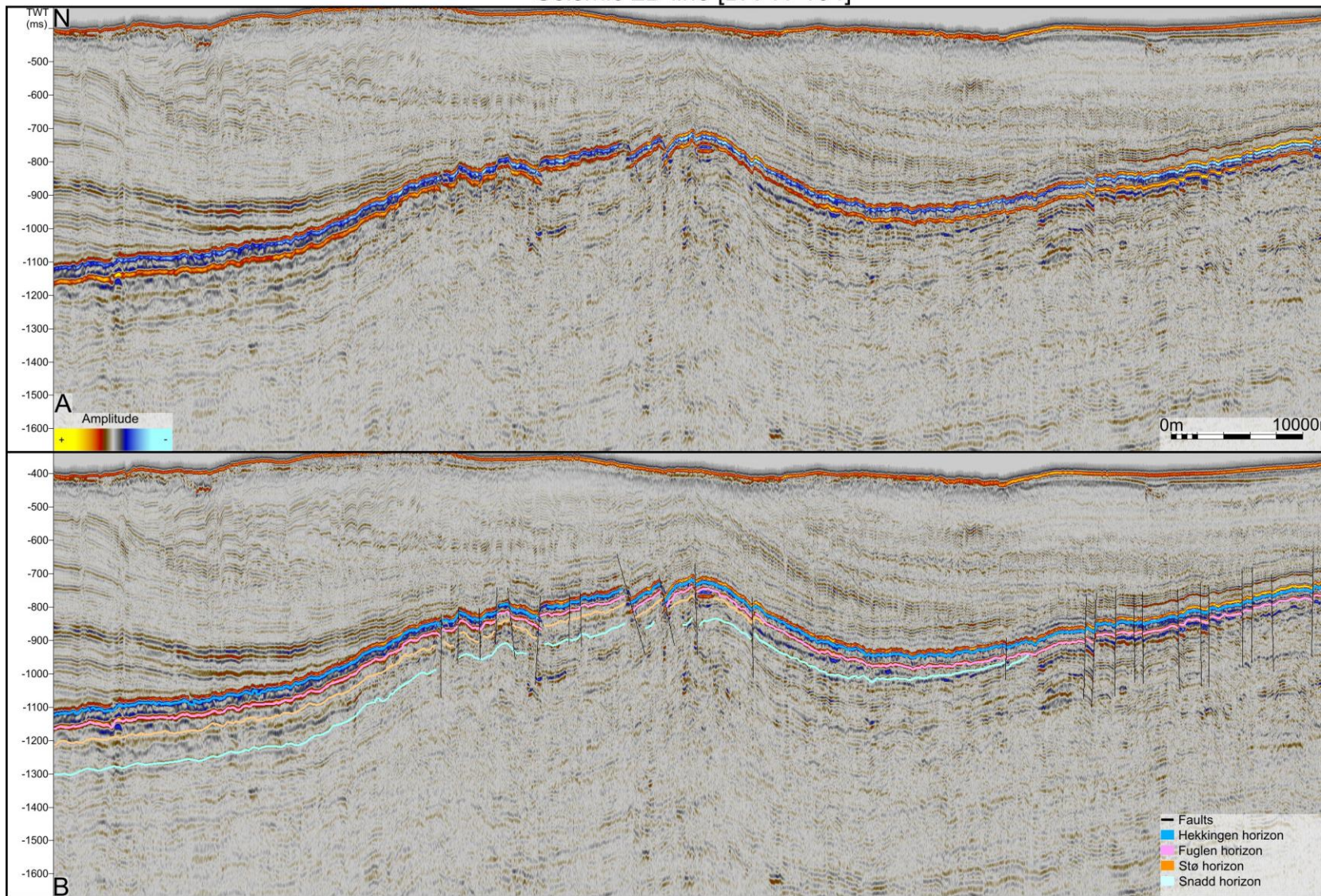


Figure 5.13  
 Seismic 2D line  
 [BA-11-104] from  
 the north margin  
 of the Signalhorn  
 Dome onto the  
 Finnmark  
 Platform in the  
 south, illustrating  
 the fault  
 influence of the  
 horizons and  
 units ontop of the  
 Signalhorn Dome  
 and the  
 truncation of the  
 Top Snadd and  
 Stø Horizons and  
 the Realgrunnen  
 subgroup and  
 Fuglen  
 Formation by the  
 Top Fuglen  
 horizon/  
 Hekkingen  
 Formation. The  
 location of the  
 profile is  
 indicated with  
 orange in (Figure  
 5.11).



### Seismic 2D line [NPD1201-029]

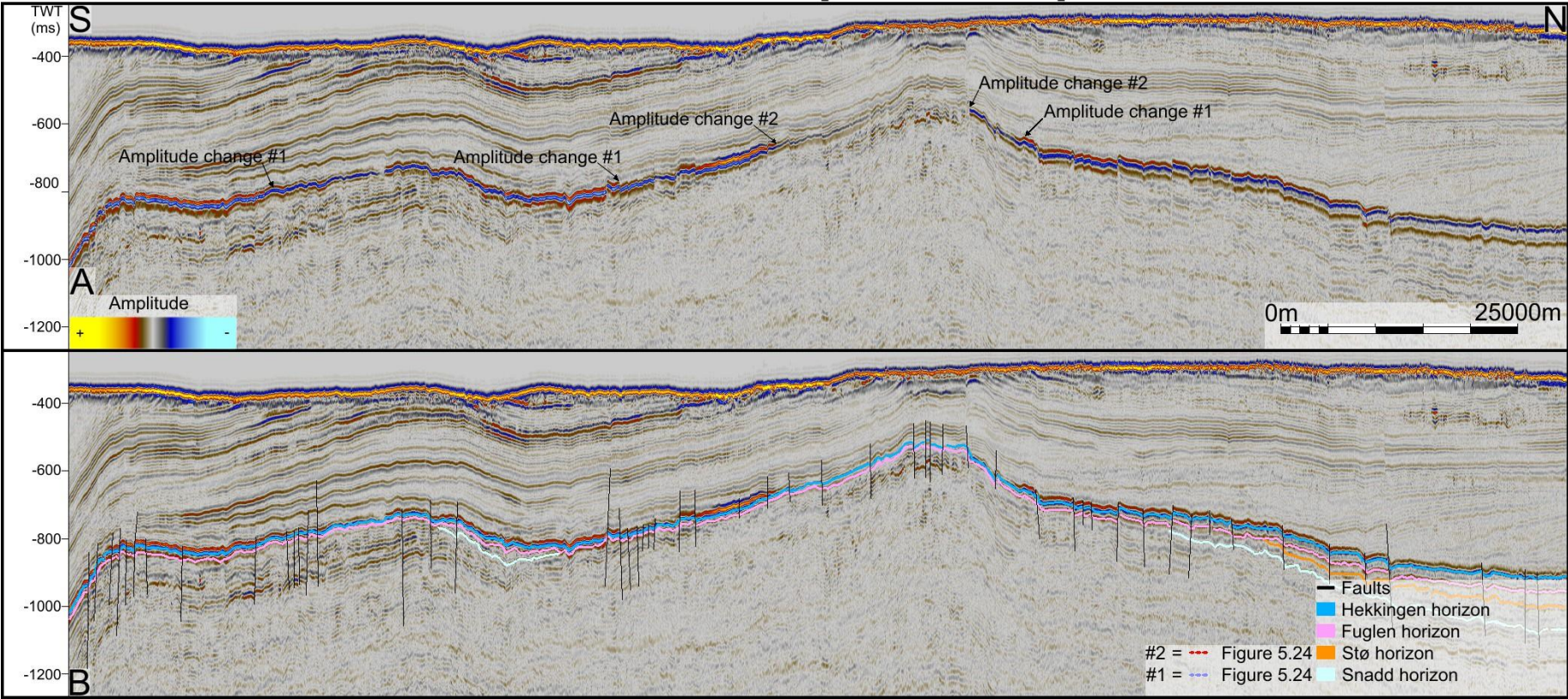


Figure 5.14 Seismic 2D line [NPD1201-029] from the south to north on the Fedynsky High, illustrating fault influence on the horizons and units onto the Fedynsky High and the truncation of the Top Snadd and Stø Horizons and the Realgrunnen Subgroup and Fuglen Formation by the Top Fuglen horizon/ Hekkingen Formation. Profile (A) has indicators pinpointing amplitude changes of the Top Hekkingen horizon as it thins on the High. Amplitude change #1 indicate the first amplitude change of the horizon. Amplitude change #2 indicate locations of abrupt decrease in amplitude, with amplitude change #1 and #2 indicated in (Figure 5.24). The location of the profile is indicated with light-blue in (Figure 5.11).



Seismic 2D line [NPD1201-008]

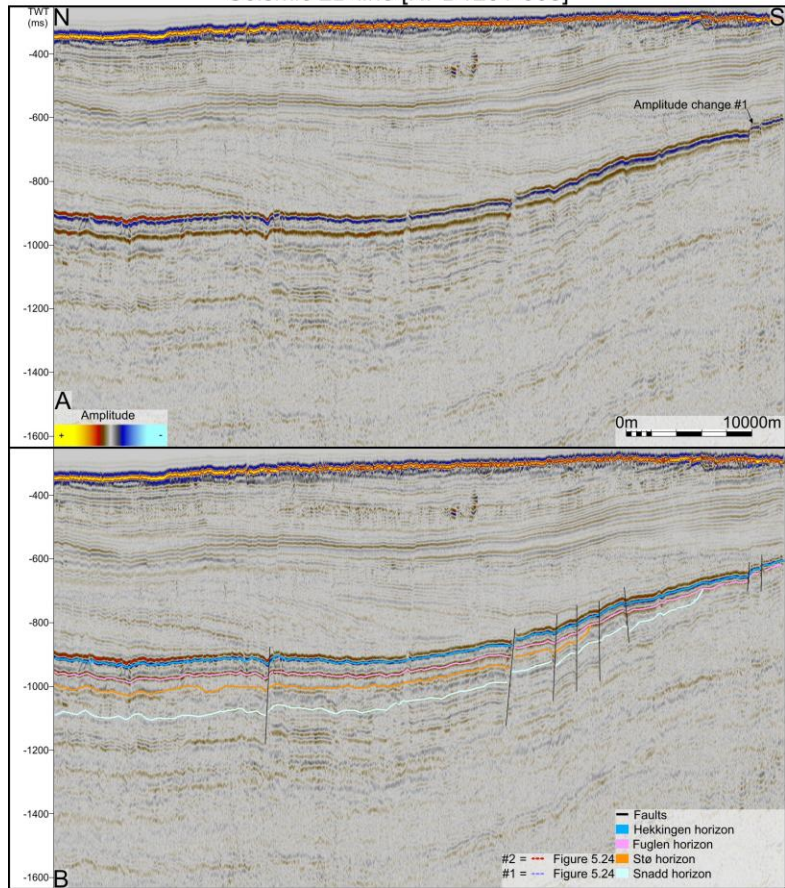


Figure 5.16 Seismic 2D line [NPD1201-008] from north to south on the north margin of the Fedynsky High, illustrating fault influence on the horizons and units onto the Fedynsky High and the truncation of the Top Snadd and Stø Horizons and the Realgrunnen subgroup and Fuglen Formation by the Top Fuglen horizon/ Hekkingen Formation. Profile (A) has indicators pinpointing amplitude changes of the Top Hekkingen horizon as it thins on the high. Amplitude change #1 indicate the first amplitude change of the horizon. Amplitude change #2 indicate locations of abrupt decrease in amplitude, with amplitude change #1 and #2 indicated in (Figure 5.24). The location of the profile is indicated with yellow in (Figure 5.11).

Seismic 2D line [NPD1201-002]

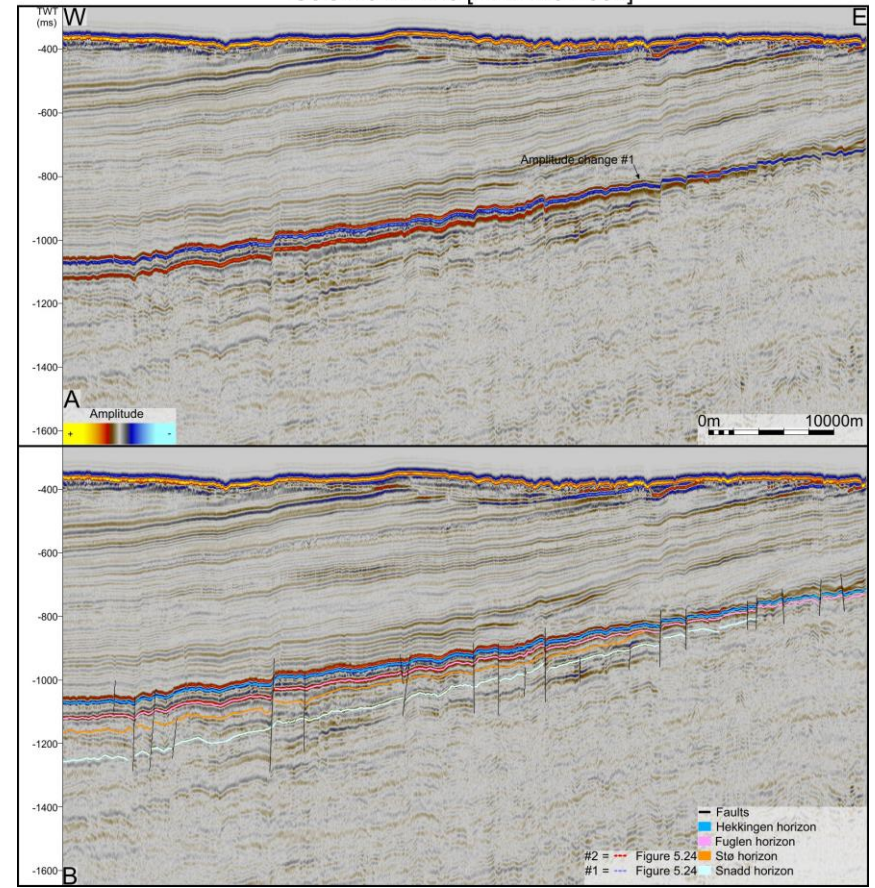


Figure 5.15 Seismic 2D line [NPD1201-002] from west to east on the west margin of the Fedynsky High, illustrating fault influence on the horizons and units onto the Fedynsky High and the truncation of the Top Snadd and Stø Horizons and the Realgrunnen subgroup and Fuglen Formation by the Top Fuglen horizon/ Hekkingen Formation. Profile (A) has indicators pinpointing amplitude changes of the Top Hekkingen horizon as it thins on the high. Amplitude change #1 indicate the first amplitude change of the horizon. Amplitude change #2 indicate locations of abrupt decrease in amplitude, with amplitude change #1 and #2 indicated in (Figure 5.24). The location of the profile is indicated with purple in (Figure 5.11).



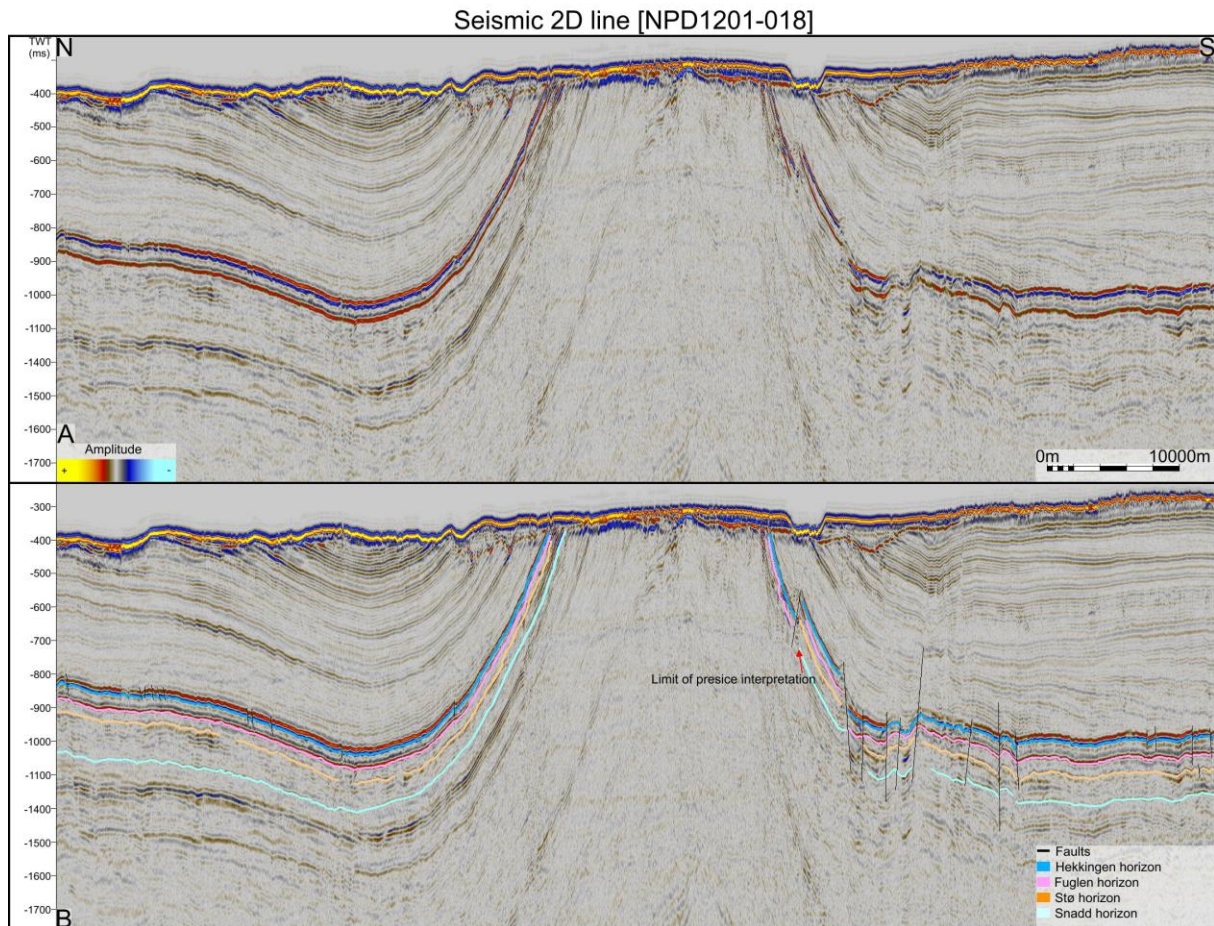


Figure 5.17 Seismic 2D line [NPD1201-018] from north to south (left to right) on the Veslekari Dome, illustrating fault influence on the horizons and units onto the Signalhorn Dome and the truncation of the horizons and units by the sea floor. The location of the profile is indicated with blue in (Figure 5.11)

The horizon follows the morphology of the larger structural elements in the area. It is at its deepest within the Nordkapp Basin (1650ms TWT), shallowing by 200ms to 400ms (TWT) along the Tor-Iversen Fault Complex and 450ms (TWT) along the Polarstjernen Fault Complex to the south and north respectively (Figure 5.18). On the Bjarmeland Platform the horizon has a low relief of 650ms (TWT) from 1200ms (TWT) at the Polarstjernen Fault Complex in the south to 550ms (TWT) in the northeast corner of the dataset (Figure 5.18). The greatest increase in relief on the Bjarmeland Platform can be found at the Haapet Dome where the Top Snadd horizon is situated at 670ms (TWT), shallowing by 250ms (TWT) from east to west and 330ms (TWT) from south to north (Figure 5.18).

In the southeast and south of the dataset the horizon is the shallowest on the Fedynsky High (630ms TWT), and the Signalhorn Dome (840ms TWT), respectively (Figure 5.18). The north section of the Finnmark Platform has a relief of around 200ms (TWT) with an overall flat morphology (Figure 5.18).

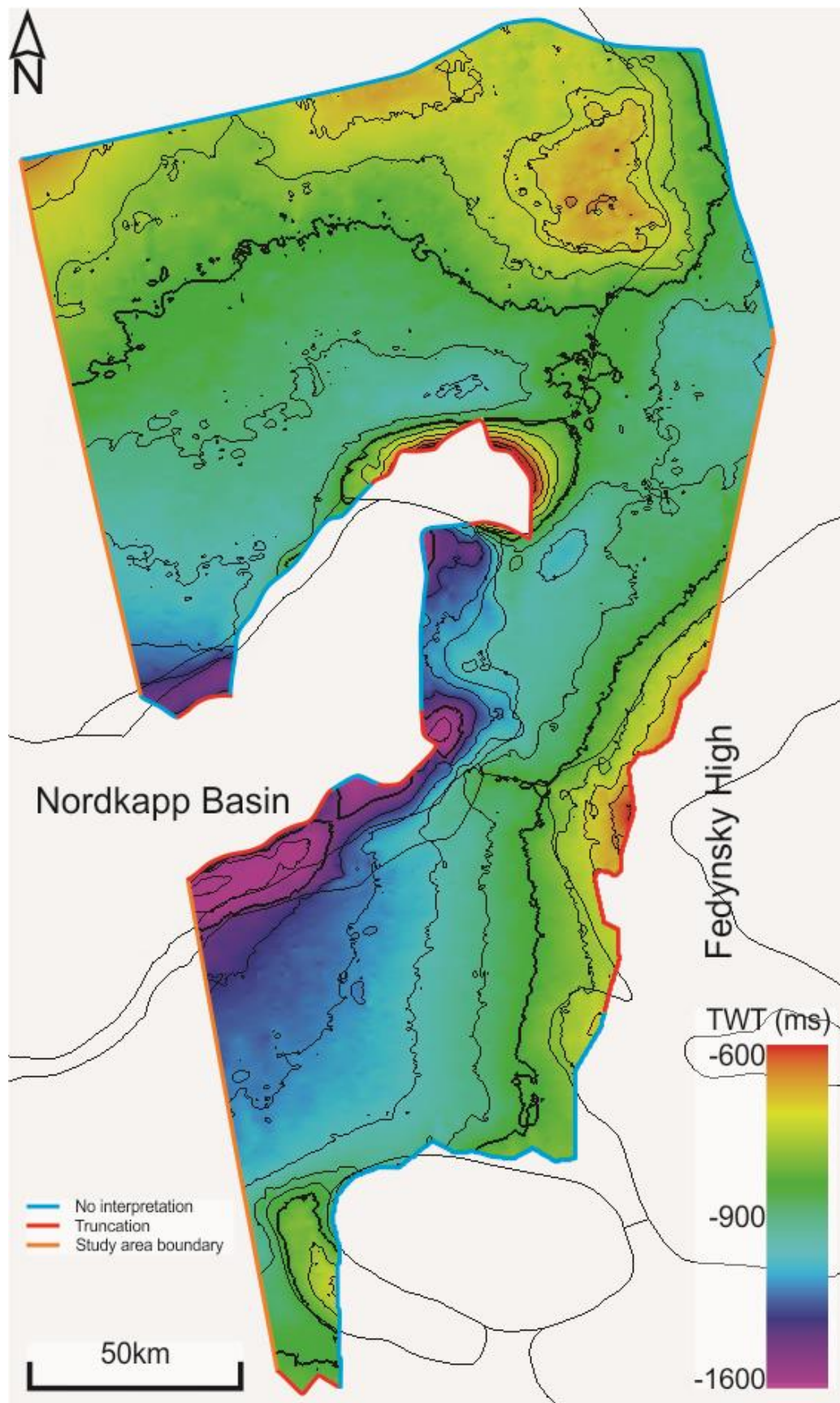


Figure 5.18 Time-structure map of the Top Snadd horizon, with depth in ms (TWT). Red lines indicate truncation of the horizon, blue lines indicate the edge of the interpreted horizon and orange lines indicate the study area boundary.

## 5.2 The Realgrunnen Subgroup (Top Snadd – Top Stø)

The time-thickness map for the Realgrunnen Subgroup is shown in (Figure 5.19). The unit is bounded at its base by the Top Snadd horizon and at its top by the Top Stø horizon (Figure 5.1). The unit is thickest in the north, on the Haapet Dome (130-180ms TWT), the northern and eastern parts of the Bjarmeland Platform (120-130ms TWT) and in the south of the Nordkapp Basin (125-135ms TWT) (Figure 5.19).

The unit is wedging out and is truncated on the Fedynsky High and Signalhorn Dome/ Finnmark Platform, at the base of the Hekkingen Formation (Figure 5.4, 5.6 and 5.13 to 5.16). The unit thins from 90ms and 80ms (TWT) in the north and west of the Fedynsky High respectively, to 30ms (TWT) as the unit is truncated on the high (Figure 5.6, 5.14 to 5.16 and 5.19). Whereas south onto the Signalhorn Dome the unit is reduced from 80ms (TWT) to 70ms (TWT), before being truncated at the south margin of the Signalhorn Dome (Figure 5.4, 5.13 and 5.19). The north section of the Finnmark Platform has a uniform thickness of 80ms (TWT). The thickness increases to <160ms (TWT) along the southern margin of the Nordkapp Basin, north of the Tor-Iversen Fault Complex (Figure 5.4 and 5.19).

On the Bjarmeland Platform the unit is 60-80ms (TWT) at its thinnest in the south by the Polarstjernen Fault Complex, increasing to more than 95ms (TWT) in the north of the platform (Figure 5.8 and 5.19). The overall thickness of the unit ranges from 60-95ms (TWT) in the west of the platform, increasing to 130-180ms (TWT) at the Haapet Dome in the east (Figure 5.7 and 5.19). This increase in thickness is also mapped onto the Haapet Dome from the south, increasing from 80ms (TWT) (to 130-180ms (TWT)) (Figure 5.6, 5.12 and 5.19). Onto the Veslekari Dome the unit has a thickness of 60-80ms (TWT) until its truncation at the sea floor (Figure 5.8, 5.17, 5.19). The Tor-Iversen Fault Complex in the south of the Nordkapp Basin is the only place within the study area where a thickness variation along fault planes is observed for the Realgrunnen Subgroup (Figure 5.4).

The Realgrunnen Subgroup can be divided into an upper and lower section. The lower section is discontinuous to chaotic, with medium to low amplitudes. The upper section has a continuous to chaotic seismic configuration, with low to high amplitudes. The internal reflection configuration of the unit appears to be continuous and sub-parallel, with a medium amplitude in the south of the Nordkapp Basin, becoming chaotic at the basin margin (Figure 5.4 and 5.9). South of the Nordkapp Basin, the internal seismic reflections of the upper section of the unit are mostly discontinuous to continuous with low to medium amplitudes



and a parallel to subparallel configuration (Figure 5.4, 5.9 and 5.16). The lower section has a parallel to subparallel, discontinuous to chaotic configuration and low to medium amplitudes, in the south and east of the basin (Figure 5.4, 5.9 and 5.16). This reflection geometry and amplitude can be followed southwards to the northern margin of the Signalthorn Dome, where the lower and upper section merge before they are truncated (Figure 5.4 and 5.13).

The amplitude of the upper section increases from a low/medium to a medium/high from west to east onto the Fedynsky High (Figure 5.16). This increase in amplitude is accompanied by the thinning of both sections and the termination of the upper and lower sections respectively. North of the Fedynsky High towards the Haapet Dome, the upper section has a medium to high amplitude (Figure 5.6), increasing to high amplitude in local areas such as at the Korpjell well (7435/12-1), situated on the Haapet Dome (Figure 5.2, 5.6 and 5.12). The seismic configuration of the upper section is parallel to subparallel, and sub-parallel for the lower section from the Fedynsky High, to the south margin of the Haapet Dome (Figure 5.6). North of this point the reflection has a discontinuous, parallel to chaotic configuration, with medium to high amplitudes (Figure 5.12).

On the Bjarmeland Platform the upper and lower section of the unit is easily identifiable in the north-south orientation, at which the lower section has a discontinuous to chaotic seismic configuration and low to medium amplitudes (Figure 5.4). The upper section has overall medium amplitudes, with a relatively continuous, parallel seismic configuration. In the east-west orientation the upper and lower sections of the unit is still identifiable as of amplitude, but their seismic continuity is greatly reduced making the identification of the internal geometry challenging (Figure 5.7). Onto the Veslekari Dome to the south, the seismic configuration becomes discontinuous to chaotic, with low amplitudes (Figure 5.5 and 5.17).



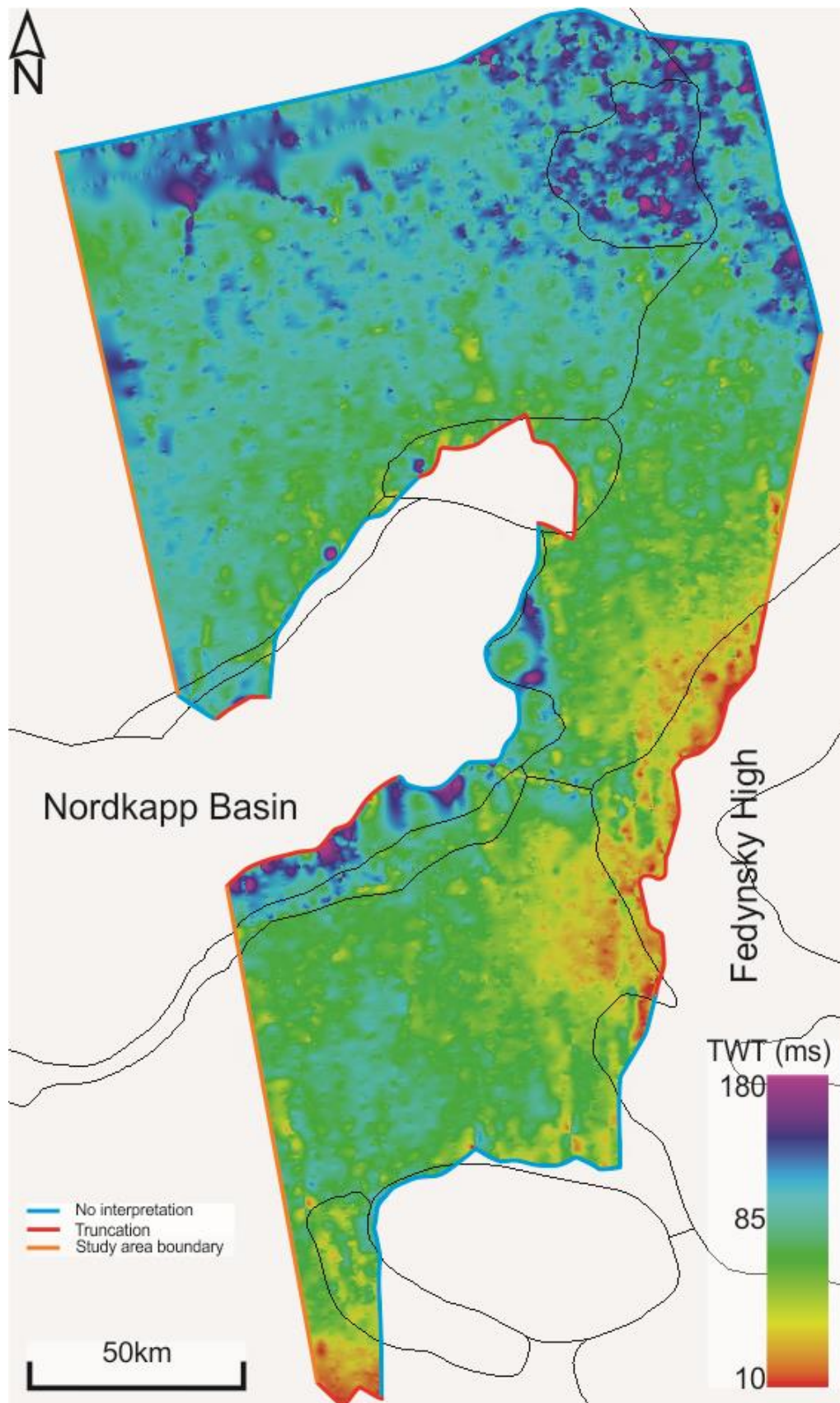


Figure 5.19 Time-thickness map of the Realgrunnen Subgroup, thickness is illustrated in TWT (ms). Red lines indicate truncation of the unit, blue lines indicate the edge of the interpreted top and base horizons of the unit and orange lines indicate the study area boundary.

### 5.3 Top Stø (Top Realgrunnen)

The Top Stø separates the Realgrunnen Subgroup from the overlying the Fuglen Formation (Figure 5.1, Section 2.3). The acoustic impedance of the boundary is represented by a negative reflection coefficient, with an average low amplitude and a continuous to discontinuous reflection geometry.

At the Bjarmeland Platform the horizon has a discontinuous reflection geometry, with a low amplitude (Figure 5.4, 5.5 and 5.7). On the Haapet Dome, the reflection geometry is discontinuous, with a high amplitude at the morphologically shallowest point of the dome (Figure 5.6, 5.7 and 5.12). The fault throw separation of the Top Stø horizon on the Haapet Dome and Bjarmeland Platform is similar to that of the Top Snadd horizon, averaging 25-50ms (TWT) (Figure 5.5, 5.7 and 5.12). At the southern margin of the dome the reflection geometry is continuous, with a medium to low amplitude (Figure 5.12). Between the Haapet Dome and Fedynsky High the horizon is represented by a discontinuous reflection geometry (Figure 5.6). Followed by a discontinuous to continuous configuration and low amplitudes onto the Fedynsky High, with an increase in amplitude from the west and decrease from the north (Figure 5.6, 5.14 to 5.16). At the Veslekari Dome the surface is represented by a discontinuous, low amplitude configuration (Figure 5.8 and 5.17).

Within the Nordkapp Basin the reflector has a discontinuous reflection geometry along the north and south basin margin, and an overall low amplitude (Figure 5.4). At the Signalhorn Dome, Tiddlybanken Basin and the north section of the Finnmark Platform the reflector alternates between a continuous to discontinuous reflection geometry with a low amplitude (Figure 5.4 and 5.13). On top of the Signalhorn Dome faults influence the horizon, separating it by 20-60ms (TWT) (Figure 5.13).

The Top Stø horizon (Figure 5.20) follows the structural morphology in much of the same way as the Top Snadd horizon (Figure 5.19). It is at its deepest within the Nordkapp Basin reaching a maximum depth of 1590ms (TWT) and 1450ms (TWT) in the southeast and northeast of the basin respectively (Figure 5.20). Towards the Polarstjernen Fault Complex and Tor-Iversen Fault Complex the horizon shallows by 100-500ms (TWT) and 30-300ms (TWT), with the most significant depth reduction in the northeast (Figure 5.4 and 5.20). This is followed by a 30-220ms (TWT) increase in relief at the Polarstjernen Fault Complex and 0-110ms (TWT) at the Tor-Iversen Fault Complex (Figure 5.4).

On the Bjarmeland Platform the horizon is situated at 1230ms (TWT) at the deepest in the southwest and 490ms (TWT) at the shallowest in the northwest (Figure 5.20). From west to east the horizon shallows from 750ms (TWT) to 530ms (TWT), with a 900ms (TWT) section in the centre of the platform (Figure 5.7 and 5.20). East and northeast of the Haapet Dome the horizon descend to a depth of 950ms (TWT), and to 1000ms (TWT) to the south by the Fedynsky High margin (Figure 5.20).

At the Veslekari Dome the horizon ascend rapidly from 1000-1120ms (TWT), being terminated by the seafloor at 300-400ms (TWT) (Figure 5.20). The margin of the dome is fault influenced, with as much as 100ms (TWT) separation of the horizon in the south and 20-30ms (TWT) in the east and west (Figure 5.8 and 5.16). Onto the Fedynsky High the horizon is located at a depth of approximately 800ms (TWT) at the shallowest (Figure 5.20). From the Tor-Iversen Fault Complex in the north to the Signalhorn Dome in the south the horizon shallows from 1360ms (TWT) to 780ms (TWT) (Figure 5.20). Interpretations of the horizon into the Tiddlybanken Basin was attempted, but with minor/ lacking results, hence the horizon interpretations are limited to the north basin margin (Figure 5.20).

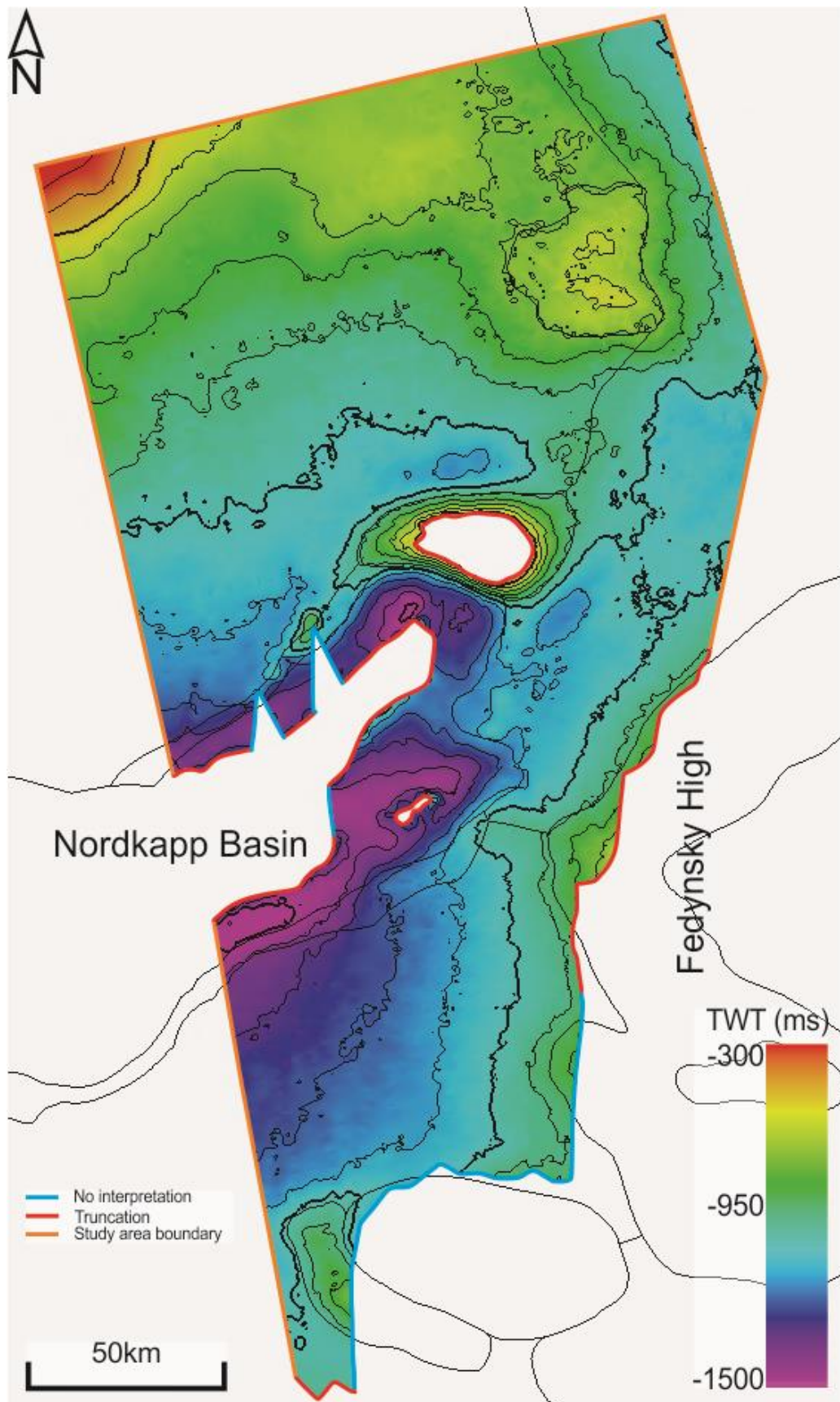


Figure 5.20 Time-structure map of the Top Stø horizon, with depth in ms (TWT). Red lines indicate truncation of the horizon, blue lines indicate the edge of the interpreted horizon and orange lines indicate the study area boundary.

## 5.4 Fuglen Formation

The time-thickness map for the Fuglen Formation is shown in (Figure 5.21). It is bounded at its base by the Top Stø horizon and at its top by the Top Fuglen horizon (Figure 5.1). It ranges in thickness from less than 10ms (TWT) at the Fedynsky High, Signalhorn Dome and local areas at the Haapet Dome, to more than 90ms (TWT) within the Nordkapp Basin (Figure 5.21).

At the Bjarmeland Platform the unit decreases from north to south and from west to east: from 50ms (TWT) in the north to 35ms (TWT) at the Polarstjernen Fault Complex in the south and 50ms (TWT) in the west to 15ms (TWT) at the Haapet Dome in the east (Figure 5.4, 5.7 and 5.21). East of the Haapet Dome the unit has a thickness of 20-80ms (TWT). In the area between the Haapet Dome in the north and the Fedynsky High margin in the south, the unit has a uniform thickness of 40-50ms (TWT) (Figure 5.6 and 5.21). Onto the Fedynsky High the unit thins, from 40-50ms to 20-30ms (TWT) in the north and west, followed by its disappearance due to the Top Stø horizon truncating at the base of the Hekkingen Formation on the high (Figure 5.14 to 5.16 and 5.21).

South of the Tor-Iversen Fault Complex, the general trend is a decrease in thickness of the unit from west to east and north to south (Figure 5.4, 5.9 and 5.21). The unit decrease in thickness, from 60ms (TWT) in the southwest of the complex, to 35-50ms (TWT) as it terminates at the base of the Hekkingen Formation on the south section of the Signalhorn Dome (Figure 5.4, 5.13 and 5.21). At the Veslekari Dome the Fuglen Formation is truncated by the sea floor, with an overall uniform thickness of 30 to 50ms (TWT) on the dome (Figure 5.8, 5.17 and 5.21).

Within the Nordkapp Basin the thickest section of the unit is located at the lowest point between the basin margin and the point at which the unit onlaps the diapir (Figure 5.4). In the north of the Nordkapp Basin the unit ranges from 55-90ms (TWT), while 50-80ms (TWT) in the south (Figure 5.21). The south margin of the Nordkapp Basin is the only place within the study area where thickness variations of the Fuglen Formation is observed across fault planes (Figure 5.4). Towards the centre of the basin, from the north and south, the unit thins and onlaps the salt diapirs (Figure 5.4).

Throughout the dataset, the unit has a parallel, continuous to chaotic internal reflection geometry, with no internal subdivisions and low amplitudes. From north to south on the

Bjarmeland Platform, the unit has a parallel seismic configuration and a transition from discontinuous to continuous approaching the Polarstjernen Fault Complex (Figure 5.4). At the Polarstjernen Fault Complex the unit is internally chaotic, followed by a sub-parallel, discontinuous reflection geometry within the Nordkapp Basin (Figure 5.4).

From the Tor-Iversen Fault Complex in the north to the Signalhorn Dome and Tiddlybanken Basin in the south, the internal configuration of the unit is discontinuous and sub-parallel (Figure 5.4 and 5.5). Onto the Fedynsky High the internal reflection geometry is parallel and discontinuous in the west, with the disappearance due to resolution as the unit decreases in thickness to the east (Figure 5.16). At the north side of the Fedynsky High the unit has a continuous, sub-parallel to parallel internal configuration, with no apparent internal reflectors to be observed close to the unit terminating (Figure 5.14 and 5.15). At the Veslekari Dome the internal reflection geometry is sub-parallel and discontinuous in both the north, south and west, with a more chaotic configuration in the east (Figure 5.5, 5.8 and 5.17). West to east on the Bjarmeland Platform the unit has an overall sub-parallel to parallel, continuous configuration, with local discontinuous intervals (Figure 5.7). On the Haapet dome the unit is parallel with a continuous to discontinuous internal configuration, with a low to medium amplitude at the dome margins and a high amplitude at the top of the dome (Figure 5.7 and 5.12).



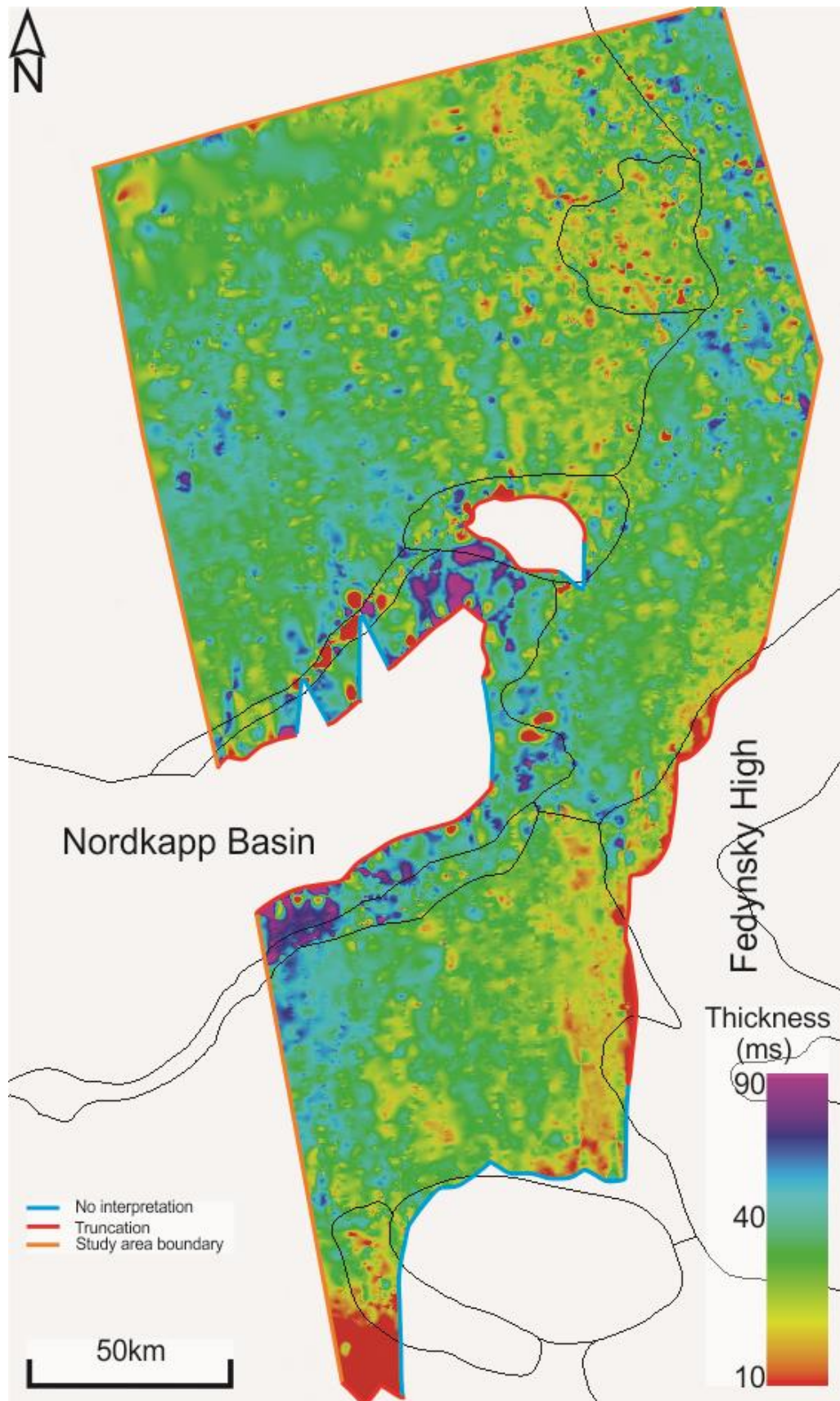


Figure 5.21 Time-thickness map of the Fuglen Formation, thickness is illustrated in TWT (ms). Red lines indicate truncation of the unit, blue lines indicate the edge of the interpreted top and base horizons of the unit and orange lines indicate the study area boundary.

## 5.5 Top Fuglen horizon

The Top Fuglen horizon separates the Fuglen Formation from the Hekkingen Formation (Figure 5.1, Section 2.3). In terms of acoustic impedance, the boundary is represented by a positive reflection coefficient, with overall high amplitudes and a continuous reflection geometry.

At the Bjarmeland Platform the horizon is generally continuous, with low to high amplitudes (Figure 5.4 and 5.7). Overall the seismic amplitude of the horizon increases from north to south (Figure 5.4, 5.5 and 5.12). It has a medium amplitude in the west, with local discontinuous, low amplitude deviations to the east, and an exemption on the Haapet Dome where the amplitudes are high (Figure 5.7). Faults influence the continuity of the surface on both the Bjarmeland Platform and Haapet Dome, separating it by an average throw of 25-50ms (TWT) (Figure 5.4, 5.5, 5.7 and 5.12).

Towards the Fedynsky High, the horizon is represented by a high amplitude that slightly decreases towards the shallower areas of the high (Figure 5.14 to 5.16). The horizon is separated by faults at several locations on the high, averaging a throw of less than 30ms (TWT). At the Veslekari Dome, the seismic signature of the horizon differs along the dome margins. To the north, east and west it has a high amplitude and a continuous configuration, while being discontinuous in the south of the dome (Figure 5.8 and 5.17). The horizon is extensively influenced by faults in the south, west and east with throws in the range of 20-100ms (TWT).

Within the Nordkapp Basin, Tiddlybanken Basin and at the Signalhorn Dome and Finnmark Platform the horizon is highly continuous with a high amplitude, illustrated in the following figures; (Figure 5.4 to 5.6, 5.10 and 5.13). The surface is extensively fault influenced at the Signalhorn Dome, with 20-60ms (TWT) throws (Figure 5.13).

The horizon is located at a depth ranging from less than 300ms (TWT) to 1500ms (TWT) within the dataset (Figure 5.22). It is deepest in the southwest and northeast of the Nordkapp and Tiddlybanken basins, at 1500ms (TWT) and 1400ms (TWT), respectively. In the south of the Nordkapp Basin the horizon shallows from 1500ms (TWT) in the west to 1220ms (TWT) at the transition out of the basin in the east (Figure 5.22).

The greatest horizon depths within the Nordkapp Basin ranges from 1350ms to 1500ms (TWT) in the south, and 1200ms to 1450ms (TWT) in the north (Figure 5.22). Towards the



centre of the basin the horizon onlaps the salt diapirs (Figure 5.4). Horizon depths are reduced by 120-250ms (TWT) towards the Tor-Iversen Fault Complex in the south and by 80-170ms (TWT) towards the Polarstjernen Fault Complex in the north (Figure 5.4). Along the Tor-Iversen Fault Complex and Polarstjernen Fault Complex fault throws of -20-90ms (TWT) and 0-210ms (TWT) influence the horizon (Figure 5.4).

At the Bjarmeland Platform the Fuglen horizon shallows from 1100ms (TWT) by the Polarstjernen Fault Complex in the southwest to 350ms (TWT) in the northwest (Figure 5.4 and 5.22). From west to east, depths decrease from 720ms to 500ms (TWT), with a 850ms (TWT) deeper section in the centre of the platform (Figure 5.7 and 5.22). The shallowest section is located on top of the Haapet Dome, with increased horizon depths off the dome to the east (Figure 5.12 and 5.22). South of the Haapet Dome the horizon tilt eastward, deepening from 850ms (TWT) in the southwest (north of the Veslekari Dome) to 1100ms (TWT) in the southeast (north of the Fedynsky High) (Figure 5.22). At the Fedynsky High there are two morphological highs, with the largest one being located to the north of the smaller one (Figure 5.14 and 5.22). The horizon is located at 425ms (TWT) at the shallowest on the northernmost high and 675ms (TWT) at the southern one.

From the Tor-Iversen Fault Complex in the north to the Finnmark Platform in the south the horizon shallows from 1000ms-1300ms (TWT) at the Tor-Iversen Fault Complex to 370ms (TWT) at the Finnmark Platform (Figure 5.4 and 5.22). At the north margin of the Signhorn Dome the depth is reduced from 1100ms to 730ms (TWT), before increasing to 980ms (TWT) at the south margin (Figure 5.13 and 5.22). Within the Tiddlybanken Basin, horizon depths range from 1250ms to 1400ms (TWT) at the deepest in the north and 1140ms to 1235ms (TWT) in the south (Figure 5.5, 5.6 and 5.22). The horizon onlaps the salt diapirs in the centre of the basin in the same manner as for the Nordkapp Basin.

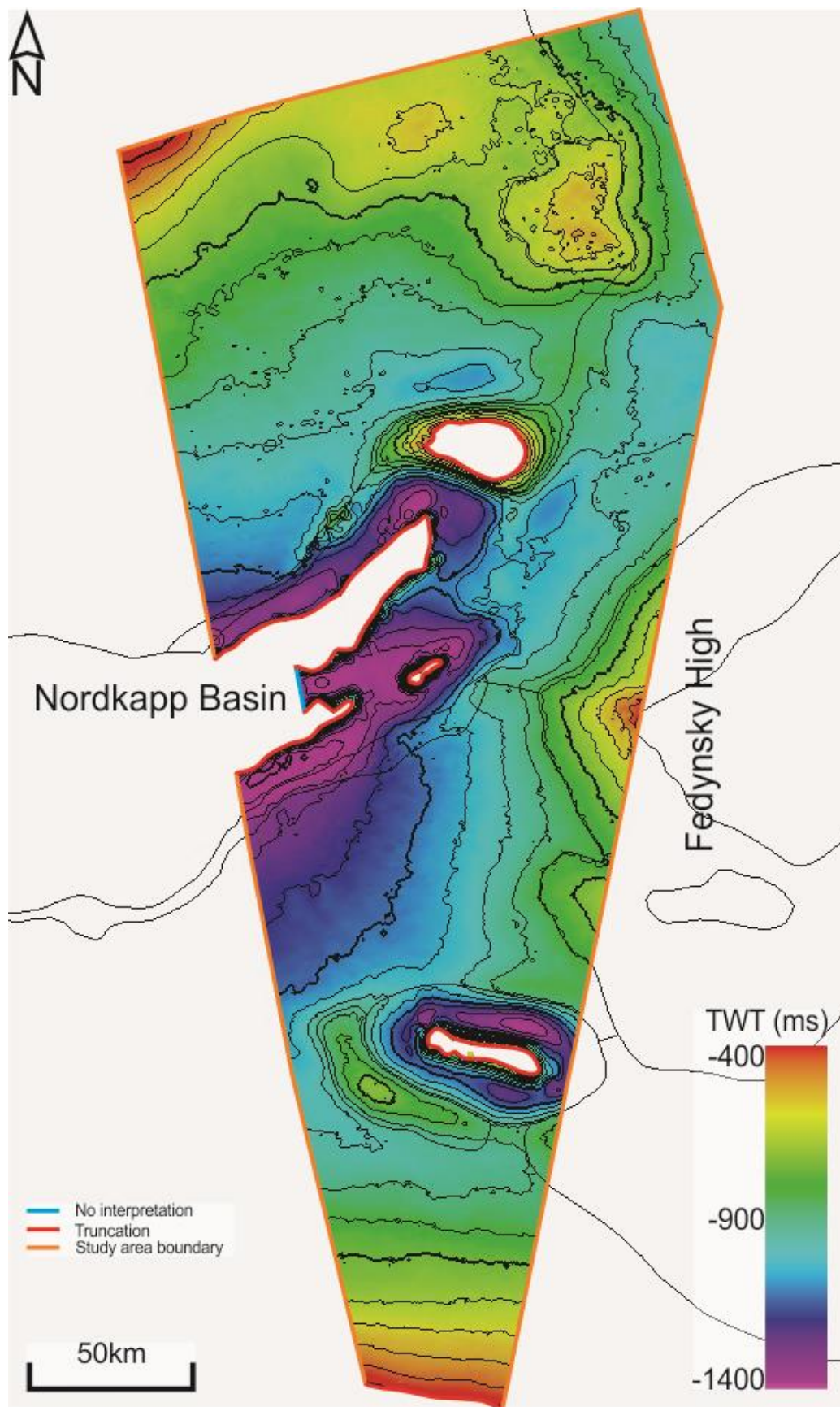


Figure 5.22 Time-structure map of the Top Fuglen horizon, with depth in ms (TWT). Red lines indicate truncation of the horizon, blue lines indicate the edge of the interpreted horizon and orange lines indicate the study area boundary.

## 5.6 Hekkingen Formation

The time-thickness map of the Hekkingen Formation (Figure 5.23) is bounded at its base by the Top Fuglen horizon and at its top by the Top Hekkingen horizon (Figure 5.1). It ranges in thickness from more than 90ms (TWT) northeast of the Haapet Dome, to less than 10ms (TWT) at the Fedynsky High and Finnmark Platform (Figure 5.23).

The time-thickness map (Figure 5.23) indicate a maximum unit thickness of 70-90ms (TWT) in the Nordkapp Basin. This thickness is reduced towards the centre of the basin in a pinch-out as the unit onlaps the diapirs (Figure 5.4). In the northwest of the basin the unit retains a constant thickness of 70ms (TWT) towards the Polarstjernen Fault Complex in the north (Figure 5.4 and 5.23). In the northeast, southeast and southwest the unit thickness decreases by 20-50ms (TWT) towards the basin margins (Figure 5.23). An increase in unit thickness is observed along the Tor-Iversen Fault Complex at the south margin of the basin (Figure 5.4).

On the Bjarmeland Platform the unit has a thickness ranging from 70-90ms (TWT) in the west and southwest, to 40ms (TWT) in the northwest and east by the Haapet Dome (Figure 5.4, 5.7 and 5.23). At the Haapet Dome in the east, the unit is overall thinner than the adjacent areas. On top of the dome the thickness ranges from 20ms to 50ms (TWT), with an average of approximately 35ms to 40ms (TWT) (Figure 5.23). The unit thickness in the adjacent areas of the dome ranges from 85ms (TWT) in the northeast to 50ms (TWT) in the southwest (Figure 5.23).

At the Veslekari Dome the unit onlaps the diapir, with a thickness of 35-45ms (TWT) in the north, south and east, being slightly thicker in the west at 60ms (TWT) (Figure 5.8, 5.17 and 5.23). The unit is truncated by the sea floor at a depth of 370ms (TWT), at which it has a thickness of 35-45ms (TWT) (Figure 5.8, 5.17 and 5.23).

The unit drapes the Fedynsky High, thinning from a thickness of 20-50ms (TWT) off the high to 10-15ms (TWT) at the shallowest point of the high (Figure 5.23). The amount of thinning is greatest from the northwest, moderate from the north and west and lowest from the south and southwest (Figure 5.15 and 5.16). From the Tor-Iversen Fault Complex to the Tiddlybanken Basin, Signalhorn Dome and Finnmark Platform, the unit thins (Figure 5.4 and 5.23). At the Tor-Iversen Fault Complex the unit is 40-50ms (TWT), being reduced to 30-35ms (TWT) at the north margin of the Tiddlybanken Basin (Figure 5.23).

Within the Tiddlybanken Basin the Hekkingen Formation increases up to 65ms (TWT) at the most but averaging at 20-35ms (TWT) (Figure 5.23). At the Signalhorn Dome the unit thickness averages 30ms (TWT) at the margins, and 10-15ms (TWT) at the shallowest section of the dome (Figure 5.13 and 5.23). To the south of the Signalhorn Dome the thickness increases to 30-35ms (TWT), followed by a decrease and truncation at the Finnmark Platform, at which the unit thickness is 10-15ms (TWT) (Figure 5.4 and 5.23).

The internal configuration of the Hekkingen Formation is parallel, with a low to medium amplitude. An observable internal configuration is identified in areas where the unit exceeds 35-50ms (TWT) in thickness, such as within the Nordkapp Basin and on the Bjarmeland Platform (Figure 5.4 and 5.23). Within the Nordkapp Basin the unit is discontinuous to continuous, having a medium to low amplitude reflection (Figure 5.4 and 5.9). In the northeast of the basin the reflections have a medium to low amplitude, and a continuous, parallel seismic configuration.

Onto the Signalhorn Dome, Finnmark Platform and into the Tiddlybanken Basin the unit lacks a seismic reflection geometry as it is close to, or below the vertical seismic resolution of the data (Figure 5.4 to 5.6 and 5.13). Onto the Fedynsky High internal seismic reflections can be identified in the thickest section of the unit, disappearing as the unit thins to below seismic resolution onto the shallower sections of the high (Figure 5.16). North on the Fedynsky High the unit is parallel and discontinuous to continuous, with a low amplitude (Figure 5.14 and 5.15). This seismic configuration is retained onto the south margin of the Haapet Dome (Figure 5.6). In the shallowest section of the dome, the unit has a low amplitude, with a parallel, discontinuous to continuous internal configuration (Figure 5.7 and 5.12). In the east of the dome the reflections are continuous, parallel with a low amplitude, while highly discontinuous with low amplitudes in the west (Figure 5.7). On the Bjarmeland Platform the seismic configuration of the unit differs from the rest of the dataset. In the east by the Haapet Dome the unit has a low amplitude and is highly discontinuous (Figure 5.7). Westward its continuity ranges from continuous to discontinuous, with a low to medium amplitude (Figure 5.7). With the increased thickness of the unit in the west, a continuous parallel configuration with a medium amplitude becomes observable (Figure 5.4, 5.7 and 5.23). From south to north on the platform the internal configuration is sub-parallel, discontinuous, with a low amplitude (Figure 5.4). At the Veslekari Dome the internal configuration of the unit is parallel and discontinuous on all sides of the dome (Figure 5.8 and 5.17).

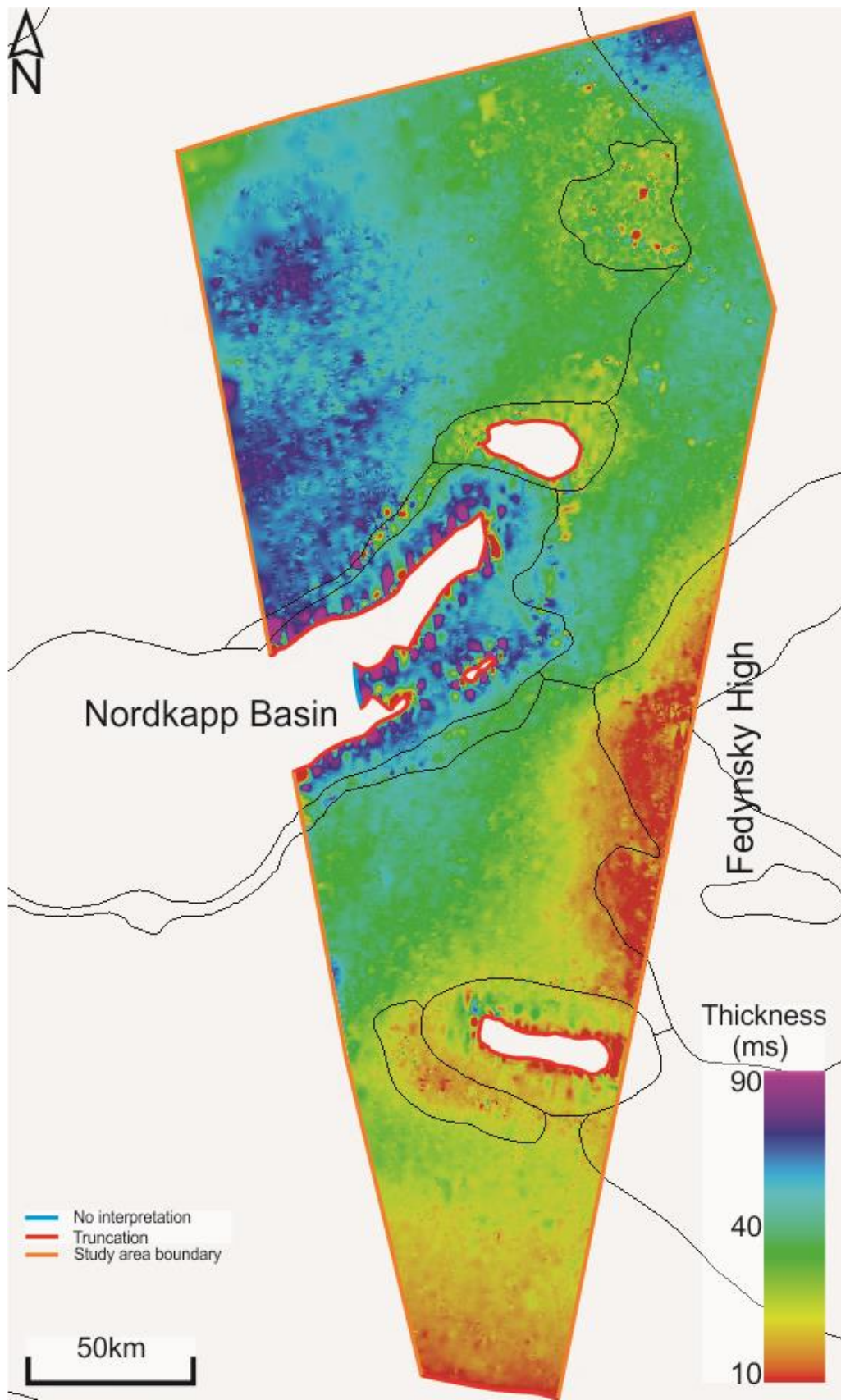


Figure 5.23 Time-thickness map of the Hekkingen Formation, thickness is illustrated in TWT (ms). Red lines indicate truncation of the unit, blue lines indicate the edge of the interpreted top and base horizons of the unit and orange lines indicate the study area boundary.

## 5.7 Top Hekkingen horizon

The Hekkingen horizon is the upper boundary of the Hekkingen Formation separating the Late Jurassic deposits from the Cretaceous deposits (Figure 5.1). The acoustic impedance of the boundary is represented by a negative reflection coefficient throughout the dataset. The reflection is continuous to discontinuous, with a high to low amplitude.

Within the Nordkapp Basin the horizon is continuous, with decreasing amplitude from high to low as the reflector onlaps the salt diapirs in the centre of the basin (Figure 5.4). At the margins of the basin, fault activity has influenced the continuity of the horizon resulting in it being discontinuous (Figure 5.4). From the Tor-Iversen Fault Complex in the north to the Finnmark Platform in the south the reflection is characterized with a high amplitude (Figure 5.4). It is mostly continuous but is influenced by fault with a throw of as much as 60ms (TWT) on the Signalhorn Dome (Figure 5.13). Within the Tiddlybanken Basin the reflection is highly continuous, with a high amplitude (Figure 5.5). Onto the Fedynsky High the horizon has a continuous reflection geometry. Its seismic amplitude is strong in the deeper sections, with a decrease in amplitude in close proximity to the shallowest points of the high (Figure 5.14 to 5.16). This decrease in seismic amplitude is mapped and illustrated in (Figure 5.24)

North of the Fedynsky High and south of the Haapet Dome, the reflection has a continuous character and high amplitude (Figure 5.6). Onto the Haapet Dome the horizon is overall continuous, influenced by faulting with average throws of 25-50ms (TWT) (Figure 5.12). The seismic amplitude of the horizon is low in several areas along the top of the dome (Figure 5.12), with the return of a strong continuous configuration north, east and west of the dome (Figure 5.7 and 5.12).

Throughout the Bjarmeland Platform the reflection has a strong amplitude (Figure 5.4 and 5.7). It is continuous on most of the platform, influenced by several smaller and larger faults averaging a throw of 25-50ms (TWT). Towards the Veslekari Dome the reflection has a continuous character from the north, with a medium to high amplitude (Figure 5.17). In the south, east and west the reflection continuity ranges from continuous to discontinuous, with a low to high amplitude (Figure 5.8 and 5.17). The horizon is influenced by faulting on the south, east and west side of the dome in the same manner as for the former horizons, with a throw of 20-100ms (TWT) separating the horizon.



The depth at which the horizon is situated ranges throughout the dataset in much of the same way as for the former horizons. Its depth ranges from 1500ms (TWT) at the deepest within the Nordkapp Basin to 250ms (TWT) at the shallowest in the northwest on the Bjarmeland Platform (Figure 5.25).

Within the Nordkapp Basin the horizon is at the deepest, situated at 1200-1500ms (TWT) in the south and 1150-1350ms (TWT) in the north (Figure 5.25). The horizon onlaps the salt diapirs in the centre of the basin, in the same manner as for the former horizons (Figure 5.4). Towards the basin margins horizon depth decreases by 180-200ms (TWT) in the south and 50-300ms (TWT) in the north (Figure 5.4 and 5.25). By the Polarstjernen Fault Complex in the north, fault throw ranges from 0-220ms (TWT) and 0-50ms (TWT) along the Tor-Iversen Fault Complex in the south (Figure 5.4).

At the Bjarmeland Platform the horizon shallows from 800-1150ms to 280-550ms (TWT) from south to north and 650ms to 520ms (TWT) from west to east (Figure 5.25). In the centre of the platform a 800ms (TWT) section is present (Figure 5.7 and 5.25). On the Haapet Dome the horizon is situated at 470ms (TWT) at its shallowest (Figure 5.17 and 5.25). At the Fedynsky High the horizon is located at 410ms (TWT) and 675ms (TWT) at its shallowest by the larger and smaller structure respectively (Figure 5.14 to 5.16 and 5.25).

At the Tor-Iversen Fault Complex the horizon depth ranges from 1000-1340ms (TWT) from west to east (Figure 5.25). The depth of the horizon is reduced to 720ms (TWT) on the Signalhorn Dome and 380ms (TWT) at the truncation of the horizon on the Finnmark Platform in the south (Figure 5.4, 5.13 and 5.25). Into the Tiddlybanken Basin depths increase from 830-1000ms (TWT) and 700-850ms (TWT) at the north and south margin, to 1200-1310ms (TWT) and 1110-1220ms (TWT) within the basin, respectively (Figure 5.5, 5.6 and 5.25). The horizon onlaps the diapirs in the centre of the basin in the same manner as within the Nordkapp Basin, truncating the sea floor at a depth of 370ms (TWT) (Figure 5.5 and 5.6). At the Veslekari Dome the horizon shallows from 920-1000ms (TWT) at the dome margins, truncating at the sea floor at 375ms (TWT) (Figure 5.8, 5.17 and 5.25).

Into the Tiddlybanken Basin depths increase from 830-1000ms (TWT) and 920-1000ms (TWT) at the north and south margin respectively, to 1200-1310ms (TWT) and 1110-1220ms (TWT) (Figure 5.5, 5.6 and 5.25). The horizon onlaps the diapirs in the centre of the basin in the same manner as within the Nordkapp Basin, truncating at the sea floor at a depth of

370ms (TWT) (Figure 5.5 and 5.6). At the Veslekari Dome the horizon shallows from 920-1000ms (TWT) at its margins, truncating at a close to identical depth as for the horizon in the Tiddlybanken Basin (Figure 5.8, 5.17 and 5.25).



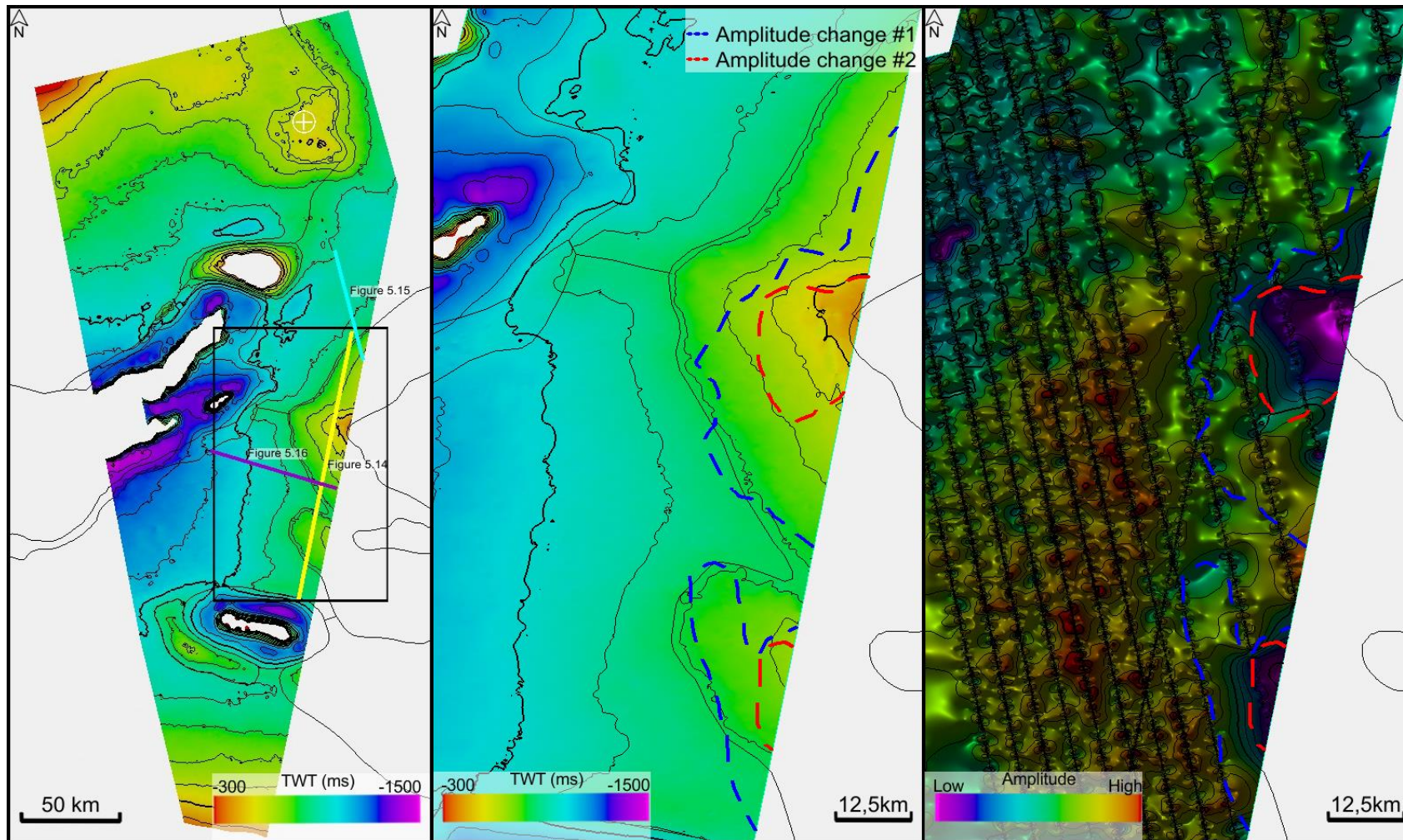


Figure 5.24 Time-structure maps (left and middle) and a RMS amplitude surface (right), illustrating the location and extent in the low amplitudes on the Fedynsky High. The blue and red line is amplitude changes documented along each individual seismic line onto the Fedynsky High. Amplitude change #1 indicate the first amplitude change of the horizon. Amplitude change #2 indicate locations of abrupt decrease in amplitude. These changes are illustrated along seismic profiles (Figure 5.14 – 5.16).

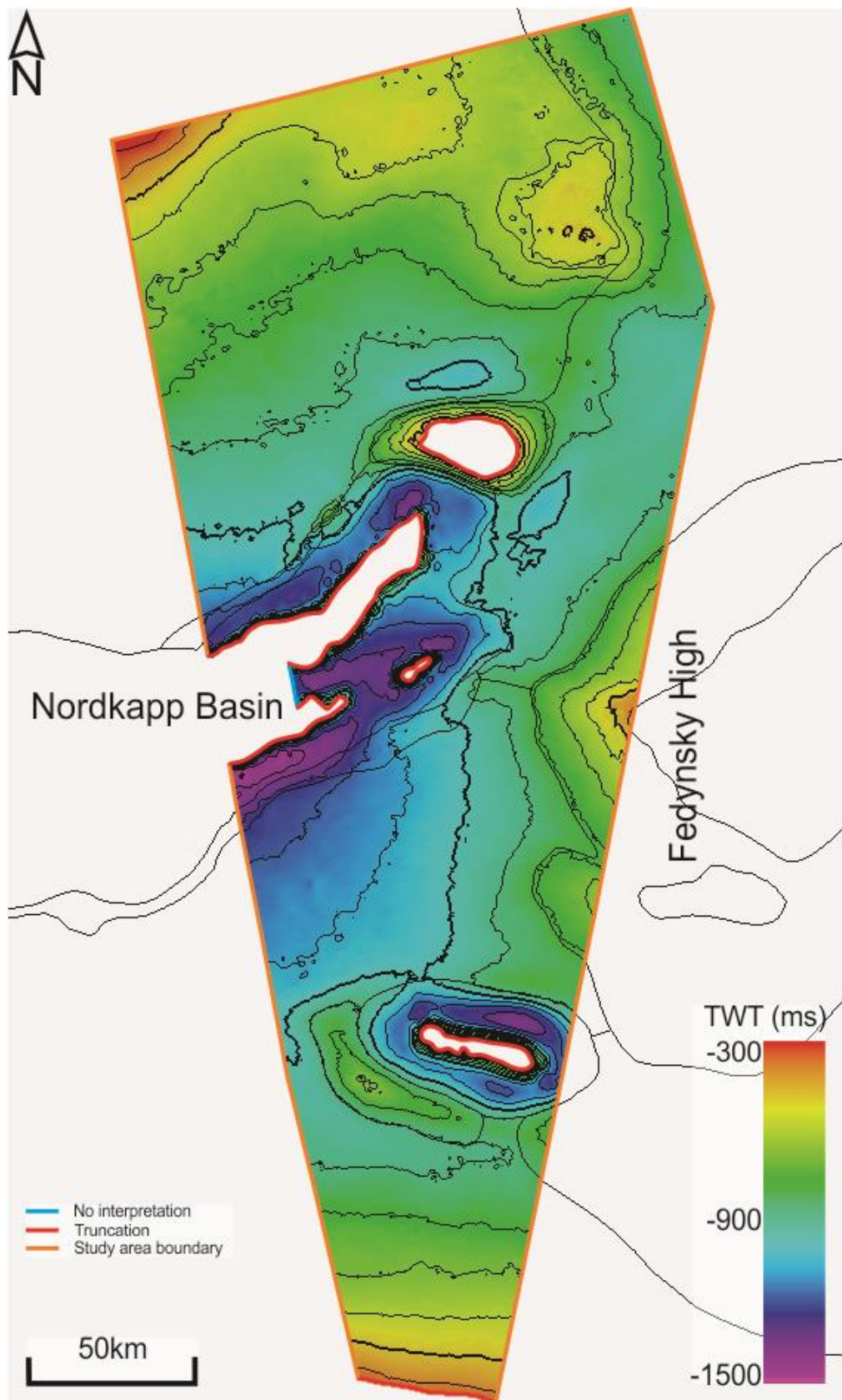


Figure 5.25 Time-structure map of the Top Hekkingen horizon, with depth in ms (TWT). Red lines indicate truncation of the horizon, blue lines indicate the edge of the interpreted horizon and orange lines indicate the study area boundary.

Table 5 Summary of the result chapter (Section 5), summarising the: amplitude, continuity, reflection configuration, fault influence, fault throw, unit thickness and truncations of the horizons and units.

Formation/Unit	Bjarmeland Platform	Haapet Dome	Veslekari Dome	Fedynsky High	Nordkapp Basin	Signalhorn Dome	Tiddlybanken Basin	Finnmark Platform
Top Hekkingen horizon (Section 5.7)	<ul style="list-style-type: none"> <li>High amplitude.</li> <li>Continuous reflection.</li> <li>Faulting; 25-50ms (TWT) average.</li> </ul>	<ul style="list-style-type: none"> <li>Low to high amplitude.</li> <li>Continuous reflection.</li> <li>Faulting; 25-50ms (TWT) average.</li> </ul>	<ul style="list-style-type: none"> <li>Medium to high amplitude, in the north.</li> <li>Low to high amplitude, in the south, east and west.</li> <li>Continuous in the north.</li> <li>Discontinuous to continuous in the south, west and east.</li> <li>Faulting; 20-100ms (TWT) average, in the south, east and west.</li> </ul>	<ul style="list-style-type: none"> <li>High to low amplitude, decrease to low by the shallowest section.</li> <li>Continuous reflection.</li> <li>Traceable on the entire high.</li> </ul>	<ul style="list-style-type: none"> <li>High to low amplitude, decrease onto the salt diapirs.</li> <li>Continuous reflection.</li> <li>Faulting; PFC: 0-220ms (TWT) average. TIFC: 0-50ms (TWT) average.</li> </ul>	<ul style="list-style-type: none"> <li>High amplitude.</li> <li>Continuous reflection.</li> <li>Faulting; as much as 60ms (TWT) throw.</li> </ul>	<ul style="list-style-type: none"> <li>Continuous reflection.</li> <li>High amplitude.</li> </ul>	<ul style="list-style-type: none"> <li>Continuous reflection.</li> <li>High amplitude.</li> </ul>
Hekkingen Formation (Section 5.6)	<ul style="list-style-type: none"> <li>Thickness of 40-90ms (TWT).</li> <li>70-90ms (TWT), west and southwest.</li> <li>40ms (TWT), east and northwest.</li> <li>Discontinuous, low amplitude in the east.</li> <li>Continuous, parallel, medium amplitude, in the west.</li> </ul>	<ul style="list-style-type: none"> <li>Average thickness of 35-40ms (TWT).</li> <li>Parallel, discontinuous to continuous.</li> <li>Low amplitude.</li> </ul>	<ul style="list-style-type: none"> <li>Thickness of 35-45ms (TWT), north, south and east.</li> <li>Thickness of 60ms (TWT), west.</li> <li>Truncated by seafloor at 370ms (TWT).</li> <li>Thickness at point of truncation, 35-45ms (TWT).</li> <li>Parallel and discontinuous.</li> </ul>	<ul style="list-style-type: none"> <li>Thickness of 20-50ms (TWT) off the high, 10-15ms (TWT) at shallowest section on the high.</li> <li>Parallel, discontinuous to continuous.</li> <li>Low amplitude</li> <li>Thins onto the high, to less than resolution.</li> </ul>	<ul style="list-style-type: none"> <li>Thickness of 70-90ms (TWT).</li> <li>Pinch-out onto diapirs.</li> <li>Discontinuous to continuous, low to medium amplitude.</li> <li>Observable thickness variations across faults. Especially in the southern sub-basin.</li> </ul>	<ul style="list-style-type: none"> <li>Thickness of 10-30ms (TWT).</li> <li>Close to, or below vertical resolution of the data.</li> </ul>	<ul style="list-style-type: none"> <li>Average thickness of 20-35ms (TWT), 65ms (TWT) at the most.</li> <li>Thickness of 30-35ms (TWT) at north margin.</li> <li>Close to, or below vertical resolution of the data.</li> </ul>	<ul style="list-style-type: none"> <li>Thickness of 10-15ms (TWT).</li> <li>Truncated at Sea-floor.</li> <li>Close to, or below vertical resolution of the data.</li> </ul>
Top Fuglen horizon (Section 5.5)	<ul style="list-style-type: none"> <li>Low to high amplitude increase from north to south</li> <li>Continuous reflection.</li> <li>Faulting; 25-50ms (TWT) average throw.</li> </ul>	<ul style="list-style-type: none"> <li>High amplitude.</li> <li>Continuous reflection.</li> <li>Faulting; 25-50ms (TWT) average throw.</li> </ul>	<ul style="list-style-type: none"> <li>High amplitude in the north, east and west.</li> <li>Continuous in the north east and west.</li> <li>Discontinuous in the south.</li> <li>Faulting; 20-100ms (TWT) throw range in the east, west and south.</li> </ul>	<ul style="list-style-type: none"> <li>High to low amplitude, decrease towards shallower section.</li> </ul>	<ul style="list-style-type: none"> <li>High amplitude.</li> <li>Continuous reflection.</li> <li>Faulting; PFC: 0-210ms (TWT) average. TIFC: -20-90ms (TWT) average.</li> </ul>	<ul style="list-style-type: none"> <li>High amplitude.</li> <li>Continuous reflection.</li> <li>Faulting; 20-60ms (TWT) average throw.</li> </ul>	<ul style="list-style-type: none"> <li>High amplitude.</li> <li>Continuous reflection.</li> </ul>	<ul style="list-style-type: none"> <li>High amplitude.</li> <li>Continuous reflection.</li> </ul>



Fuglen Formation (Section 5.4)	<ul style="list-style-type: none"> <li>Thickness range, 15-50ms (TWT).</li> <li>45ms to 50ms (TWT), from south to north.</li> <li>15ms to 50ms (TWT), from east to west.</li> <li>Internal configuration; parallel, discontinuous to continuous from north to south.</li> <li>Sub-parallel to parallel, continuous configuration, with local discontinuous intervals.</li> </ul>	<ul style="list-style-type: none"> <li>Average thickness of 15ms (TWT).</li> <li>Parallel, continuous to discontinuous.</li> <li>Low to medium amplitudes at margins and high at the top of the dome.</li> </ul>	<ul style="list-style-type: none"> <li>Uniform thickness of 30-50ms (TWT).</li> <li>Truncated by sea-floor.</li> <li>Sub-parallel, discontinuous in the north, south and west.</li> <li>Chaotic in the east.</li> </ul>	<ul style="list-style-type: none"> <li>Truncated at the base of the Hekkingen Formation.</li> <li>West: Parallel, discontinuous, below resolution at shallower section.</li> <li>North: continuous, sub-parallel to parallel and no apparent internal reflectors close to the unit termination.</li> </ul>	<ul style="list-style-type: none"> <li>Thickness of 55-90ms (TWT), north.</li> <li>Thickness of 50-80ms (TWT), south.</li> <li>Onlaps the salt diapirs.</li> <li>Internal configuration; sub-parallel, discontinuous.</li> <li>Observable thickness variations across faults.</li> </ul>	<ul style="list-style-type: none"> <li>Truncated at the base of the Hekkingen Formation.</li> <li>Discontinuous and sub-parallel.</li> </ul>	-	-
Top Stø horizon (Section 5.3)	<ul style="list-style-type: none"> <li>Low amplitude.</li> <li>Discontinuous reflection.</li> <li>Faulting; 25-50ms (TWT) average throw.</li> </ul>	<ul style="list-style-type: none"> <li>High amplitude.</li> <li>Discontinuous reflection.</li> <li>Faulting; 25-50ms (TWT) average throw.</li> </ul>	<ul style="list-style-type: none"> <li>Low amplitude.</li> <li>Discontinuous reflection.</li> <li>Faulting; average throw of 100ms (TWT) in the south and 20-30ms (TWT) in the east and west.</li> </ul>	<ul style="list-style-type: none"> <li>Low amplitudes.</li> <li>Discontinuous to continuous reflection.</li> <li>Decreasing amplitude onto high from north.</li> <li>Increasing amplitude onto high from west.</li> <li>Terminating at the base of the Hekkingen Formation.</li> </ul>	<ul style="list-style-type: none"> <li>Low amplitude.</li> <li>Discontinuous reflection.</li> <li>Faulting; PFC: 30-220ms (TWT) average throw.</li> <li>TIFC: 0-110ms (TWT) average throw.</li> </ul>	<ul style="list-style-type: none"> <li>Low amplitude.</li> <li>Continuous to discontinuous reflection.</li> <li>Faulting; 20-60ms (TWT) average throw.</li> <li>Terminating at the base of the Hekkingen Formation.</li> </ul>	-	-
Realgrunnen Subgroup (Section 5.2)	<ul style="list-style-type: none"> <li>Lower section: discontinuous to chaotic, low to medium amplitudes.</li> <li>Upper section: continuous, parallel, medium amplitudes.</li> <li>Thinning north to south, 95ms (TWT) north, 60-80ms (TWT) south)</li> </ul>	<ul style="list-style-type: none"> <li>Medium to high amplitudes.</li> <li>Discontinuous, parallel to chaotic configuration.</li> <li>Thickness of 130-180ms (TWT)</li> </ul>	<ul style="list-style-type: none"> <li>Discontinuous to chaotic.</li> <li>Low amplitudes.</li> <li>Thickness, 60-80ms (TWT).</li> <li>Truncated at the seafloor.</li> </ul>	<ul style="list-style-type: none"> <li>Upper section: Amplitudes increase from low/medium to medium/high, from west to east.</li> <li>Lower section: Low to medium amplitudes.</li> <li>Discontinuous to continuous reflections. Parallel to subparallel configuration.</li> </ul>	<ul style="list-style-type: none"> <li>Continuous, subparallel in the south.</li> <li>Low to medium amplitudes.</li> <li>Thickness, 125-135ms (TWT). Observable thickness variations across faults.</li> </ul>	<ul style="list-style-type: none"> <li>Discontinuous to continuous reflections. Parallel to sub-parallel configuration.</li> <li>Low to medium amplitudes.</li> <li>Truncated at the base of the Hekkingen Formation.</li> </ul>	-	-

				<ul style="list-style-type: none"> <li>Truncated at the base of the Hekkingen Formation.</li> </ul>				
<p>Top Snadd horizon (Section 5.1)</p>	<ul style="list-style-type: none"> <li>Continuous reflection.</li> <li>Low amplitude</li> <li>Faulting; 25-50ms (TWT) average throw.</li> </ul>	<ul style="list-style-type: none"> <li>Low amplitude.</li> <li>Discontinuous reflection.</li> <li>Faulting; 25-50ms (TWT) average throw.</li> </ul>	<ul style="list-style-type: none"> <li>Low amplitude.</li> <li>Discontinuous reflection.</li> <li>Extensively faulted in the south and west.</li> </ul>	<ul style="list-style-type: none"> <li>Continuous reflection.</li> <li>Low amplitude</li> <li>Terminating at the base of the Hekkingen Formation</li> </ul>	<ul style="list-style-type: none"> <li>Continuous to semi-continuous reflection.</li> <li>Low amplitude</li> <li>Faulting; TIFC: &lt;70ms (TWT) throw.</li> <li>Limited seismic correlation into basin.</li> </ul>	<ul style="list-style-type: none"> <li>Discontinuous reflection.</li> <li>Low to medium amplitude.</li> <li>Faulting; 20-60ms (TWT) average throw.</li> <li>Terminating at the base of the Hekkingen Formation</li> </ul>	-	-

## 6 Discussion

The Realgrunnen Subgroup, Fuglen Formation and Hekkingen Formation all display regional and local differences in thickness and internal seismic facies. These differences are observed laterally within each individual unit, as well as stratigraphically between the units. In the following chapter, the suggested syn- and post-depositional evolution of each unit will be discussed. Lateral and stratigraphic differences of the intervals will be integrated with, and discussed in light of, the large-scale structural evolution of the study area.

The discussion is structured as follows. For each unit discussed, first, the observed internal seismic facies is evaluated as indications of depositional environments, in combination with the observed regional thickness trends of the respective unit. Following this the implications for the structural evolution will be addressed, with emphasis to the detailed mapping of the unit.

### 6.1 Depositional and structural development

Previously conducted detailed work on the late Norian to Tithonian structural and depositional evolution within the Barents Sea South East is limited. The structural development of the study area has been proposed by several authors (Mattingsdal et al., 2015; Gernigon et al., 2018; Müller et al., 2019; Hassaan et al., 2020), whereas the depositional and lithological aspects of the area are significantly less explored. Regional studies (Smelror et al., 2009; Henriksen et al., 2011) has been important in the correlation of depositional environment and lithology, as well-data is limited.

#### **Late Norian to Bajocian – the Realgrunnen Subgroup**

The Realgrunnen Subgroup (late Norian to Bajocian) in the Norwegian Barents Sea South, is represented by coastal and deltaic deposits (Müller et al., 2019). This unit displays a southward thinning trend with, 120-130ms (TWT) to the north and 70ms (TWT) to the south, a change of 60ms (TWT) over a distance of 290 km (Section 5.2). The thickness trend of the unit could possibly reflect a regional trend of slightly increased accumulation space in the north of the study area during the late Norian to Bajocian (Figure 6.1, A-B).

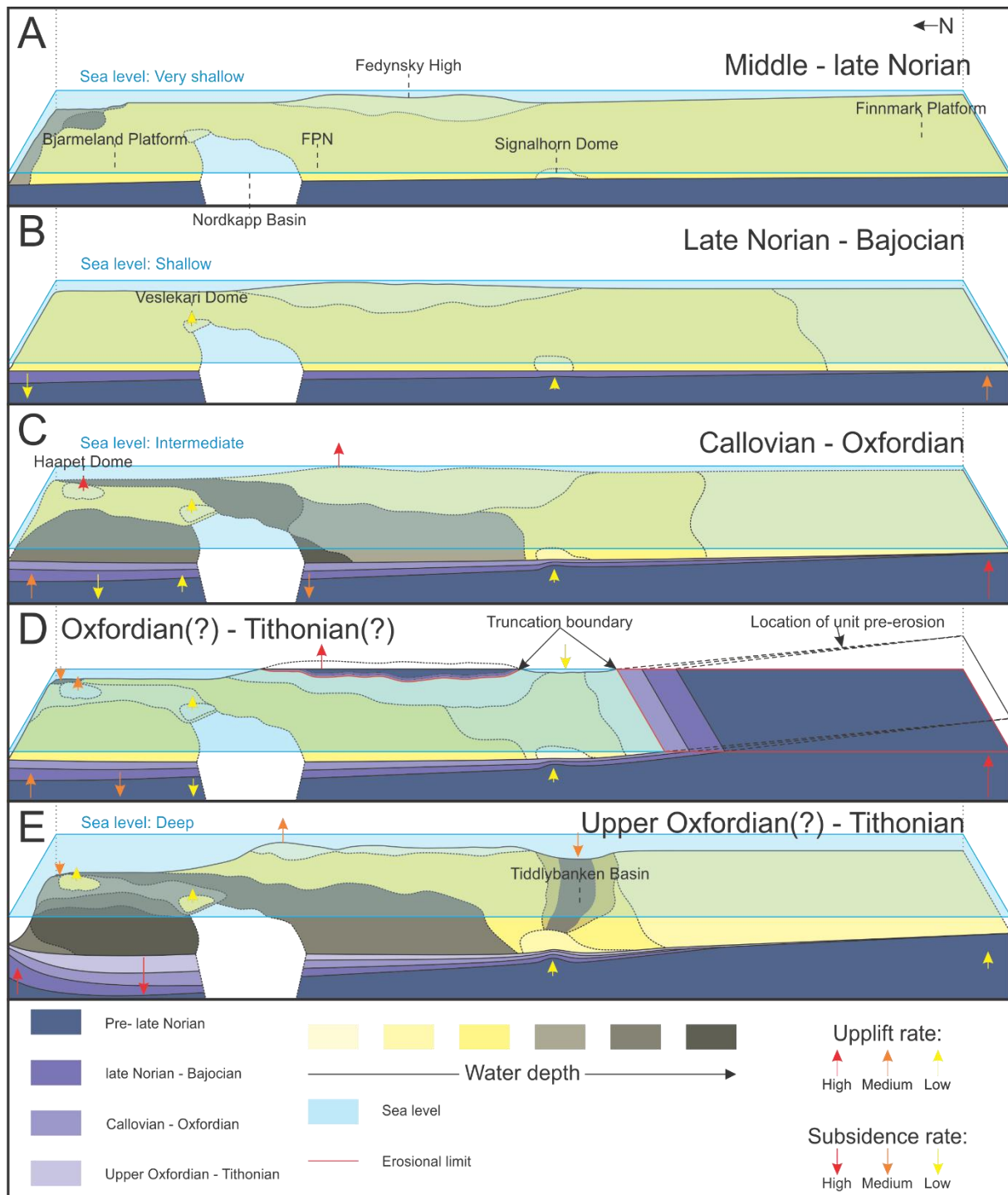


Figure 6.1, A-E, Conceptual model of the suggested depositional environment and structural evolution of the late Norian to Tithonian. A) Middle – late Norian structural configuration of the study area pre-deposition of late Norian – Bajocian, Realgrunnen Subgroup. B) Late Norian – Bajocian uplift/ subsidence, Bajocian water depths and the late Norian – Bajocian structural influence on the units. C) Callovian - Oxfordian uplift/ subsidence, Oxfordian water depths and the late Norian – Oxfordian structural influence on the units. D) Oxfordian(?) – Tithonian(?) regression event, as a result of possible local uplifting of the Fedynsky High and Finnmark Platform. Syn-Fulgen Formation, Pre-Hekkingen Formation uplift/subsidence and syn-erosional sea level. E) Post-regression (upper Oxfordian) – Tithonian uplift/ subsidence, Tithonian water depths and the late Norian – Tithonian structural influence on the units. Red, orange and yellow arrows illustrate the rate of uplift/ subsidence, concurrent to the subsequent deposits of the time interval illustrated. The dark purple to light purple illustrate the documented thickness variations of the late Norian – Tithonian deposits in a north-south orientation.

The Realgrunnen Subgroup is represented by seismic discontinuous to chaotic, medium to low amplitudes in the lower section and a relatively continuous, medium amplitudes in the upper section (Section 5.2), believed to indicate an upwards change in lithology and/ or depositional environment of the unit. The discontinuous reflection geometry may imply a fluctuating energy regime during deposition or, post-depositional deformation of the unit (Mitchum et al., 1977b; Veeken, 2007). The discontinuous to chaotic configuration of the upper section is limited to the extensively faulted areas along the north and south margin of the Nordkapp Basin and the Haapet Dome (Figure 5.4, 5.6 and 5.12). This suggests the chaotic configuration of the upper section to be the possible result of post-depositional deformation. The discontinuous to chaotic configuration of the lower section is not limited to the extensively faulted part of the study area. The prevalence of the discontinuous to chaotic configuration could possibly suggest a volatile, high-energy depositional regime. The regression event of the Late Triassic – Early Jurassic (Section 2.2.1.1 and 2.2.1.2), would possibly facilitate a shallow-marine environment or sedimentary bypassing, which are commonly associated with high-energy regimes (Mitchum et al., 1977b; Catuneanu et al., 2011). The continuous configuration of the upper section could reflect the following transgression in the Early – Middle Jurassic (Section 2.2.1.2), in which a higher sea level may have reduced the fluctuation of the energy regime, aiding the deposition of sediments in the observed continuous seismic configuration (Veeken, 2007; Catuneanu et al., 2011). A regression is documented to have occurred in retrospect of the Early – Middle Jurassic transgression (Section 2.2.1.2), whereas no clear indication of this event was observed in the seismic data. The constant medium amplitude of the upper section may imply minimal lateral variation in the lithological composition of the section (Mitchum et al., 1977b). The suggested high-energy regime of the lower section of the unit, would primarily promote the deposition of coarse-grained sandy sediments (Mitchum et al., 1977b). The Stø and Nordmela formations, presumably of the upper section, has a sandy lithology documented in the 7435/12-1 (Korpfjell) well by Equinor in 2018 (NPD, 2019). The upper and lower section is thus suggested have a sandy composition. The decrease in amplitude from the upper to the lower section, imply a downwards decrease in acoustic impedance contrast within the Realgrunnen Subgroup (Section 3). Kearey et al. (2013) states that the velocity and density of



sedimentary deposits can be influenced by post-depositional processes, such as cementation, compaction and fluid content (Section 3).

In the northeast part of the study area, at the Haapet Dome and within the south of the Nordkapp Basin, noticeably thicker (80-180ms TWT) accumulations of sediments are documented (Figure 5.19, Section 5.2). This observation might suggest that these areas represent local areas of increased accumulation (Figure 6.1, A-B and 6.2, A). The thickness trend of the diapiric rim synclines and thickness increase across faults into the Nordkapp Basin could reflect syn-depositional subsidence and fault movements. The current dome configuration of the Haapet Dome would not facilitate such a thicker sediment accumulation over a high, thus suggesting a basin configuration of the element during the late Norian to Bajocian (Figure 6.1, A and 6.2, A).

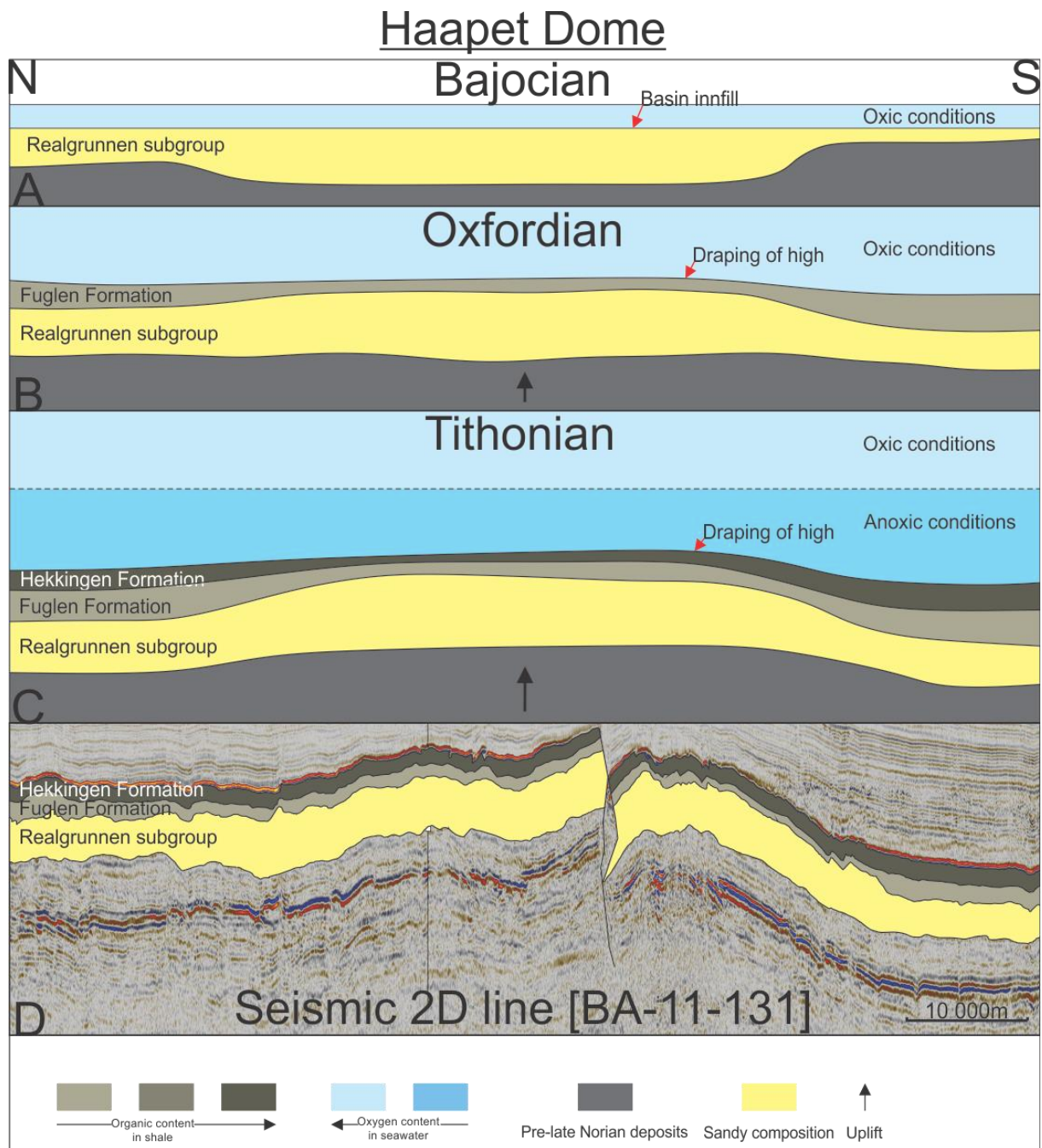


Figure 6.2 Conceptual model of the Haapet Dome, from the Bajocian (1) to the Tithonian (5). 1) Bajocian: The Realgrunnen Subgroup has been deposited, and an additional accumulation of sediments has infilled the late Norian basin configuration of the Haapet Dome. Slight uplifting has possibly commenced during the late Norian to Bajocian. 2) Oxfordian: The Fulgen Formation has been deposited during the Callovian to Oxfordian, coinciding with an inversion of the basin into a dome. This is observable through the observable thinning and draping of the Haapet Dome, by the Fuglen Formation. 3) Tithonian: The upper Oxfordian – Tithonian Hekkingen Formation has been deposited, draping the dome in a similar manner as for the Fuglen Formation. Anoxic deep water conditions commenced during the deposition of the Hekkingen Formation, illustrated by the dotted line. 4) Present-day configuration: Seismic 2D line [BA-11-131] (Figure, 5.2 and 5.12), illustrating the thickness and configuration of the units across the dome and the configuration of the Haapet Dome.

On the Bjarmeland Platform, the thickness of the unit is relatively constant at 80-90ms (TWT) throughout the platform areas, with a slight thickness increase to 120-130ms (TWT) towards the north of the platform (Figure 5.19). The thickness increase of the unit follows the northward thickening trend of the entire Realgrunnen Subgroup, believed to be the result of a pre- and/ or syn- depositional subsidence in the northern region of the platform (Figure 6.1, A-B). This is also believed to be the case for the north section of the Finnmark Platform (Figure 6.1, A-B). The uniform thickness of the Realgrunnen Subgroup across faults in both areas (Section 5.2), could possibly reflect a minimal amount of syn-depositional fault influence on the two areas. The Bjarmeland Platform and the north section of the Finnmark Platform are thus believed to have been relatively stable platforms during the late Norian to Bajocian (Figure 6.1, A-B).

The Realgrunnen Subgroup thins towards the Fedynsky High and Finnmark Platform (Figures 5.6, 5.9 and 5.14-5.16), and is truncated along the lower boundary of the Hekkingen Formation on both structural elements. This reflects the occurrence of an erosional event, making the lateral south- and eastward extent of the interval uncertain in these areas (Figure 5.6, 5.9, 5.10, 5.13-5.16 and 6.1, D). The thinning of the unit is observed in the north and west of the Fedynsky High and north of the Finnmark Platform (Section 5.1-5.3). This could imply that the Realgrunnen Subgroup possibly overlapped both the Fedynsky High and Finnmark Platform prior to the erosional event, reflecting their presence as elevated areas during the late Norian to Bajocian (Figure 6.1, A-B and 6.3, A-B). The angular difference between the Hekkingen Formation base and the lower and upper boundary of the Realgrunnen Subgroup, implies that both the Fedynsky High and Finnmark Platform experienced significant uplift and erosion (Figure 5.13-5.16, 6.1, A-D and 6.3, A-D). There are no clear signs of syn-depositional brittle deformation of the Realgrunnen Subgroup, in terms of thickness variations within the study area, except for the Nordkapp Basin (Section 5.1-5.3). This does imply that the primary cause for uplift and subsidence of the structural elements could be related to the reactivation of deep lineaments. The reactivation of such deep seated lineaments would coincide time-wise with the documented final upthrusting of the Novaya Zemlya which occurred in the Late Triassic –Early Jurassic (Hassaan et al., 2020). In Müller et al. (2019) the uplift and erosion of the Fedynsky High are linked as a response to the Novaya Zemlya.

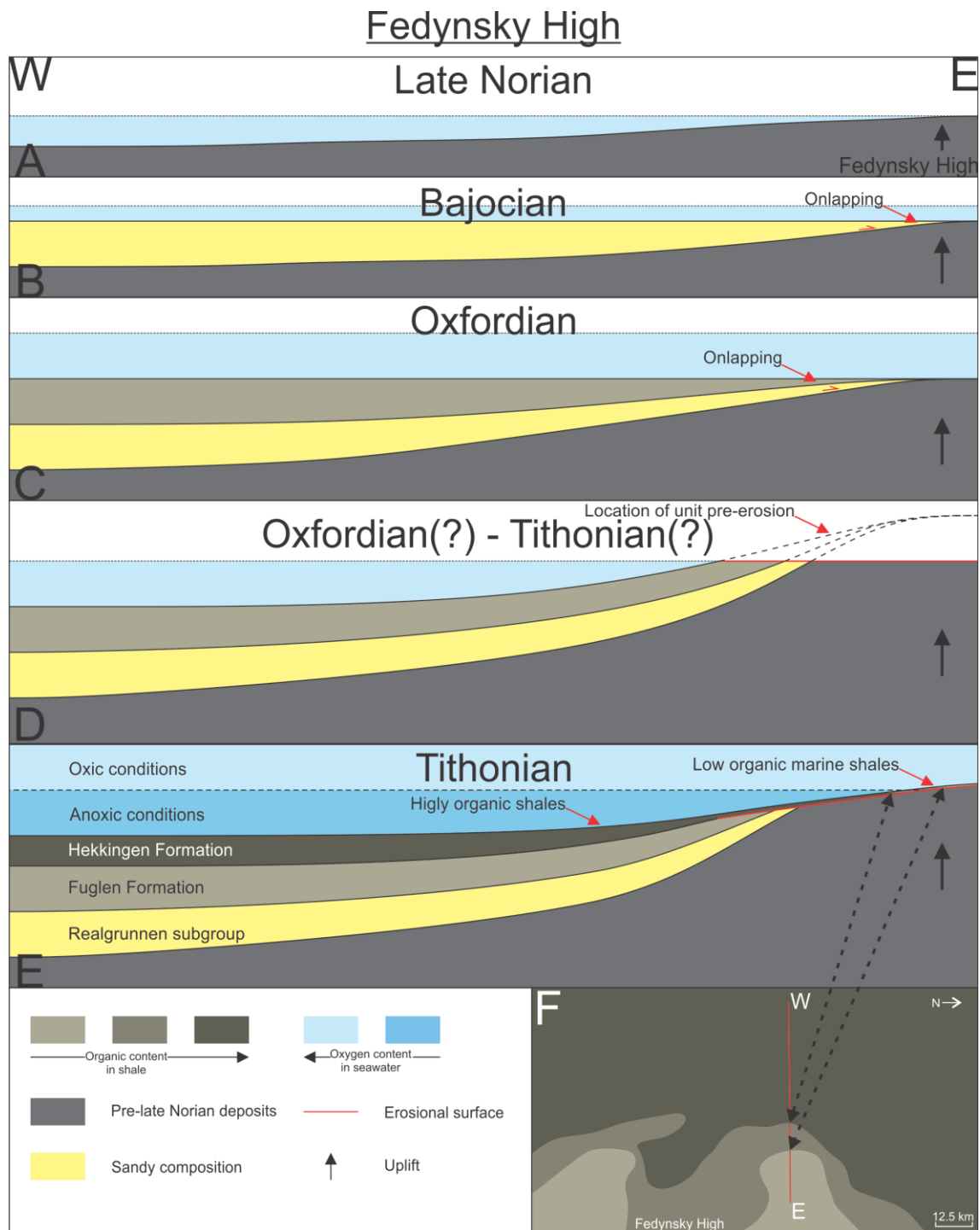


Figure 6.3 Conceptual model of the suggested structural and depositional evolution at the Fedynsky High of the late Norian (A) to Tithonian (E). A) Late Norian structural configuration of the Fedynsky High. B) Bajocian: The Realgrunnen Subgroup has been deposited, having a sandy composition. The unit is onlapping the Fedynsky High, with no significant uplift influencing the Subgroup. C) Oxfordian: The Fulgen Formation has been deposited, with minor uplifting influencing the underlying Realgrunnen Subgroup. D) Oxfordian(?) – Tithonian(?): Significant uplifting and erosion occurred in the transition between the deposition of the Fuglen and Hekkingen formations, causing the truncation of the Realgrunnen Subgroup and Fuglen Formation. E) Tithonian: The Hekkingen Formation has been deposited, overlying the truncated Realgrunnen Subgroup and Fuglen Formation. Anoxic conditions dominated in the deeper sections of the shelf during the upper Oxfordian - Tithonian, during which high organic shales were deposited (dark brown). F) Map of the Fedynsky High, illustrating the organic content of the Hekkingen Formation onto the Fedynsky High. The map were created with the use of (Figure 5.14 – 5.16 and 5.24) as references and is oriented with its north arrow pointing right.

A minor decrease in thickness of 10ms and 10-20ms (TWT) of the Realgrunnen Subgroup are observed across the Signalhorn and Veslekari domes, respectively (Section 5.2, Figure 5.13, 5.17 and 5.19). The decrease in thickness implies that both represented, structurally elevated areas during the late Norian to Bajocian (Figure 6.1, A-B and 6.4, A). This initial doming of the Signalhorn Dome possibly occurred in Middle Triassic to Jurassic. This coincides with the estimates made for the Signalhorn Dome by several authors (Mattingsdal et al., 2015; Gernigon et al., 2018; Hassaan et al., 2020), where respectively a pre-Cretaceous, Lower Triassic to Cretaceous and uppermost Triassic to Middle Jurassic age of the doming are estimated. As for the Veslekari Dome, a pre-Bajocian doming is estimated (Figure 6.4, A). This timing of doming could correspond with the Triassic activation estimate made by Gernigon et al. (2018), and the Late Triassic estimate suggested by Hassaan et al. (2020), linking the initial diapiric doming to the final up-thrusting of the Novaya Zemlya.

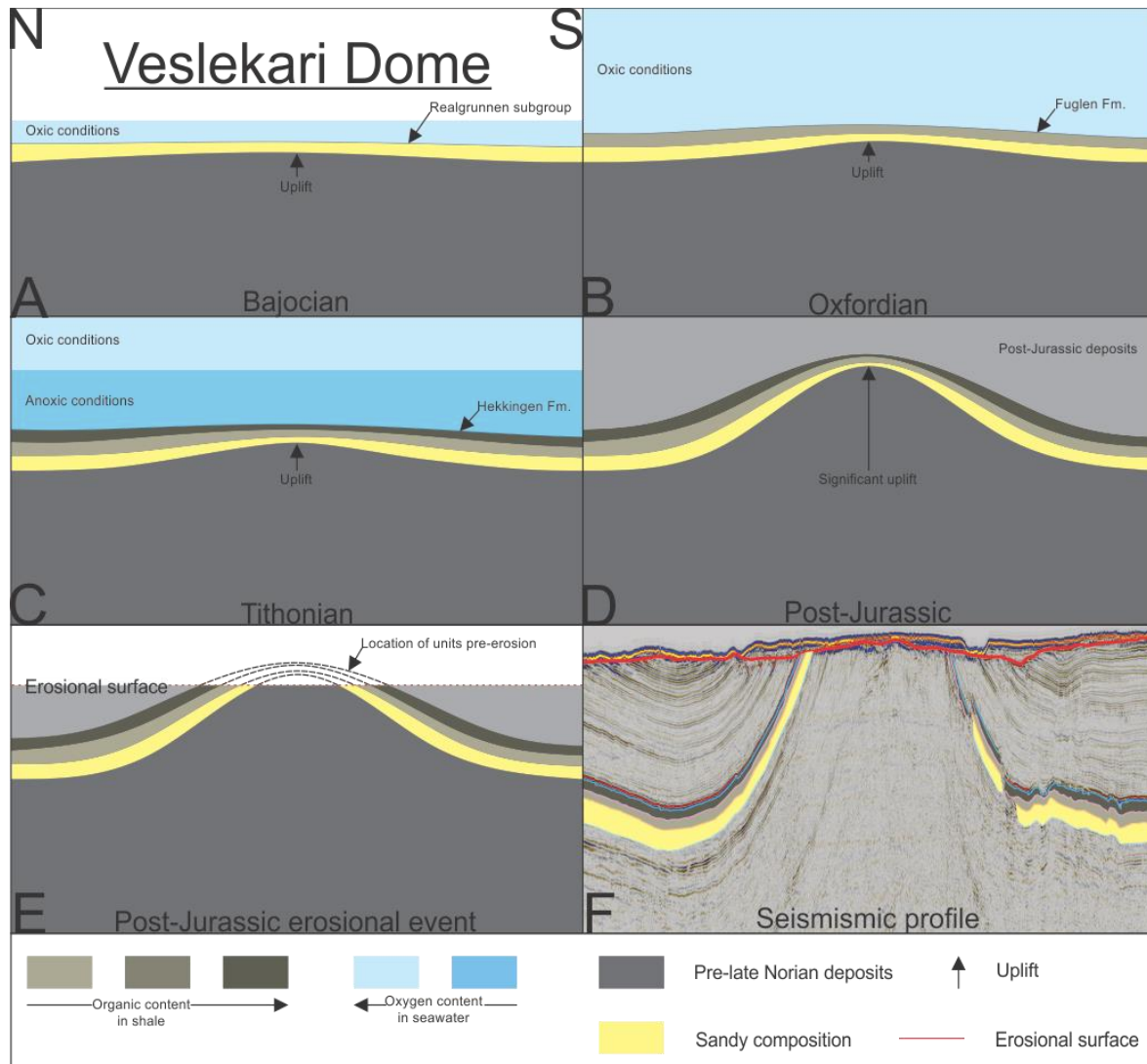


Figure 6.4 Conceptual model of the Veslekari Dome, from the Bajocian (1) to the post-Jurassic erosional event (5). 1) Minor uplifting can be observed at the Veslekari Dome through the Realgrunnen Subgroup, time-thickness map (Figure 5.19). 2) Oxfordian: The Fuglen Formation has been deposited alongside continued uplifting of the dome. 3) Tithonian: Anoxic conditions has been established within the Barents Sea during the upper Oxfordian – Tithonian, resulting in the deposition of the High organic Hekkingen Formation. 4) Post-Jurassic: Significant uplift of the dome due to halite migration occurs. 5) An erosional event occurs, removing the upper section of the dome. 6) Seismic 2D line [NPD1201-018], illustrating the seismic section of the Veslekari Dome. Profile (6), taken from (Figure 5.17).

## **Callovian to Oxfordian – the Fuglen Formation**

For the Fuglen Formation (Callovian to Oxfordian) more local thickness variations are observed (Figure 5.21), as opposed to the regional north-south thinning trends of the below Realgrunnen Subgroup (late Norian to Bajocian) (Section 5.2 and 5.4). The Haapet Dome, Veslakari Dome, Signalhorn Dome, Finnmark Platform and Fedynsky High, all represent areas where the Fuglen Formation is thinning. The thickest parts can be found within the Nordkapp Basin and in the northeast section of the study area (reaching up to 90ms TWT (Section 5.4)). On the Bjarmeland Platform and the north section of the Finnmark Platform, the unit is thinning eastwards to 15ms (TWT) on the Haapet Dome (Figure 5.21, Section 5.4). The Fuglen Formation is, as the older Realgrunnen Subgroup, truncated at the Fedynsky High, Finnmark Platform, Nordkapp Basin and Veslekari Dome (Section 5.4).

The positive reflection coefficient at the Hekkingen/ Fuglen interface (Section 5.5), implies an increased density and/ or velocity of the Fuglen Formation relative to the Hekkingen Formation. This could possibly be due to the suggested low density, high organic shale of the Hekkingen Formation, which is further discussed later. The parallel to sub-parallel, locally continuous reflection geometry of the unit is commonly associated with a stable environmental setting and uniform depositional rates (Mitchum et al., 1977b) (Section 5.4). A stable environmental setting and uniform depositional rates may have been facilitated by the documented regional transgression at the time (Section 2.2.1.2). The increased sea level would increase the distance of the study area to the sediment supply, promoting the deposition of fine-grained sediments (Veeken, 2007). The low amplitudes of the unit, may reflect a minimal internal acoustic impedance contrast and thus a possible uniform lithological composition of the unit (Prather et al., 1998). The discontinuous to chaotic reflection geometry of the unit (Section 5.4), are primarily located within fault influenced areas, suggesting post-depositional deformation as a plausible cause of the configuration (Mitchum et al., 1977b; Veeken, 2007). The northern part of the Finnmark Platform is not extensively fault influenced, which may imply a syn-depositional origin for the discontinuous, sub-parallel configuration (Mitchum et al., 1977b; Veeken, 2007; Catuneanu et al., 2011). A non-stable energy regime, is suggested to may have been facilitated by a gradual southward shallowing of the study area at the time of deposition (Figure 6.1, C). The primary composition of the Fuglen Formation in the Barents Sea South East is thus believed to share similarities to the fine-grained, offshore deposits documented by Klausen et al. (2017a), in the Barents Sea South West.

The Fuglen Formation thins towards the Haapet Dome, Veslekari Dome, Signalhorn Dome, Finnmark Platform and Fedynsky High (Section 5.4). The unit drapes both the Haapet and Signalhorn domes, reflecting their presence as elevated areas during the Callovian to Oxfordian (Figure 6.1, C and 6.2, B). The Fuglen Formation is believed to have been draping the Veslekari Dome, in advance of the erosional event which eroded the top section of the dome (Figure 5.5, 5.7, 5.17 and 6.4, B). This is suggested by the low thinning rate of the unit in addition to the relatively parallel configuration of both the base and top of the formation (Figure 5.5, 5.7 and 5.17). Whether the Fuglen Formation draped or overlapped the Veslekari Dome are debatable, as any actual evidence has been removed by later erosion (Figure 6.4, D-F). The truncation of the Fuglen Formation, along with a high dip (incline) of the unit onto the dome, suggest significant post-Oxfordian uplifting and erosion of the Veslekari Dome (Figure 6.4, A-F).

A late Norian to Bajocian doming is previously suggested in this study for both the Signalhorn and Veslekari domes (Figure 6.1, A-B). However, the rate of doming during the Callovian to Oxfordian is debateable. There are no clear observations indicating any significant erosion on top of the Signalhorn Dome, implying that it most likely did not experience terrestrial exposure (Figure 6.1 C-D). The compared time-thickness maps of the Realgrunnen Subgroup and Fuglen Formation, suggest a possible increase in the uplift of the Signalhorn Dome, between the deposition of the Realgrunnen Subgroup (late Norian to Bajocian) and the Fuglen Formation (Callovian to Oxfordian) (Figure 5.19 and 5.21). This is due to the additional thinning of the Fuglen Formation on the north section of the dome, compared to the Realgrunnen Subgroup (Figure 5.19 and 5.21). The base and top of the Realgrunnen Subgroup and Fuglen Formation follow much of the same trend onto the Veslekari Dome, being relatively parallel, with a slight thickness decrease of the units (Figure 5.8, 5.17, 5.19 and 5.21). This implies a possible continued, low rate uplifting of the dome from the late Norian through the Oxfordian (Figure 6.4, A-B). The uncertainties related to the uplift estimation are significant, as the top section of the dome has been removed by erosion (Figure 5.8, 5.17 and 6.4, D-F).

The thickness trends of the Realgrunnen Subgroup and the Fuglen Formation at the Haapet Dome are distinctly different (Figure 5.19 and 5.21). The previously established elevation of the dome suggested by the thinning of the Fuglen Formation, imply a pre-Callovian(?) inversion of the structural element following the deposition of the Realgrunnen Subgroup (late Norian to Bajocian) (Figure 6.1, A-C and 6.2, A-B). An inversion of the dome has



previously been documented by Mattingsdal et al. (2015) and Hassaan et al. (2020). Observations made by Mattingsdal et al. (2015), suggest a lower Cretaceous inversion, as no thinning in the Triassic and Jurassic strata were documented in this study. This is questioned by Hassaan et al. (2020) who suggest a Late Triassic - Early Jurassic inversion as a far-field response to the final up-thrusting of the Novaya Zemlya. The observed thinning of the Fuglen Formation in this study, thus disagrees with observations made in Mattingsdal et al. (2015), while supporting the assumed time of activation in Hassaan et al. (2020).

The truncation of the Fuglen Formation has several similarities to the Realgrunnen Subgroup on the Fedynsky High and Finnmark Platform (Figure 5.6, 5.9, 5.10 and 5.13-5.16). Both units are truncated, and overlain by the Hekkingen Formation, suggesting the previously documented erosional event to have occurred at the transition from top-Fuglen Formation to base-Hekkingen Formation (Figure 6.1, C-D and 6.3, C-E). There is a higher dip (incline) of the Realgrunnen Subgroup compared to the Fuglen Formation, which suggests continued uplifting of both structural elements following the deposition of the Realgrunnen Subgroup (Figure 5.13, 5.16, 6.1, C-D and 6.3, B-D). The truncation of the unit can be traced along the margin of both structural elements, establishing their presence as structurally elevated areas at the time of erosion (Figure 6.1, D and 6.3, D-E). The thinning of the unit, which is traceable until the erosional contact is reached, is a possible result of the Fuglen Formation overlapping both structural elements in advance of the erosional event, in a similar manner as suggested for the Realgrunnen Subgroup (Figure 6.3, C-E). This supports a continued established elevation of the Fedynsky High and Finnmark Platform through the Callovian to Oxfordian (Figure 6.1, C-D and 6.3, B-C). The greater unit thickness on the Finnmark Platform, implies its additional accumulation space and/ or sediment supply, relative to the Fedynsky High during the deposition of the Realgrunnen Subgroup and Fuglen Formation (Figure 6.1, A-D). It also suggests a significantly greater uplift of the Finnmark Platform than for the Fedynsky High, following the deposition of the Fuglen Formation and up until the erosional event (Figure 6.1, A-D).

The eastward to south-eastward thinning trend of the Fuglen Formation, compared to the more southward thinning trend of the below Realgrunnen Subgroup, could reflect a westward to north-westward tilting of the study area during the Bajocian – Callovian (Figure 6.1, B-D). No measurable change in unit thickness is observed across faults within the study area, excluding the north and south margin of the Nordkapp Basin. The uniform thickness along fault planes might reflect a possible post-Fuglen Formation origin of the faults.

An increase in unit thickness between the Realgrunnen Subgroup and Fuglen Formation, in the west on the Bjarmeland Platform and the north section of the Finnmark Platform reflect that subsidence possibly has acted alongside uplifting of the Haapet Dome, Fedynsky High and Finnmark Platform in the east and south-southeast (Figure 5.19, 5.21 and 6.1, C-D). The two areas are thus believed to have represented relatively tectonically stable sections of the study area during the Callovian to Oxfordian, with a small basin setting in the west and structural highs in the east (Figure 6.1, C). A basin configuration and thereby subsidence is also inferred for the northeast section of the study area, as the unit is noticeably thicker (60ms TWT) than on the structural highs to the west and south (Figure 5.21 and 6.1, C). This possibly correlates with Müller et al. (2019), who signifies that areas immediately to the north and south of the Fedynsky High have experienced additional sedimentary accumulations and reduced erosion parallel to the Novaya Zemlya forebulging.

The thickness of the Fuglen Formation within the Nordkapp Basin is similar to that of the Realgrunnen Subgroup (Figure 5.19 and 5.21). The formation is thicker in the basin than in the adjacent platform areas (20ms TWT), implying that it was a local area of increased accumulation during the Callovian to Oxfordian (Section 5.3-5.5). The additional accumulation space can possibly be related to syn-depositional subsidence within the basin, as an un-uniform thickness is observable along faults (Figure 5.4). A similarity in the thickness of the Realgrunnen Subgroup and the Fulgen Formation, could reflect a continued late Norian – Oxfordian subsidence of the Nordkapp Basin.

### **Upper Oxfordian – Tithonian – the Hekkingen Formation**

The upper Oxfordian – Tithonian, Hekkingen Formation has a larger and more regional extent than the underlying late Norian – Oxfordian deposits (Figure 5.19, 5.21 and 5.23). The thickness of the Hekkingen Formation follows much of the same trends as for the Fuglen Formation, with a thinning onto the Haapet Dome, Veslekari Dome, Signalhorn Dome, Fedynsky High and Finnmark Platform (Section 5.2, 5.4 and 5.6). The unit is truncated by the seafloor within the Tiddlybanken Basin, on the Veslekari Dome and within the Nordkapp Basin in the same manner as for the late Norian – Oxfordian deposits (Figure 5.4 and 5.5). It is draping the Fedynsky High, with a thickness of 10-15ms (TWT) at the thinnest, and it is truncated towards the seafloor in the south of the Finnmark Platform (Section 5.5-5.7). The most significant unit thickness is found within the northeast section of the study area and within the Nordkapp Basin (70-90ms TWT), with the addition of the west section of the

Bjarmeland Platform (70-90ms TWT, Figure 5.23). On the north section of the Finnmark Platform the unit has a similar thickness trend to that of the Callovian to Oxfordian deposits, which is a thicker unit in the west, with a gradual thinning to the east and south-southeast (Figure 5.19, 5.21 and 5.23).

The parallel, continuous configuration of the Hekkingen Formation could possibly reflect a stable environmental setting and uniform depositional rates, as that previously suggested for the Fuglen Formation (Section 5.6) (Mitchum et al., 1977b). The draping of some structural elements by the unit may reinforce this suggestion, as draping according to (Prather et al., 1998; Veeken, 2007) reflects hemipelagic/ pelagic suspension fall-out, and thus a low-energy environment. The negative reflection coefficient of the upper boundary is believed to reflect a density decrease (Section 3). The combined high amplitude and reflection coefficient of the top (negative) and base (positive) of the unit, could suggest that the unit represents a source rock (Løseth et al., 2011). Marine shales with a high organic content has previously been documented to have a lower bulk density than shales with a lower organic content (Løseth et al., 2011). The seismic configuration and amplitude of the Hekkingen Formation within the study area thus support that the unit is a marine shale with a high organic content (Section 2.3.5, Figure 6.3, E-F). This coincides with the documented regional prevalence of the unit and the organic composition of the formation in the Barents Sea South West and gamma ray readings in well 7435/12-1 (Section 2.3.5, Figure 6.3, E-F) (Dallmann, 1999, p. 136; Henriksen et al., 2011). A highly organic content of the Hekkingen Formation would imply a stratification of the water column concurrent to the deposition of the unit (Figure 6.2, 6.3 and 6.4) (Lee, 1992). This would imply a limited amount of water circulation was present at the time (Van Cappellen et al., 1998). Løseth et al. (2011) suggest that variations in amplitude laterally within source rocks can be correlated to the internal distribution and total amount of organic content of the unit. This could imply that the lateral variations in the continuity of the Hekkingen Formation within the study area, might be related to the organic content of the unit.

The suggested low-energy depositional environment for the Hekkingen Formation, implies a submersion of both the Fedynsky High and Finnmark Platform following the erosion at the Fuglen/ Hekkingen transition (Figure 6.1, D-E and 6.3, D-E). Sea level rise is suggested to have occurred at the time (Figure 6.1, D-E and 6.3, D-E, Section 2.2.1.2).

The thinning of the Hekkingen Formation implies the continued elevation of the Fedynsky High and Finnmark Platform during the upper Oxfordian – Tithonian (Figure 6.1, D-E and

6.3, D-E). As for the Finnmark Platform, the slight thinning and high seismic amplitude of the Hekkingen Formation from north to south, reflect a slight northward tilt of the platform during the deposition of the Hekkingen Formation (Figure 6.1, D-E).

The low seismic amplitude of the shallowest section of the Hekkingen Formation on the Fedynsky High differs from the high amplitudes observed on the Finnmark Platform (Section 5.7). A reduction in amplitude implies a potential decrease in seismic impedance contrast at the reflection boundary, hence a resemblance in velocity and/ or density of the over and underlying unit (Section 3.1). This could therefore suggest an increased lithological resemblance of the Hekkingen Formation to the overlying deposits on the high (Figure 6.3, E-F). A fine-grained sedimentary composition on top of the high is suggested by the previously established low-energy depositional environment which may have prevailed at the time. Løseth et al. (2011) correlate the total organic content and the unit thickness to the amplitude strength along the top reflector of source rocks. They suggest an increase in amplitude with an increase in total organic content, as long as the separation of the upper (negative) and the lower (positive) reflection coefficient is sufficient (Løseth et al., 2011). The close to identical thickness of the unit on the Fedynsky High and Finnmark Platform excludes thickness as a probable cause for the amplitude decrease (Figure 5.21 and 5.23). This suggests that the reduced amplitude of the Hekkingen Formation onto the Fedynsky High is the possible effect of a reduction in the organic content of the formation (Figure 6.3, E-F). A reduced organic content could be the effect of a continued uplifting of the high, elevating the shallowest section above the anoxic condition, which is suggested to have prevailed during the deposition of the Hekkingen Formation (Figure 6.3, E-F). This would also imply a greater elevation of the Fedynsky High, in relation to the Finnmark Platform during the Oxfordian – Tithonian (Figure 6.1, E and 6.3, E).

A uniform thickness of the Fuglen and Hekkingen formations on the north section of the Finnmark Platform are interpreted to represent a stable Callovian to Tithonian platform setting (Figure 5.21, 5.23 and 6.1, E).

The Hekkingen Formation has a thickness of 70-90ms (TWT) in the west on the Bjarmeland Platform and 85ms (TWT) in the northeast of the Haapet Dome (Figure 5.23). The Haapet Dome is located between these two areas, where the unit has a thickness of 20-50ms (TWT) (Figure 5.23). The increased unit thickness at these two areas possibly suggest that they acted as depocentres during the upper Oxfordian – Tithonian (Figure 6.1, D-E). The accumulations



of the Hekkingen Formation are significantly more pronounced than for the Fuglen Formation in these areas (Figure 5.21 and 5.23), which possibly implies an increased subsidence rate for these two areas during the upper Oxfordian – Tithonian (Figure 6.1, D-E). The thickness of the unit appears to be increasing towards the boundary of the study area in the west of the Bjarmeland Platform and northeast of the Haapet Dome (Figure 5.23). This suggests that the area influenced by subsidence is likely to exceed the extent of the study area both to the west on the Bjarmeland Platform and to the northeast of the dataset. Both the Hekkingen Formation and Fuglen Formation are influenced by brittle deformation, reflected by the separation of both formations along several fault planes within the study area (Figure 5.4-5.10 and 5.12-5.17). There is no sign of any thickness variations across these faults, implying that they were formed after the deposition of the Hekkingen Formation. The subsidence and uplift within the study area, are thus believed to be related to the reactivation of deep-seated structural lineament during both the deposition of the Fuglen and Hekkingen formations, in a similar manner as for the Realgrunnen Subgroup. A time equivalent structural episode is the Jurassic – Early Cretaceous rift episode, related to the pre-breakup rifting of the North-Atlantic (Faleide et al., 2008). This possibly suggests that the study area was located beyond the extensional forces of the northward propagation of the Atlantic rifting acting on the West Barents Sea. The pre-North-Atlantic rifting in the Late Jurassic – Early Cretaceous re-activated deep-seated lineaments, which caused the uplifting of the Fedynsky High and Finnmark Platform and the subsidence of the west section of the Bjarmeland Platform.

The subsidence that influenced the older units within the Nordkapp Basin is assumed to have persisted through upper Oxfordian – Tithonian. This is reflected by the similarities in the thickness trends of the diapiric rim synclines (Figure 5.4) and location of increased unit thickness on the time-thickness maps (Figure 5.21 - 5.23). The presence of a thicker Hekkingen Formation in the northwest section of the Tiddlybanken Basin (Figure 5.23), reflects that it represented a topographic low during the upper Oxfordian – Tithonian (Figure 6.1, D-E). This suggests a pre-Oxfordian diapiric activation, due to the additional accumulation space close to the diapiric structures at the basin centre and the presence of rim synclines (Section 5.6). Gernigon et al. (2018) attributed the additional accumulation space to salt withdrawal and diapiric migration during the Lower to Upper Triassic. The truncation of the Hekkingen Formation at the seafloor suggests significant diapirism and erosion, following the deposition of the unit.

Continued doming through the upper Oxfordian – Tithonian is proposed for the Signalhorn Dome, as a more prominent thickness decrease is observed in the upper Oxfordian – Tithonian unit compared to the late Norian – Oxfordian deposits (Figure 5.19, 5.21 and 5.23). The unit appears to be draping the dome, while onlap by the internal reflectors cannot be excluded as a possibility due to the limiting resolution of the dataset. Significant thinning of the unit onto the Haapet Dome and Veslekari Dome, indicates the prominence of the two structural elements at the time (Figure 5.12 and 5.17). The thinning is believed to be the result of continued doming through the upper Oxfordian – Tithonian, in combination with an increased subsidence of the adjacent areas to the west and northeast of the Haapet Dome (Figure 6.1, E, 6.2, C and 6.4, D-E). Significant post-Jurassic diapirism of the Veslekari Dome is suggested, as the late Norian – Tithonian units are truncated by the sea floor (Figure 5.8, 5.17 and 6.4, D-E). It is suggested by Hassaan et al. (2020) that a reactivation of salt resulted in uplifting and erosion of the dome in the earliest Cretaceous.

## 7 Conclusion

- Variations in thickness and termination patterns of the Realgrunnen Subgroup (late Norian to Bajocian), the Fuglen Formation (Callovian to Oxfordian) and the Hekkingen Formation (upper Oxfordian to Tithonian) have given insights to the tectono-stratigraphic evolution of the Barents Sea South East (BSSE).
- During the late Norian to Bajocian, the topography of the BSSE was characterized by uplifted regions in the areas of the Fedynsky High, Finnmark Platform, Veslekari Dome and Signalhorn Dome. This is inferred from thinning of the Realgrunnen Subgroup towards these areas. A uniform thickness and minimal amount of syn-depositional fault influence of the Realgrunnen Subgroup, suggest a relatively stable platform configuration for the Bjarmeland Platform and northern section of the Finnmark Platform. Prominent depocenters and thereby basin configurations are interpreted for the Nordkapp Basin, Haapet Dome and the area northeast of the dome structure.
- The Callovian to Oxfordian is interpreted as a period of uplift of the Finnmark Platform, and Fedynsky High are represented by the onlap and thinning of the Fuglen Formation towards these structures. The dome structures; the Haapet Dome in the north, the Veslekari Dome and the Signalhorn Dome to the south also appears to have been active based on the associated thinning of the Fuglen Formation. Increased thickness of the Fuglen Formation on the Bjarmeland Platform, northern parts of the Finnmark Platform, northeast of the Haapet Dome and in the Nordkapp Basin, are assumed to represent increased accommodation space due to subsidence of these structural elements.
- In late Oxfordian to Tithonian submersion of the Fedynsky High and Finnmark Platform is suggested by draping and onlap of the Hekkingen Formation. Thinning, draping and onlap of the Hekkingen Formation also suggest a continued uplift of the domes, the Haapet-, Veslekari-, and Signalhorn domes. The subsidence as described above during Callovian to Oxfordian in the west on the Bjarmeland Platform, the area northeast of the Haapet Dome and Nordkapp Basin, appears from increased thickness of the Hekking Formation to have continued in this period. The Tiddlybanken Basin also show increased thickness of the Hekkingen Formation, suggesting subsidence of these areas.

- Reactivation of deep lineaments by the final upthrusting of the Novaya Zemlya (Late Triassic – Early Jurassic) and the Atlantic rifting (Late Jurassic – Early Cretaceous) are suggested as the large scale tectonic events for the structural movements and differences within the study area from the late Norian to Tithonian.

## 8 Future work

This study has provided information on the possible tectonic- and evolutionary differences between the major structural elements of the BSSE during the uppermost Triassic to lower Cretaceous.

To further investigate the geological development of the area, some possible future work might be indicated:

- Acquisition and use of additional seismic 3D data, combined with well information would facilitate an increased understanding of the seismic stratigraphic development of the study area.
- Investigate the possible causes for the (uppermost Triassic to lower Cretaceous) tectonic movements within the study area, with an emphasis on the later stages of the Novaya Zemlya forebulging and the Atlantic rifting.
- Correlate seismic and well data of the BSSE to the BSSW, facilitating a possible enhanced understanding of the depositional and structural evolution of the Norwegian Barents Sea.





## References

- Aminzadeh, F., & Dasgupta, S. N. (2013). Fundamentals of Petroleum Geophysics. In Geophysics for petroleum engineers (1 ed., Vol. 60, pp. 37-92). AE Amsterdam: Elsevier.
- Bacon, M., Simm, R., & Redshaw, T. (2003). 3-D seismic interpretation(pp. 225). doi:<https://doi.org/10.1017/CBO9780511802416>
- Berzin, R., Oncken, O., Knapp, J., Perez-Estaun, A., Hismatulin, T., Yunusov, N. t., & Lipilin, A. (1996). Orogenic evolution of the Ural Mountains: results from an integrated seismic experiment. *Science*, 274(5285), 220-221. doi:<https://doi.org/10.1126/science.274.5285.220>
- Brown, A. R. (2004). Interpretation of three-dimensional seismic data (J. C. Lorenz & G. T. Schuster Eds. 6th ed. ed. Vol. 42). Tulsa, Okla: American Association of Petroleum Geologists and the Society of Exploration Geophysicists.
- Bugge, T., Elvebakk, G., Fanavoll, S., Mangerud, G., Smelror, M., Weiss, H. M., Gjelberg, J., Kristensen, S. E., & Nilsen, K. (2002). Shallow stratigraphic drilling applied in hydrocarbon exploration of the Nordkapp Basin, Barents Sea. *Marine and Petroleum Geology*, 19(1), 13-37. doi:[https://doi.org/10.1016/S0264-8172\(01\)00051-4](https://doi.org/10.1016/S0264-8172(01)00051-4)
- Catuneanu, O., Galloway, W. E., Kendall, C. G. S. C., Miall, A. D., Posamentier, H. W., Strasser, A., & Tucker, M. E. (2011). Sequence stratigraphy: methodology and nomenclature. *Newsletters on stratigraphy*, 44(3), 173-245. doi:<https://dx.doi.org/10.1127/0078-0421/2011/0011>
- Chopra, S., & Marfurt, K. J. (2008). Emerging and future trends in seismic attributes. *The Leading Edge*, 27(3), 298-318. doi:<http://dx.doi.org/10.1190/1.2896620>
- Dalland, A., Worsley, D., & Ofstad, K. (1988). A lithostratigraphic scheme for the Mesozoic and Cenozoic succession offshore mid-and northern Norway, NPD-Bulletin No. 4NPD-Bulletin No 4 (Vol. 4, pp. 87).

- Dallmann, W. K. (1999). Lithostratigraphic lexicon of Svalbard: review and recommendations for nomenclature use : Upper Palaeozoic to Quaternary bedrock. Tromsø: Norsk polarinstitutt.
- Doré, A. G. (1995). Barents Sea Geology, Petroleum Resources and Commercial Potential. *Arctic*, 48(3), 207-221.
- Faleide, J. I., Bjørlykke, K., & Gabrielsen, R. H. (2010). Geology of the Norwegian Continental Shelf. In *Petroleum Geoscience: From Sedimentary Environments to Rock Physics* (pp. 467-499). Berlin, Heidelberg: Springer Berlin Heidelberg.
- Faleide, J. I., Tsikalas, F., Breivik, A. J., Mjelde, R., Ritzmann, O., Engen, O., Wilson, J., & Eldholm, O. (2008). Structure and evolution of the continental margin off Norway and the Barents Sea. *Episodes*, 31(1), 82-91.  
doi:<https://doi.org/10.18814/epiiugs/2008/v31i1/012>
- Faleide, J. I., Vågnes, E., & Gudlaugsson, S. T. (1993). Late Mesozoic-Cenozoic evolution of the south-western Barents Sea in a regional rift-shear tectonic setting. *Marine and Petroleum Geology*, 10(3), 186-214. doi:[https://doi.org/10.1016/0264-8172\(93\)90104-Z](https://doi.org/10.1016/0264-8172(93)90104-Z)
- Gabrielsen, R. H., Færseth, R. B., Jensen, L. N., Kalheim, J. E., & Fridtjof, R. (1990). Structural elements of the Norwegian Continental shelf: The Barents sea region. *NPD-Bulletin No 6* (Vol. 6, pp. 47).
- Gee, D. G., & Pease, V. (2004). The Neoproterozoic Timanide Orogen of eastern Baltica: introduction. *Geological Society, London, Memoirs*, 30(1), 1-3.  
doi:<https://doi.org/10.1144/GSL.MEM.2004.030.01.01>
- Gernigon, L., Brønner, M., Dumais, M.-A., Gradmann, S., Grønlie, A., Nasuti, A., & Roberts, D. (2018). Basement inheritance and salt structures in the SE Barents Sea: Insights from new potential field data. *Journal of Geodynamics*, 119, 82-106.  
doi:<https://doi.org/10.1016/j.jog.2018.03.008>

- Glørstad-Clark, E., Birkeland, E. P., Nystuen, J. P., Faleide, J. I., & Midtkandal, I. (2011). Triassic platform-margin deltas in the western Barents Sea. *Marine and Petroleum Geology*, 28(7), 1294-1314. doi:<https://doi.org/10.1016/j.marpetgeo.2011.03.006>
- Glørstad-Clark, E., Faleide, J. I., Lundschieen, B. A., & Nystuen, J. P. (2010). Triassic seismic sequence stratigraphy and paleogeography of the western Barents Sea area. *Marine and Petroleum Geology*, 27(7), 1448-1475. doi:<https://doi.org/10.1016/j.marpetgeo.2010.02.008>
- Halland, E., Bjørnestad Andreas, Gjeldvik Ine, Bjørheim Maren, Magnus Christian, Meling Ida, Mujezinović Jasminka, Riis Fridtjof, Rød Rita, Pham Van T. H., & Tappel Inge. (2014). The Barents Sea. In CO2 atlas for the Norwegian continental shelf (pp. 1-39): NPD.
- Hassaan, M., Faleide, J. I., Gabrielsen, R. H., & Tsikalas, F. (2020). Carboniferous graben structures, evaporite accumulations and tectonic inversion in the southeastern Norwegian Barents Sea. *Marine and Petroleum Geology*, 112, 1-26. doi:<https://doi.org/10.1016/j.marpetgeo.2019.104038>
- Henriksen, E., Ryseth, A. E., Larssen, G. B., Heide, T., Rønning, K., Sollid, K., & Stoupakova, A. V. (2011). Chapter 10 Tectonostratigraphy of the greater Barents Sea: implications for petroleum systems. *Geological Society, London, Memoirs*, 35(1), 163-195. doi:<https://doi.org/10.1144/M35.10>
- Jensen, Ø. (2011). Current Legal Developments, The Barents Sea: Treaty between Norway and the Russian Federation concerning Maritime Delimitation and Cooperation in the Barents Sea and the Arctic Ocean *International Journal of Marine and Coastal Law*, 26, 151-168. Retrieved from <https://www.fni.no/getfile.php/131499-1467549392/Filer/Publikasjoner/OYJ-ESTU-2011.pdf>. (Accessed 11.11.2019)
- Kearey, P., Brooks, M., & Hill, I. (2013). *An introduction to geophysical exploration (Vol. 3)*: John Wiley & Sons.
- Klausen, T. G., Müller, R., Poyatos-Moré, M., Olausson, S., & Stueland, E. (2019). Tectonic, provenance and sedimentological controls on reservoir characteristics in the Upper

Triassic–Middle Jurassic Realgrunnen Subgroup, SW Barents Sea. Geological Society, London, Special Publications, 495. doi:<https://doi.org/10.1144/SP495-2018-165>

Klausen, T. G., Müller, R., Slama, J., & Helland-Hansen, W. (2017a). Evidence for Late Triassic provenance areas and Early Jurassic sediment supply turnover in the Barents Sea Basin of northern Pangea. *Lithosphere*, 9(1), 14-28.  
doi:<https://doi.org/10.1130/L556.1>

Klausen, T. G., Müller, R., Sláma, J., Olaussen, S., Rismyhr, B., & Helland-Hansen, W. (2017b). Depositional history of a condensed shallow marine reservoir succession: stratigraphy and detrital zircon geochronology of the Jurassic Stø Formation, Barents Sea. *Journal of the Geological Society*, 175(1), 130-145.  
doi:<https://doi.org/10.1144/jgs2017-024>

Klausen, T. G., Ryseth, A. E., Helland-Hansen, W., Gawthorpe, R., & Laursen, I. (2015). Regional development and sequence stratigraphy of the Middle to Late Triassic Snadd Formation, Norwegian Barents Sea. *Marine and Petroleum Geology*, 62, 102-122.  
doi:<https://doi.org/10.1016/j.marpetgeo.2015.02.004>

Klitzke, P., Faleide, J. I., Scheck-Wenderoth, M., & Sippel, J. (2015). A lithosphere-scale structural model of the Barents Sea and Kara Sea region. *Solid Earth*, 6(1), 153-172.  
doi:10.5194/se-6-153-2015

Koyi, H., Talbot, C. J., & Torudbakken, B. O. (1995). Analogue models of salt diapirs and seismic interpretation in the Nordkapp Basin, Norway. *Petroleum Geoscience*, 1(2), 185-192. doi:<https://doi.org/10.1144/petgeo.1.2.185>

Larsen, G., Elvebakk, G., Henriksen, L. B., Kristensen, S., Nilsson, I., Samuelsen, T., Svånå, T., Stemmerik, L., & Worsley, D. (2002). Upper Palaeozoic lithostratigraphy of the Southern Norwegian Barents Sea. *Norwegian Petroleum Directorate Bulletin*, 9, 76.

Lee, C. (1992). Controls on organic carbon preservation: The use of stratified water bodies to compare intrinsic rates of decomposition in oxic and anoxic systems. *Geochimica et*



Cosmochimica Acta, 56(8), 3323-3335. doi:[https://doi.org/10.1016/0016-7037\(92\)90308-6](https://doi.org/10.1016/0016-7037(92)90308-6)

Lundschieen, B. A., Høy, T., & Mørk, A. (2014). Triassic hydrocarbon potential in the Northern Barents Sea; integrating Svalbard and stratigraphic core data. In Atle Mørk, B. A. Lundschieen, & T. Høy (Eds.), Norwegian Petroleum Directorate Bulletin No.11 (Vol. 11, pp. 3-20).

Løseth, H., Wensaas, L., Gading, M., Duffaut, K., & Springer, M. (2011). Can hydrocarbon source rocks be identified on seismic data? *Geology*, 39(12), 1167-1170.  
doi:<https://doi.org/10.1130/G32328.1>

Mattingsdal, R., Høy, T., Simonstad, E., & Brekke, H. (2015). An updated map of structural elements in the southern Barents Sea. In. 31st Geological Winter Meeting in Stavanger: NPD.

Mitchum, R. M., Vail, P., & Thompson Iii, S. (1977a). Seismic stratigraphy and global changes of sea level: Part 2. The depositional sequence as a basic unit for stratigraphic analysis: Section 2. Application of seismic reflection configuration to stratigraphic interpretation. In C. E. Payton (Ed.), *Seismic Stratigraphy — Applications to Hydrocarbon Exploration* (Vol. 26, pp. 53-62): American Association of Petroleum Geologists.

Mitchum, R. M., Vail, P. R., & Sangree, J. B. (1977b). Seismic stratigraphy and global changes of sea level: Part 6. Stratigraphic interpretation of seismic reflection patterns in depositional sequences: Section 2. Application of seismic reflection configuration to stratigraphic interpretation. In C. E. Payton (Ed.), *Seismic Stratigraphy — Applications to Hydrocarbon Exploration* (Vol. 26, pp. 53-62): American Association of Petroleum Geologists.

Mulrooney, M. J., Rismyhr, B., Yenwongfai, H. D., Leutscher, J., Olaussen, S., & Braathen, A. (2018). Impacts of small-scale faults on continental to coastal plain deposition: Evidence from the Realgrunnen Subgroup in the Goliat field, southwest Barents Sea,

- Norway. *Marine and Petroleum Geology*, 95, 276-302.  
doi:<https://doi.org/10.1016/j.marpetgeo.2018.04.023>
- Müller, R., Klausen, T., Faleide, J., Olaussen, S., Eide, C., & Suslova, A. (2019). Linking regional unconformities in the Barents Sea to compression-induced forebulge uplift at the Triassic-Jurassic transition. *Tectonophysics*, 765, 35-51.  
doi:<https://doi.org/10.1016/j.tecto.2019.04.006>
- Mørk, A., Lundschieen, B. A., & Høy, T. (2014). Results from the Norwegian Petroleum Directorate's activities in the northern Barents Sea and Svalbard (2006-2014). In Atle Mørk, B. A. Lundschieen, & T. Høy (Eds.), *NPD-Bulletin No 11 (Vol. No.11)*.
- Nagell, T. C., & Berthelsen, O. (2016). Announcement 23rd licensing round awards [Press release]. Retrieved from <https://www.regjeringen.no/en/aktuelt/announcement-23rd-licensing-round-awards/id2500936/>. (Accessed 11.11.2019)
- NPD. (2013). *The Petroleum Resources on the Norwegian Continental Shelf*(pp. 63).
- NPD. (2017). *Geological assesment of petroleum resources in eastern part of the Barents Sea north*(pp. 40).
- NPD. (2019). *Factpages from Oljedirektoratet* <https://factpages.npd.no/nb-no/wellbore/pageview/exploration/wdss/8228>. (Accessed 28.04.2020)
- Nygaard, H. H., Løvstad, K., Müller, R., & Jahren, J. (2017). Clay coating preserving high porosities in deeply buried intervals of the Stø Formation. *Marine and Petroleum Geology*, 88, 648-658. doi:<https://doi.org/10.1016/j.marpetgeo.2017.09.011>
- O'leary, N., White, N., Tull, S., Bashilov, V., Kuprin, V., Natapov, L., & Macdonald, D. (2004). Evolution of the Timan–Pechora and south barents sea basins. *Geological Magazine*, 141(2), 141-160. doi:<https://doi.org/10.1017/S0016756804008908>
- Prather, B. E., Booth, J. R., Steffens, G. S., & Craig, P. A. (1998). Classification, lithologic calibration, and stratigraphic succession of seismic facies of intraslope basins, deep-water Gulf of Mexico. *AAPG Bulletin*, 82(5), 701-728.

- Puchkov, V. N. (2009). The evolution of the Uralian orogen. Geological Society, London, Special Publications, 327(1), 161-195. doi:<https://doi.org/10.1144/SP327.9>
- Ritzmann, O., & Faleide, J. I. (2009). The crust and mantle lithosphere in the Barents Sea/Kara Sea region. *Tectonophysics*, 470(1-2), 89-104.  
doi:<https://doi.org/10.1016/j.tecto.2008.06.018>
- Ryseth, A. (2014). Sedimentation at the Jurassic-Triassic boundary, south-west Barents Sea. In *Depositional Systems to Sedimentary Successions on the Norwegian Continental Margin* (1 ed., Vol. 46, pp. 187-214). Chichester, England :: John Wiley & Sons.
- Rønnevik, H., Beskow, B., & Jacobsen, H. P. (1982). Structural and Stratigraphic Evolution of the Barents Sea Arctic. *Arctic Geology and Geophysics*, 8(4), 431-440.
- Sheriff, R. E. (2002). *Encyclopedic dictionary of applied geophysics* (Vol. 4). Tulsa, Oklahoma, USA: Society of exploration geophysicists.
- Smelror, M., Basov, V. A., & Norges geologiske, u. (2009). *Atlas : geological history of the Barents Sea* (Morten Smelror, Oleg V. Petrov, Geir Birger Larsen, & S. Werner Eds.). Trondheim, Norway: Geological Survey of Norway.
- Vail, P., & Mitchum, R. (1977). Seismic Stratigraphy and Global Changes of Sea Level: Part 1. Overview: Section 2. Application of Seismic Reflection Configuration to Stratigraphic Interpretation. In C. E. Payton (Ed.), *Seismic Stratigraphy — Applications to Hydrocarbon Exploration* (Vol. 26, pp. 51-52): American Association of Petroleum Geologists.
- Van Cappellen, P., Viollier, E., Roychoudhury, A., Clark, L., Ingall, E., Lowe, K., & Dichristina, T. (1998). Biogeochemical cycles of manganese and iron at the oxic–anoxic transition of a stratified marine basin (Orca Basin, Gulf of Mexico). *Environmental science & technology*, 32(19), 2931-2939.  
doi:<https://doi.org/10.1021/es980307m>

Van Wagoner, J., Mitchum Jr, R., Posamentier, H., & Vail, P. (1987). Seismic stratigraphy interpretation using sequence stratigraphy: Part 2: key definitions of sequence stratigraphy. *Atlas of Seismic Stratigraphy*, 1(27), 11-14.

Veeken, P. C. (2007). *Seismic stratigraphy, basin analysis and reservoir characterisation* (1 ed. Vol. 37): Elsevier.

Worsley, D. (2008). The post-Caledonian development of Svalbard and the western Barents Sea. *Polar Research*, 27(3), 298-317. doi:<https://doi.org/10.1111/j.1751-8369.2008.00085.x>

